Vilnius University

Faculty of Physics

Laboratory of Atomic and Nuclear Physics

Experiment No. 7

STUDY OF THE COMPTON EFFECT

by Andrius Poškus

(e-mail: andrius.poskus@ff.vu.lt)

2026-11-24

Contents

Objective of the work **1**

1. Tasks **1**

2. Control questions **1**

Literature 1

3. Gamma radiation and its interaction with matter **2**

3.1. Photonic theory of electromagnetic radiation 2

3.2. Photoeffect. Einstein's equation 2

3.3. Compton effect 3

3.4. Concepts of interaction cross section and differential interaction cross section 4

3.5. Types of ionizing radiation 8

3.6. Interaction of gamma radiation with matter 9

3.6.1. Classical scattering and Compton scattering 10

3.6.2. Relations between photon energy, electron energy and scattering angle 12

3.6.3. Classical expressions for Rayleigh and Thomson scattering cross sections 13

3.6.4. Compton scattering cross section 17

3.6.5. Photoelectric effect 19

3.6.6. Electron and positron pair production 20

3.6.7. Attenuation coefficients 21

4. Scintillation Detectors **27**

4.1. Introduction 27

4.2. The elementary process of scintillation in an inorganic scintillator 27

4.3. Structure of a Scintillation Detector 29

5. Gamma Spectroscopy Using Scintillation Detectors **31**

5.1. Pulse Height Spectra 31

5.2. Detector Energy Resolution 32

5.2.1. Pulse height response function and pulse height resolution 32

5.2.2. Energy response function and energy resolution 33

5.3. Gamma Radiation Spectrum. Gamma Spectrometer. Secondary Electrons 34

5.4. Energy spectrum of secondary electrons 35

5.5. Shapes of response functions for detectors of various sizes 37

5.6. Structure and Main Parameters of a Gamma Spectrometer 41

5.7. Energy Calibration of a Spectrometer 45

6. Measurement methodology **46**

6.1. Theory of the measurement method 46

6.1.1. Measurement schematic 46

6.1.2. Calculation of the full-energy peak centroid by non-linear least squares fitting 46

6.1.3. Calculation of the confidence interval for the experimental wavelength 49

6.2. Equipment and measurement procedure 50

6.3. Analysis of measurement data 54

6.3.1. Generation of the text file with initial approximation data in "Measure" 55

6.3.2. Calculation of the calibration spectrum peak centroid by non-linear least squares fitting 56

6.3.3. Calculation of the scattered spectrum peak centroid by non-linear least squares fitting 61

6.3.4. Verification of the Compton formula and calculation of the Compton wavelength . . . 64

Objective of the work

Experimentally investigate the Compton scattering phenomenon, and verify the Compton formula.

1. Tasks

1. Measure the γ radiation energy spectra of a ^{137}Cs sample scattered at angles of 45°, 60°, 75°, 90°, 105°, 120°, and 135°.
2. Determine the change in wavelength of the scattered γ radiation and its uncertainty for each scattering angle.
3. Compare the measurement results of the wavelength change with the results of theoretical calculations (Compton formula).

2. Control questions

1. Concept of electromagnetic radiation scattering. Thomson, Rayleigh, and Compton scattering.
2. Laws of conservation of energy and momentum in the case of Compton scattering. Compton effect. Compton formula (with derivation).
3. Concept of scattering cross section. Relationship between scattering cross section and mean free path.
4. Concept of differential scattering cross section.
5. Physical mechanisms of gamma radiation interaction with matter. Attenuation coefficient concept.
6. Operating principle and schematic of a scintillation detector.
7. Scintillation processes in an inorganic scintillator.
8. Concept of differential pulse amplitude spectrum.
9. Definitions of the detector's response function and energy resolution.
10. Operating principles of scintillation γ spectrometers. Energy spectrum of secondary electrons.
11. General shape of the detector's response function.
12. Main components of a γ spectrometer. Calibration of a spectrometer.

Literature

1. Krane K. S. Introductory Nuclear Physics. New York: John Wiley & Sons, 1988. p. 198 – 204, 207 – 213.
2. Lilley J. Nuclear Physics: Principles and Applications. New York: John Wiley & Sons, 2001. p. 136 - 142.
3. Knoll G. F. Radiation Detection and Measurement. 3rd Edition. New York: John Wiley & Sons, 2000. p. 48 - 55, 307 –317.
4. Photon cross sections and attenuation coefficients. – https://kaeri.re.kr
5. Press W. H. , Teukolsky S. A., Vetterling W. T., Flannery B. P. Numerical Recipes in C: The Art of Scientific Computing. Second Edition, Cambridge: Cambridge University Press, 1992, 994 p.

3. Gamma radiation and its interaction with matter

3.1. Photonic theory of electromagnetic radiation

Based on the hypothesis of the German physicist Max Planck about the discreteness (quantization) of the energy of a harmonic oscillator, another German physicist, Albert Einstein, developed the quantum (photonic) theory of light in 1905. According to Einstein, electromagnetic radiation exists in the form of discrete portions of energy. A quantum of electromagnetic radiation energy can be considered a material particle that moves at the speed of light c and carries energy

$$E = h\nu = h\frac{c}{\lambda}. \tag{3.1.1}$$

This particle is called a **photon**. Since a photon acts as a material particle, it possesses mass and momentum. The mass of a photon m_f can be expressed using Einstein's relativistic relationship between energy and mass: $h\nu = m_\mathrm{f}c^2$. From this:

$$m_\mathrm{f} = \frac{h\nu}{c^2} = \frac{h}{c\lambda}. \tag{3.1.2}$$

It must be borne in mind that this is the mass of a photon moving at the speed of light: *the rest mass of a photon is equal to zero*. In this respect, the photon differs from material particles (such as the electron, proton, and neutron), whose rest mass is non-zero and which can be at rest, while its speed is always equal to the speed of light c. The momentum of a photon p_ph (the product of mass and velocity) is

$$p_\mathrm{ph} = m_\mathrm{ph}c = \frac{h\nu}{c} = \frac{h}{\lambda}. \tag{3.1.3}$$

The photon momentum vector $\mathbf{p}_\mathrm{ph}$ is related to its wave vector $\mathbf{k}$ as follows:

$$\mathbf{p}_\mathrm{ph} = \hbar\mathbf{k}. \tag{3.1.4}$$

Thus, electromagnetic radiation can be characterized not only by wave parameters λ and ν, but also by quantities m_ph and p_ph, which are used in mechanics to describe the motion of material particles. This shows that electromagnetic radiation manifests a **wave-particle duality**: certain phenomena (interference, diffraction, and polarization) show that electromagnetic radiation has a wave nature, while other phenomena (the properties of thermal radiation and the photoeffect and Compton effect described below) show that electromagnetic radiation is discrete, or a **quantum** process caused by the action of individual particles (photons).

3.2. Photoeffect. Einstein's equation

At the end of the 19th century, an optical phenomenon was discovered that could not be explained on the basis of classical laws of physics. It was observed that when a negatively charged metal plate is illuminated with ultraviolet light, the metal gradually loses its charge, but if the metal is positively charged, it does not lose its charge when illuminated. This shows that light releases negative electrical charge from the metal. The nature of this negative charge was determined in 1900 by the German physicist F. Lenard. He proved that the negative charge carriers released from the metal by light are electrons. The electron is an elementary particle discovered in 1897 by the English physicist J. J. Thomson. The absolute value (modulus) of the electron charge is usually denoted by the letter e and is equal to $1.6022 \cdot 10^{-19}$ C. This charge is called the **elementary charge**, because all charges of particles existing in nature are multiples of the charge e. The rest mass of an electron is equal to $m_\mathrm{e} = 9.10939 \cdot 10^{-31}$ kg.

The laws of the photoeffect were explained in 1905 by Einstein using the photonic hypothesis of the nature of light. According to Einstein, a photon hitting a metal can impart its energy $h\nu$ to a single electron. Part of this energy is consumed for the work A required to release the electron from the metal (**electron work function**), and the remaining part becomes the kinetic energy of the released electron. The speed of the released electron is equal to the maximum speed of photoelectrons v_max, and its kinetic energy is equal to $m_\mathrm{e}v_\mathrm{max}^2/2$. According to the law of conservation of energy, the photon energy must be equal to the sum of the work function A and the kinetic energy of the released electron:

$$h\nu = A + \frac{m_\mathrm{e}v_\mathrm{max}^2}{2}. \tag{3.2.1}$$

This is **Einstein's photoeffect equation**. Photoelectrons lose part of their energy interacting with the atoms of the metal. Therefore, they emerge from the metal with a speed that is less than or equal to the maximum speed v_{max}.

3.3. Compton effect

Another phenomenon in which the corpuscular (quantum) properties of light are particularly clearly manifested is the Compton effect. In 1922, the American physicist Arthur Compton, studying the scattering of short-wavelength X-rays in various substances, noticed that the wavelength of the scattered radiation is larger than the wavelength of the incident radiation. This increase in the wavelength of electromagnetic radiation during scattering is called the **Compton effect**.

Classical theory, which is based on the wave model of radiation, cannot explain the Compton effect. According to classical theory, the wavelength of electromagnetic waves should not change during scattering. Classical theory explains the scattering of electromagnetic waves as follows. Ions and electrons of the material, acted upon by the electric field of the electromagnetic wave, vibrate at a frequency equal to the wave frequency. An accelerating electrical charge (in this case, an ion or an electron) radiates electromagnetic waves. In this case, when the acceleration of the charge carrier's motion is a harmonic function of time, the charge carrier radiates secondary monochromatic waves of the same frequency. These are the scattered waves. Thus, classical theory asserts that the radiation frequency does not change during scattering.

From the standpoint of the photon theory, the event of electromagnetic radiation scattering is a collision of two particles—a photon and an electron, or a photon and an atom (by "collision" we will mean any brief interaction where only the states of the particles before and after the interaction are of interest). Here we will discuss only the interaction of a photon with a free electron (the interaction with an atom will be discussed in Section 3.6). The collision of a photon and a free electron is **elastic**, because during it the sum of the kinetic energies of the interacting particles remains unchanged (kinetic energy is only redistributed among the particles). A photon, whose energy is equal to $h\nu_0$, interacting with an electron, transfers a part of its energy to it. Due to this interaction, the electron acquires a certain velocity, and the photon changes its direction of motion (see Fig. 1). Since a part of the photon's energy is transferred to the electron, it is clear that the energy of the scattered photon is less than that of the incident photon. Since the photon energy is proportional to the frequency, as the photon energy decreases, the frequency of the radiation also decreases, and the wavelength increases.

Therefore, the Compton effect is a purely corpuscular phenomenon: it is described in the same way as an elastic collision between two spheres. This phenomenon shows that the increase in wavelength during Compton scattering can be expressed using the laws of conservation of energy and momentum. The only difference compared to the elastic collision of two spheres is that the photon energy must be calculated

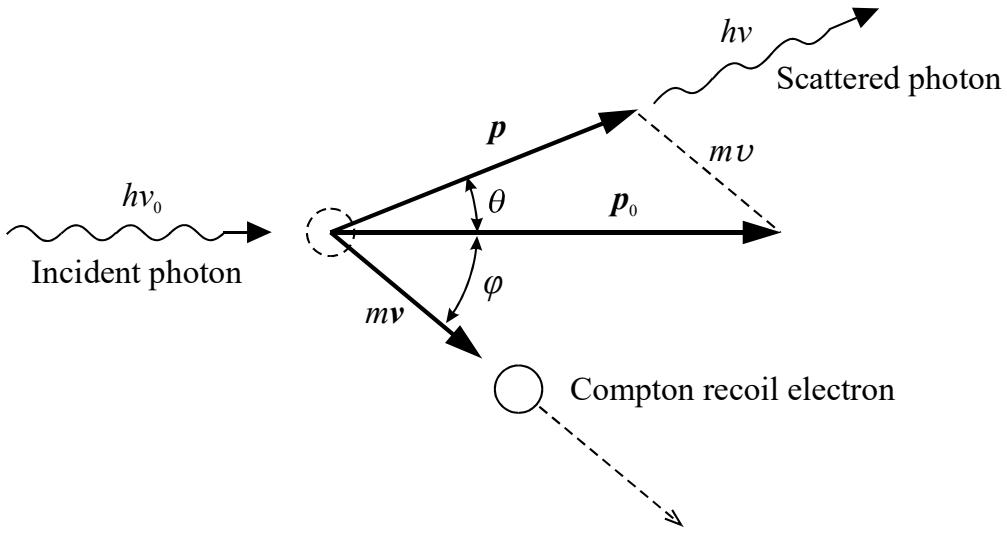


Fig. 1. Momentum conservation law when a stationary free electron scatters a photon: ν_0 and $h\nu_0$ – incident photon frequency and energy, ν and $h\nu$ – scattered photon frequency and energy, **v** and m**v** – electron velocity vector and momentum, $\mathbf{p}_0$ and **p** – photon momentum vectors before and after collision, θ – photon scattering angle, ϕ – electron recoil angle, h – Planck constant, m – electron mass.

according to Eq. (3.1.1), and the photon momentum according to Eq. (3.1.3). Since the electron can acquire a relativistic speed, we will use the relativistic expression for the electron kinetic energy $(m - m_e)c^2$ in the expression of the law of conservation of energy, where m_e is the rest mass of the electron and m is the relativistic mass of the electron:

$$m = \frac{m_e}{\sqrt{1 - (v/c)^2}}, \tag{3.3.1}$$

where v is the electron speed. This same expression for the mass m (3.3.1) must be used in the expression for the electron momentum $m\mathbf{v}$. The relativistic laws of conservation of energy and momentum, when a photon elastically collides with a stationary electron, have the following form:

$$h\nu_0 = h\nu + (m - m_e)c^2, \tag{3.3.2a}$$

$$\mathbf{p}_0 = \mathbf{p} + m\mathbf{v} \tag{3.3.2b}$$

(see Fig. 1). Here ν_0 and ν are the photon frequencies before and after the collision, $\mathbf{v}$ and m are the electron velocity vector and mass after the collision, $\mathbf{p}_0$ and $\mathbf{p}$ are the photon momentum vectors before and after the collision (the moduli of these vectors are $p_0 = h\nu_0/c$ and $p = h\nu/c$). In Eq. (3.3.2b), we move $\mathbf{p}$ to the left side and square both sides of this equation:

$$h\nu_0 = h\nu + (m - m_e)c^2, \tag{3.1.3a}$$

$$(mv)^2 = \left(\frac{h\nu_0}{c}\right)^2 + \left(\frac{h\nu}{c}\right)^2 - 2\frac{h\nu_0}{c}\frac{h\nu}{c}\cos\theta. \tag{3.1.3b}$$

Here θ is the angle between the vectors $\mathbf{p}$ and $\mathbf{p}_0$, i.e., the scattering angle (see Fig. 1). Substituting (3.3.1) into (3.3.3a,b), we have a system of two equations with respect to two unknowns v and ν. Having solved it and using the relationship between wavelength λ and frequency $\nu = c/\lambda$, we derive the following expression for the change in photon wavelength:

$$\lambda - \lambda_0 = c\left(\frac{1}{\nu} - \frac{1}{\nu_0}\right) = \frac{h}{m_e c}(1 - \cos\theta), \tag{3.3.4}$$

where λ_0 is the initial wavelength.

Thus,

$$\lambda - \lambda_0 = \lambda_C(1 - \cos\theta), \tag{3.3.5}$$

$$\lambda_C \equiv \frac{h}{m_e c} = 2.4263 \cdot 10^{-12}\ \text{m} = 2.4263\ \text{pm}. \tag{3.3.6}$$

Eq. (3.3.5) is called the **Compton formula**, and the quantity λ_C is called the **Compton wavelength** (more precisely – "the Compton wavelength of the electron", because the rest mass of the electron appears in the denominator of the expression (3.3.6)).

The Compton formula (3.3.5) is derived without any restrictions on the electron speed v. Therefore, this formula is valid for both small and relativistic speeds. Consequently, even if non-relativistic expressions for kinetic energy and momentum ($(m - m_e)c^2 \approx m_e v^2/2$ and $m_e\mathbf{v}$, respectively) are used instead of relativistic ones during derivation, the final result does not change.

A more detailed analysis of Compton scattering will be provided in Sections 3.6.1–3.6.4.

3.4. Concepts of interaction cross section and differential interaction cross section

The consequence of any possible interaction ("collision") between two particles will be called an "event". The probability of a specific event (e.g., radiative neutron capture or Compton scattering of a photon) is expressed using the concept of a cross section: each target particle (e.g., an electron, an atom, or an atomic nucleus) is represented by a flat disk perpendicular to the direction of the incident particles, and its area is chosen such that the probability of the event (e.g., capture of a neutron being simulated or Compton scattering) is equal to the probability that the incident particle will hit this disk. The area σ defined in this way is called the **interaction cross section** or simply the **cross section**. Thus, it is said that knowing the cross section σ, the probability of an event can be calculated using geometric probability calculation rules in the manner described below.

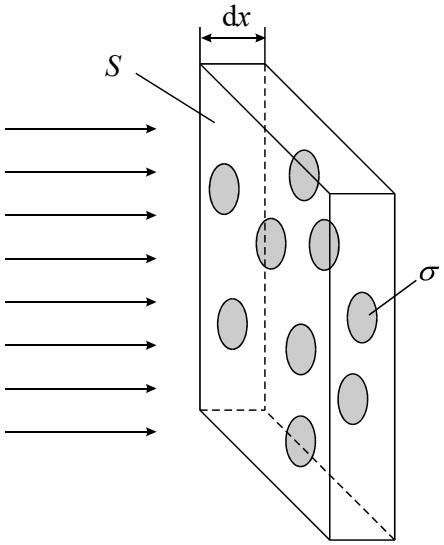


Fig. 2. Explanation of the interaction cross section σ.

If the concentration of target particles is n, then the area S and the vanishingly small thickness dx of a layer of substance contain $n \cdot S \cdot \mathrm{d}x$ target particles. The total "area" dS' of these particles, which covers a part of the area S, is equal to the sum of the cross sections, i.e., $\mathrm{d}S' = \sigma \cdot n \cdot S \cdot \mathrm{d}x$ (see Fig. 2). Since the positions of these target particles are random, the probability dP that an incident particle will "hit" a target particle located in a layer of thickness dx is equal to the ratio of the areas:

$$\mathrm{d}P = \frac{\mathrm{d}S'}{S} = \sigma n \mathrm{d}x. \tag{3.4.1}$$

This relation can also be considered as the definition of the interaction cross section σ: the interaction cross section σ is equal to the ratio of the interaction probability dP to the number of particles per unit area $n \cdot \mathrm{d}x$.

Each event is characterized by its own cross section. For example, the cross section for elastic scattering of a neutron in the general case differs from the cross section for radiative capture of the incident neutron. According to the addition rule for probabilities of mutually exclusive events, the sum of cross sections for all possible events determines the total interaction (collision) cross section of the particles:

$$\sigma = \sum_i \sigma_i, \tag{3.4.2}$$

where σ_i is the collision cross section of the i-th type.

The total (or specific interaction) cross section when several types of targets exist is calculated analogously. Then the interaction cross section is equal to

$$\sigma = \sum_i p_i \sigma_i, \tag{3.4.3}$$

where p_i is the relative abundance of target particles of the i-th type (i.e., the ratio of the concentration of target particles of that type to the total concentration of target particles), and σ_i is the cross section for the given type of interaction (or the total cross section for several interactions) when interacting precisely with target particles of that type.

Cross sections of nuclear reactions are usually expressed in barns (b). 1 b = 10^{-28} m^2.

From (3.4.1) it follows that the collision probability dP is proportional to the distance x covered by the particle. The average distance l traveled by a particle before the probability dP becomes equal to unity is called the particle's **mean free path** in the given material (the word "average" will often be omitted hereafter). The physical meaning of this quantity is the average distance traveled by a particle between two collisions. According to (3.4.1), the mean free path is equal to

$$l = \frac{1}{\sigma n}. \tag{3.4.4}$$

This expression for the free path can be obtained in a slightly more visual way. As a particle moves, it interacts only with those particles of the material that belong to a "cylinder" that encloses the particle's

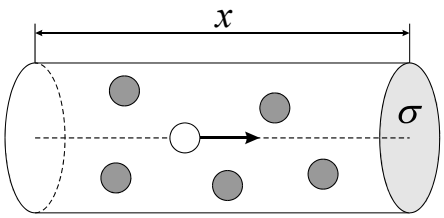


Fig. 3. Calculation of the mean free path.

trajectory and whose cross-sectional area is equal to the interaction cross section σ (see Fig. 3). The number of material particles N in this cylinder is equal to the product of its volume σx and the particle concentration n:

$$N = \sigma x n, \tag{3.4.5}$$

where x is the length of the particle's trajectory. It is clear that the average distance traveled by a particle between two collisions is equal to the ratio of the total distance x traveled to the number of collisions. Since the number of collisions is equal to the number of particles N in the "cylinder" mentioned above, the free path is equal to

$$l = \frac{x}{N} = \frac{x}{\sigma x n} = \frac{1}{\sigma n}. \tag{3.4.6}$$

It should be kept in mind that the term "free path" describes the path of free motion of a particle, i.e., the distance a particle covers between two interactions of *any* type. Therefore, strictly speaking, expression (3.4.6) has the meaning of a free path only when σ is the *total* interaction cross section. If the partial interaction cross section for one specific type of interaction is used in expression (3.4.6) instead of the total interaction cross section σ, then the meaning of the obtained value is the average path of the particle between two collisions of *that specific type*. If several interaction processes are possible, this path is not "free" in the literal sense of the word, because interactions of other types are also possible between two collisions of that type. However, for brevity, this path is sometimes also called the "free path" (with respect to the specific type of collision), although it is always greater than the true mean free path (if collisions of other types are possible). From (3.4.2) and (3.4.6) it follows that for the true mean free path l, the reciprocal is equal to the sum of the reciprocals of the "partial" free paths:

$$\frac{1}{l} = \sum_i \frac{1}{l_i}, \tag{3.4.7}$$

where l_i is the average path of the particle between two collisions of the i-th type.

The product of the event cross section σ and the target particle concentration n, σn, is called the **macroscopic cross section** (Σ) of the event. Thus, it can be stated that the macroscopic cross section is the total interaction cross section of the target particles contained in a unit volume of the target. According to (3.4.1), the macroscopic cross section describes the probability of an interaction event per unit path of an incident particle, and according to (3.4.4), the macroscopic cross section is equal to the reciprocal of the mean free path between two interactions of a given type:

$$\Sigma = \frac{\mathrm{d}P}{\mathrm{d}x} = \sigma n = \frac{1}{l}. \tag{3.4.8}$$

In certain cases, the macroscopic cross section is equal to a component of the radiation attenuation coefficient associated with a given type of interaction (such a case will be discussed in Section 3.6.7 when speaking about γ radiation attenuation in matter).

Usually, we are interested not in the interaction probability of a single incident particle with the target, but in the total number of interaction events per unit time in a given volume V. This quantity divided by the unit volume V is called the interaction probability per unit time ($\mathrm{d}P/\mathrm{d}t$) multiplied by the concentration of incident particles n_{kr} divided by the time $\mathrm{d}t$, over which the particle travels a distance $\mathrm{d}x$. Thus,

$$\frac{\mathrm{d}P}{\mathrm{d}t} = \sigma n v, \tag{3.4.9}$$

where v is the speed of the incident particle. The number of interaction events per unit time in a given volume V will be denoted by the letter R ("reaction rate"). This quantity is obtained by multiplying the number of

incident particles in the volume V by the interaction probability per unit time $\mathrm{d}P/\mathrm{d}t$. Assuming that the concentration of incident particles n_{kr} is constant, their number in the volume V is equal to $n_{\mathrm{kr}}V$. Therefore,

$$R = \sigma n v n_{\mathrm{kr}} V = \sigma N v n_{\mathrm{kr}} = \sigma N j = \Sigma j V, \tag{3.4.10}$$

where $N = nV$ is the total number of target particles in the volume V, and $j = vn_{\mathrm{kr}}$ is the flux density of the incident particles (the number of particles crossing a unit area per unit time).

Interaction (reaction) products (e.g., scattered neutrons or photons emitted during radiative capture) can be emitted in various directions. Often, the angular distribution of the reaction products (secondary particles) provides information about the properties or structure of the target matrix. To characterize this angular distribution, the concept of a differential interaction cross section is used. The differential interaction cross section is defined as follows. Suppose that the probability $\mathrm{d}P$, which is on the left side of equality (3.4.1), is the probability of a specific interaction event after which a secondary particle emerges into a vanishingly small solid angle $\mathrm{d}\Omega$ in a given direction specified by angles θ and ϕ (see Fig. 4). [The solid angle Ω is the ratio of the area of a sphere segment to the square of the sphere radius. Since the area of a sphere of radius r is $4\pi r^2$, the maximum possible value of Ω is 4π.] Since $\mathrm{d}\Omega$ is a vanishingly small quantity, the probability $\mathrm{d}P$ is also a vanishingly small quantity for a given direction, so the ratio $\mathrm{d}P/\mathrm{d}\Omega$ is finite. Thus, the ratio $\frac{1}{n \cdot dx}\frac{\mathrm{d}P}{\mathrm{d}\Omega}$ is called the **differential interaction cross section with respect to the solid angle** or the **angular interaction cross section**. We denote it by σ_Ω. Thus, the differential cross section is a partial cross section per unit solid angle in a given direction of secondary particle emission (possible values – from 0 to 4π). The differential cross section is expressed in barns per steradian (b/sr). As shown in Fig. 4, θ is the angle between the direction of motion of the primary particle and the direction of emission of the secondary particle (possible values – from 0 to π), and ϕ describes the projection of the last direction onto a plane perpendicular to the direction of incidence (possible values – from 0 to 2π). If we look at the direction of motion of the primary particle as the axis of a spherical coordinate system, then angles θ and ϕ are the coordinates of a point on the sphere surface in a polar coordinate system, where θ is the polar angle, and ϕ is the azimuthal angle. Angle θ is sometimes called the **scattering angle**. The total ("integral") cross section is equal to the integral of the differential cross section over all directions[1]:

$$\sigma = \int_{4\pi} \sigma_\Omega \mathrm{d}\Omega \equiv \int_0^{2\pi} \mathrm{d}\phi \int_0^{\pi} \sigma_\Omega \sin\theta \mathrm{d}\theta. \tag{3.4.11}$$

In the general case, σ_Ω depends on both angles θ and ϕ. However, when the incident radiation is not polarized (i.e., when all directions perpendicular to the direction of incidence are equivalent), σ_Ω does not depend on ϕ. Then Eq. (3.4.11) simplifies:

$$\sigma = 2\pi \int_0^{\pi} \sigma_\Omega \sin\theta \mathrm{d}\theta. \tag{3.4.12}$$

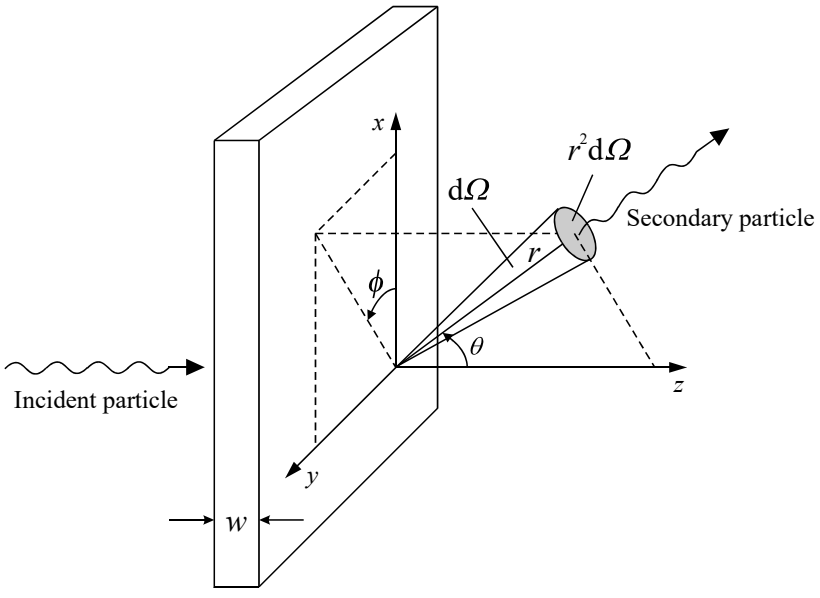


Fig. 4. Explanation of the calculation of the differential interaction cross section.

[1] According to the definition of a solid angle, a sphere plot element is $r^2\mathrm{d}\Omega$. In spherical coordinates, this plot element is expressed as follows: $r^2 \sin\theta \mathrm{d}\theta \mathrm{d}\phi$. Therefore $\mathrm{d}\Omega = \sin\theta \mathrm{d}\theta \mathrm{d}\phi$.

According to (3.4.1), the differential cross section can be measured as follows. A layer of target material of thickness w is illuminated by a parallel flux of particles Φ_0 (electrons, atoms, or atomic nuclei per unit time). The measured flux of secondary particles $\Delta\Phi$ into a given small solid angle $\Delta\Omega$ (these are secondary particles emitted in directions belonging to this solid angle per unit time). The ratio $\Delta\Phi/\Phi_0$ describes the probability ΔP that an incident particle will emit into the solid angle $\Delta\Omega$:

$$\Delta P = \Delta\Phi/\Phi_0. \tag{3.4.13}$$

On the other hand, according to (3.4.1) this probability is equal to

$$\Delta P = \Delta\sigma \cdot n \cdot w, \tag{3.4.14}$$

where $\Delta\sigma$ is the cross section for emission into the solid angle $\Delta\Omega$. Equating (3.4.14) and (3.4.13), we get:

$$\Delta\sigma = \frac{\Delta\Phi}{\Phi_0 nw}. \tag{3.4.15}$$

If $\Delta\Omega$ is sufficiently small, then the differential cross section in a given direction can be calculated approximately:

$$\sigma_\Omega \approx \Delta\sigma/\Delta\Omega. \tag{3.4.16}$$

When deriving a theoretical expression for the differential cross section, it is convenient to express it in terms of particle flux *density*. Flux density of particles is their flux per unit area (i.e., number of particles per unit time and unit area). Let j denote the *flux density* of secondary particles created due to interaction with a *single* target particle and propagating in a given direction specified by angles (θ, ϕ). Then the *flux* of secondary particles created due to interaction with *all* target particles and propagating into a vanishingly small solid angle $\mathrm{d}\Omega$ in the same direction is equal to

$$\mathrm{d}\Phi = Njr^2\mathrm{d}\Omega = S \cdot w \cdot n \cdot jr^2\mathrm{d}\Omega, \tag{3.4.17}$$

where r is the distance from the target scattering region to the observation point (assuming that this distance is much larger than the dimensions of the scattering region), $r^2\mathrm{d}\Omega$ is the area of a sphere surface element that fits into the solid angle $\mathrm{d}\Omega$, $N = S \cdot w \cdot n$ is the number of target particles, and S is the surface area of the ”illuminated” layer. The flux of incident particles is equal to

$$\Phi_0 = Sj_0, \tag{3.4.18}$$

where j_0 is the flux density of incident particles. Substituting the flux expressions into (3.4.15), changing to vanishingly small quantities, and taking into account (3.4.17) and (3.4.18), we get:

$$\sigma_\Omega = \frac{j}{j_0} r^2 \tag{3.4.19}$$

(since $j \sim 1/r^2$, the differential cross section does not depend on r).

3.5. Types of ionizing radiation

Ionizing radiation is a stream of subatomic particles (e.g., photons, electrons, positrons, nucleons, nuclei) whose interaction with matter causes atoms of the material to become ionized, meaning electrons are liberated from the atoms. To liberate an electron from an atom, a certain amount of work must be performed. This work is equal to the reduction in energy of the radiation particles or the secondary kinetic energy produced by the radiation effect. Therefore, ionization becomes possible only when the energy of the radiation particles or secondary particles is greater than a certain threshold value—the **ionization energy**, which is equal to the minimum binding energy of the atomic electrons. This energy is usually on the order of 10 eV (1 eV = $1.6022 \cdot 10^{-19}$ J).

Ionizing radiation can have various physical origins. **Directly ionizing radiation** consists of high-energy charged particles that ionize atoms of the material due to the Coulomb interaction with their electrons. These include, for example, electrons (beta radiation), ^{4}He nuclei (alpha radiation), and other nuclei. **Indirectly ionizing radiation** consists of neutral particles that do not directly ionize atoms or do so relatively rarely;

Table 1. Scale of electromagnetic waves

Spectral region	Approximate wavelength range	Approximate photon energy range
Radio waves	100000 km – 1 mm	$1 \cdot 10^{-14}$ eV – 0.001 eV
Infrared rays	1 mm – 0.75 μm	0.001 eV – 1.7 eV
Visible light	0.75 μm – 0.4 μm	1.7 eV – 3.1 eV
Ionizing electromagnetic radiation:		
Ultraviolet rays	0.4 μm – 10 nm	3.1 eV – 100 eV
X-rays	10 nm – 0.001 nm	100 eV – 1 MeV
Gamma (γ) rays	< 0.1 nm	> 10 keV

Table 2. Energy of particulate ionizing radiation

Type of radiation	Approximate particle energy range
Alpha (α) particles (^{4}He nuclei)	4 MeV – 9 MeV
Beta (β) particles (electrons and positrons)	10 keV – 10 MeV
Thermal neutrons	< 0.4 eV
Epithermal neutrons	0.4 eV – 200 keV
Fast neutrons	> 200 keV
Nuclear fragments and recoil nuclei	1 MeV – 100 MeV

however, by interacting with the medium, they can create high-energy free charged particles that easily ionize atoms directly. These include, for example, high-energy photons (ultraviolet, X-ray, and gamma radiation) and neutrons of any energy. The particle energies of various types of radiation are presented in the two tables below (Table 1 lists the lower-energy electromagnetic photon radiation types).

The characteristics of particle interaction with matter depend on the nature of the particles (more precisely, on their mass and electric charge). Therefore, it is most convenient to analyze the main interaction processes separately for these types of ionizing radiation:

1. heavy charged particles,
2. light charged particles,
3. photons (particles having no electric charge and whose rest mass is equal to zero),
4. neutrons (heavy particles having no electric charge).

3.6. Interaction of gamma radiation with matter

Like the interaction of charged particles (e.g., electrons, protons, α particles), the interaction of γ quanta with matter is of an electromagnetic nature. However, the physical mechanism of this interaction is different from that of charged particles, because:

1. γ quanta have no electric charge, so they do not participate in the Coulomb interaction. Compared to charged particles, γ quanta interact much less frequently with electrons and atomic nuclei. A γ quantum interacts with an electron in a very small region of space, whose dimensions are on the order of 10^{-13} m, i.e., three orders of magnitude smaller than interatomic distances. Therefore, the cross section for the interaction of a γ quantum with an atom or a free electron is much smaller than the cross section for the interaction of charged particles.

2. The rest mass of a γ quantum is equal to zero, so its speed is always equal to the speed of light. In a material medium, a γ quantum cannot be slowed down. It can only be absorbed or scattered. During each interaction event, the nature of the γ quantum changes fundamentally: it either ceases to exist, or the scattering event can significantly alter its direction of motion (in addition, the energy of the γ quantum changes during scattering). In comparison, charged particles lose energy continuously, moving relatively slowly, while a particle moving in a medium interacts simultaneously with many atoms located near its trajectory.

In matter, γ radiation is absorbed and scattered. The **absorption** of a photon (γ quantum) means that the photon disappears, and all its energy is transferred to the atoms of the material or turned into kinetic energy of secondary particles. The two primary physical mechanisms of γ quantum absorption are the photoelectric effect and electron-positron pair production (these will be discussed in sections 3.6.5 and 3.6.6). **Scattering** means that the photon changes its direction of motion (possibly transferring a part of its energy to the material atom or a free electron). If the sample is exposed to a parallel beam of radiation, then during measuring the beam passing through the sample along that same direction, scattering and absorption manifest themselves identically: due to both phenomena, the flux density of the radiation decreases. Therefore, the total effect of these two phenomena is measured by the total linear attenuation coefficient μ. The **attenuation coefficient** is the reciprocal of the material thickness over which the intensity of the transmitted radiation decreases by a factor of $e = 2.7183$. Thus, the attenuation coefficient determines the absorption and scattering. Therefore, in practice, the attenuation coefficient is often called the **attenuation coefficient**. However, these terms differ from one another, because the attenuation coefficient describes the total flux of photons (in all directions). Scattering is studied by measuring the intensity of the scattered radiation in directions that differ from the initial direction of radiation propagation.

3.6.1. Classical scattering and Compton scattering

As mentioned in section 3.3, classical electrodynamics states that the radiation frequency does not change during scattering. Scattering of electromagnetic radiation during which the wavelength does not change is called **coherent scattering** (as opposed to scattering where the wavelength changes, which is called **incoherent scattering**). If electromagnetic waves are scattered by free electrons, then such classical coherent scattering is called **Thomson scattering**, and if it is scattered by atomic electrons and the wavelength is much larger than atomic dimensions, then such classical coherent scattering is called **Rayleigh scattering**[2].

From the quantum mechanics standpoint, the scattering event is an interaction of two particles—a photon and an electron, or a photon and an atom. If a photon collides with a free electron, then such an interaction is elastic, because during it the kinetic energy sum of the particles does not change. The equations of energy and momentum conservation for this collision match the energy and momentum conservation expressions for an elastic collision (see Fig. 1 in section 3.3). From these conservation equations, it follows that due to electron recoil, the scattered photon loses a part of its energy to the kinetic energy of the recoiling electron. Because of this photon energy and frequency reduction (and corresponding wavelength increase), this scattering is un-coherent. This phenomenon, which in 1922 was described by the American physicist A. Compton, became one of the key milestones of quantum mechanics. Such scattering, which manifests the corpuscular (quantum) properties of electromagnetic radiation, is called **Compton scattering**, and the resulting reduction of frequency (or an increase of wavelength) is called the **Compton effect**. A photon typically transfers a large fraction of its energy to the electron. Those fast electrons resulting from Compton scattering are called **Compton recoil electrons**. They lose energy in the material due to ionization of atoms and due to bremsstrahlung.

When a photon interacts with a polyatomic molecule or solid, it can undergo incoherent Raman scattering, whereby the photon's energy either increases or decreases by transferring energy to or from the molecule's vibrational or rotational states. While a partial classical explanation exists, Raman scattering is fundamentally described by quantum mechanics. This process is disregarded in further discussion because its intensity is much lower than coherent scattering, it only occurs at low electron-volt photon energies, and it requires interaction with polyatomic systems rather than isolated atoms.

The Compton effect is the primary factor responsible for the energy transfer of hard X-rays and medium-energy gamma radiation (i.e., electromagnetic radiation with a quantum energy between 0.1 MeV and 1 MeV) to materials composed of light-element atoms (such as water and organic compounds). In practice, the Compton effect is applied when setting up protection against gamma radiation using low-density materials (concrete, bricks, iron, etc.), in which absorption is weak at the initial photon energy. This is because as the photon's energy decreases due to multiple collisions with electrons, its probability of absorption (the photoelectric effect) increases.

Photons can be scattered not only by free electrons but also by atoms (more precisely, by atomic electrons). If part of the photon's energy is converted into the atom's internal energy during such scattering, the

[2] If the wavelength is not much larger than the dimensions of the atom, the scattering properties depend on atomic structure, which requires quantum mechanics to describe. Therefore, classical electrodynamics formulas are not applicable in this case.

scattering is also called Compton scattering. Thus, Compton scattering resulting from a photon's interaction with an atom (rather than with a free electron) is inelastic. During Compton scattering, the atom can be either ionized or merely excited (without ionization). In either case, almost the entire decrease in the photon's energy is equal to the increase in the atom's internal energy (the kinetic energy of the atomic recoil is relatively small and can be neglected). If the atom is ionized, then (neglecting the recoil energy of the atom) the photon's energy loss consists of two parts: the kinetic energy of the Compton recoil electron and the binding energy of that electron in the atom (the **electron binding energy** is the work required to remove an electron from a given electron shell).

The role of the electron binding energy or the excitation energy of atoms during Compton scattering becomes important only when the photon energy is not much greater than the average excitation energy of the atom $\bar{I}$. However, then the probability of Compton scattering becomes much smaller than the probability of other interaction processes—the photoelectric effect and elastic scattering. Therefore, in practice, Compton scattering needs to be taken into account only when the photon energy is much greater than $\bar{I}$. In such a case, during Compton scattering, the atom is almost always ionized and the scattering occurs in almost the same way as scattering by a free electron. The average excitation energy of atoms is less than 1 keV for mid-weight elements. Therefore, when atomic electrons scatter photons whose energy is greater than 100 keV, the free electron approximation can be applied. Furthermore, since the probability of the photoelectric effect is small when the binding energy of the K-shell electrons is much smaller than the incident photon energy, it can be stated in this case that γ quanta, whose energy is less than 1 MeV, interact with matter only due to scattering.

If the photon energy is not much (at least 100 times) greater than the binding energy of the K-shell electrons, then in addition to Compton scattering, another type of scattering occurs—photon elastic scattering by atoms. During such scattering, the atom is neither ionized nor excited, and the photon energy remains practically unchanged (this follows from the laws of conservation of energy and momentum). Thus, such scattering is coherent. Such an event is most probable when a γ quantum is scattered by inner-shell electrons of heavy atoms, whose minimum excitation energy is relatively high. Coherent scattering manifests itself by the presence of an un-shifted wavelength component in the scattered γ radiation. Coherent scattering becomes the dominant scattering mechanism when the photon energy is less than 10 keV (the larger the atomic number of the element, the wider the energy interval over which coherent scattering dominates). For example, during the scattering of X-rays with a wavelength of 50−250 pm (5−25 keV photon energy) in crystals, coherent scattering occurs. It is precisely due to this that the diffraction of X-rays of such wavelengths in crystals is possible. Coherent scattering can be described by the methods of classical physics. As the γ quantum energy decreases or as the atomic number of the scattering material increases, the probability of coherent scattering increases. During the scattering of γ quanta of medium and high energy (> 500 keV) in materials of low atomic number (e.g., in aluminum), coherent scattering practically does not manifest itself, and it can be considered that Compton scattering is the only scattering process.

The other limiting case where the classical description applies is the scattering of visible light or lower frequency electromagnetic radiation by free electrons. As proven in Section 3.3, the increase in the radiation wavelength caused by the Compton effect does not depend on the radiation frequency and is less than 5 pm. Therefore, when the radiation wavelength exceeds 100 nm, the *relative* increase in wavelength caused by the Compton effect becomes almost unnoticeable, so the scattering can be considered coherent (Thomson) scattering.

The regularities and definitions formulated above are summarized in Table 3. In this table, $h\nu_0$ is the primary photon energy, and $m_e c^2 = 511$ keV is the rest energy of the electron (m_e is the electron rest mass, and c is the speed of light).

Table 3. Types of electromagnetic radiation scattering

	Classical physics		Quantum physics		
	Name	**Coher.**	**Name**	**Coher.**	**Limiting cases**
Scattering by free electrons[3]	Thomson scattering	Yes	Compton scattering	No	When $h\nu_0 \ll m_e c^2$, Compton scattering by free electrons can be treated as Thomson scattering (i.e., described by classical physics methods).
Inelastic scattering by atoms	—	—	Compton scattering	No	When $h\nu_0 > m_e c^2$, scattering by atoms can be described in the same way as scattering by free electrons; the atom is ionized during the interaction. In this case, Compton scattering is the dominant scattering process. When $h\nu_0$ becomes less than the binding energy of the valence electrons, ionization becomes impossible and inelastic scattering by atoms is accompanied by excitation. Furthermore, in this case, inelastic scattering occurs much less frequently than coherent scattering. When $h\nu_0$ is less than the lowest excitation energy, inelastic scattering becomes impossible. Then only coherent scattering occurs.
Elastic scattering by atoms	Rayleigh scattering	Yes	Coherent scattering	Yes	When $h\nu_0 > 500$ keV, coherent scattering occurs much less frequently than Compton scattering. When $h\nu_0 < 10$ keV, coherent scattering is the dominant scattering process.

3.6.2. Relations between photon energy, electron energy and scattering angle

Further in the analysis of Compton scattering, we will rely on the assumption that photons are scattered by free electrons (not by atoms), because, as mentioned in Section 3.6.1, the electron binding energy in the atom does not usually have a major influence on Compton scattering. As shown in Fig. 1 (Section 3.3), due to Compton scattering, instead of the primary photon with energy $h\nu_0$, a scattered photon appears with energy $h\nu < h\nu_0$, while the electron that scattered the photon acquires a kinetic energy $E_C = h\nu_0 - h\nu$.

Using the laws of conservation of energy and momentum, it is possible to obtain a relation between the scattered photon energy $h\nu$, the incident photon energy $h\nu_0$, and the photon scattering angle θ, as well as a relation between the Compton recoil electron energy E_C and its emission angle ϕ (angles θ and ϕ are measured from the initial direction of photon motion as shown in Fig. 1, Section 3.3):

$$\begin{cases} h\nu = \dfrac{h\nu_0}{1 + (1 - \cos\theta)\gamma}, \\ E_C = \dfrac{2h\nu_0\gamma}{1 + 2\gamma + (1+\gamma)^2 \operatorname{tg}^2\phi} = h\nu_0 \dfrac{\gamma(1 - \cos\theta)}{1 + \gamma(1 - \cos\theta)}, \\ \operatorname{tg}\left(\dfrac{\theta}{2}\right) = \dfrac{\operatorname{ctg}\phi}{1+\gamma}, \quad \text{where } \gamma \equiv \dfrac{h\nu_0}{m_e c^2}. \end{cases} \tag{3.6.1}$$

Since the radiation wavelength λ and frequency ν are related by the expression $\nu = c/\lambda$, the first equation of system (3.6.1) can be written as follows:

$$\lambda - \lambda_0 = \lambda_C(1 - \cos\theta), \tag{3.6.2}$$

where $\lambda - \lambda_0$ is the increase in the photon wavelength due to Compton scattering, θ is the scattering angle, and λ_C is the electron **Compton wavelength**: $\lambda_C = h/(m_e c) = 2.4263$ pm. Eq. (3.6.2) is called the **Compton formula** (it was derived in Section 3.3).

[3] Photon scattering due to interaction with a free electron is always elastic, because during it the sum of the kinetic energies of the electron and the photon does not change.

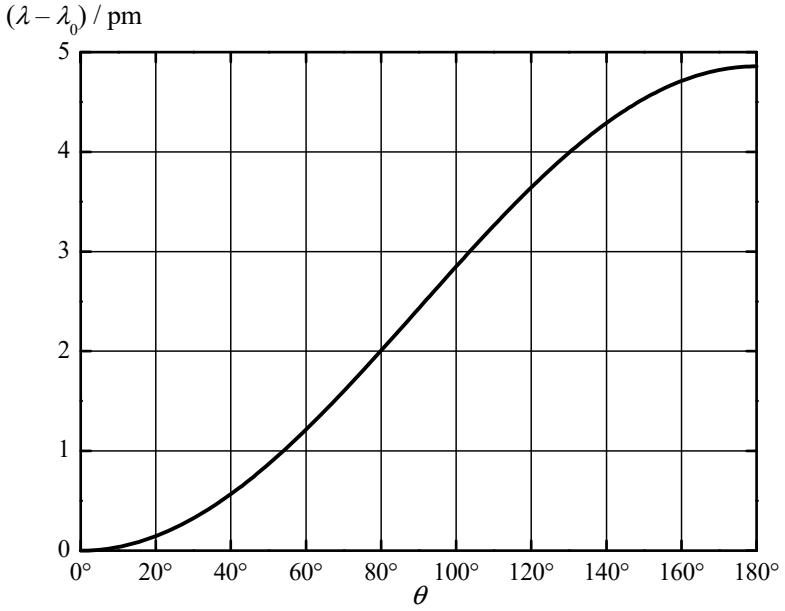


Fig. 5. Dependence of the wavelength change due to the Compton effect on the scattering angle.

From the Compton formula (3.6.2) it follows that the Compton effect strengthens with an increasing scattering angle θ (see Fig. 5). In other words, as the scattering angle increases, the energy transferred by the photon to the electron (recoil energy) increases. The maximum possible increase in wavelength corresponds to scattering at an angle $\theta = \pi$ (when the photon's direction of motion changes to the opposite direction): then $\lambda - \lambda_0 = 2\lambda_C = 4.8526$ pm. Perpendicular to the initial direction ($\theta = \pi/2$), $\lambda - \lambda_0$ is equal to λ_C.

From the second equation of system (3.6.1), it follows that the Compton recoil electron energy is at its maximum when $\phi = 0$ (i.e., when $\theta = \pi$), and this maximum energy is equal to:

$$E_{C\,max} = \frac{h\nu_0}{1 + \dfrac{m_e c^2}{2h\nu_0}}. \tag{3.6.3}$$

When the photon energy is greater than 1 MeV, it can be stated that:

$$E_{C\,max} \approx h\nu_0 - \frac{m_e c^2}{2} \approx h\nu_0 - 0.25\ \text{MeV}, \tag{3.6.4}$$

and the average recoil electron energy is approximately equal to half of the incident photon energy.

The energy spectrum of Compton recoil electrons is continuous: a photon can transfer any fraction of its energy to the electron—from zero to the maximum energy specified by Eq. (3.6.3).

The expressions and numerical values of the scattering cross section for the classical case and the Compton scattering case are given in Sections 3.6.3 and 3.6.4 (the concept of cross section is defined in Section 3.4).

3.6.3. Classical expressions for Rayleigh and Thomson scattering cross sections

The general expression for the differential interaction cross section is (3.4.19). In analyzing photon scattering, j is the flux density of scattered photons, and j_0 is the flux density of incident photons. Since the concept of a "photon" is not used in classical physics, to apply the relation (3.4.19) when calculating the classical scattering cross section, the quantities j and j_0 must be replaced by the corresponding energy fluxes I and I_0 (energy flux density is the amount of energy transported per unit time through a unit surface area perpendicular to the direction of propagation):

$$\sigma_\Omega = \frac{I}{I_0} r^2. \tag{3.6.5}$$

We will refer to the energy flux density of the radiation simply as the radiation **intensity**. Thus, I is the intensity of the radiation scattered by a single electron at a distance r in a given direction, and I_0 is the

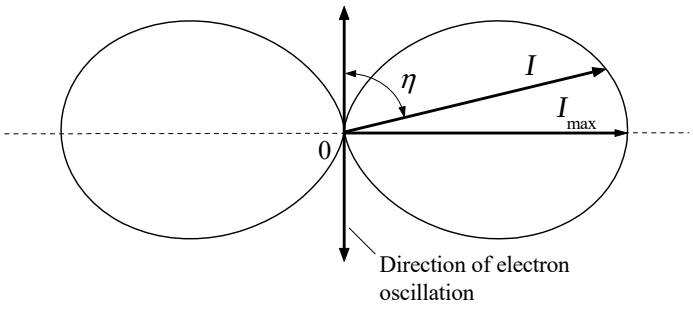


Fig. 6. Angular distribution of the radiation intensity (I) of an electron vibrating according to a harmonic law: polar coordinates (η, I) represent a plot where the length of the vector from the origin describes the intensity in the given direction. The spatial dependence is obtained by rotating the curve around the vibration direction of the electron. The maximum intensity $I_{\max}$ is expressed by Eq. (3.4.9).

intensity of the incident radiation. In classical electrodynamics, it is proven that the intensity of a plane electromagnetic wave is equal to:

$$I_0 = \frac{1}{2} c \varepsilon_0 \mathscr{E}_0^2, \tag{3.6.6}$$

where $\mathscr{E}_0$ is the amplitude of the wave's electric field strength vector $\mathscr{E}$ (the letter "E" has been used so far to denote energy, but here the electric field strength is denoted by a different font), c is the speed of light, and ε_0 is the electric constant. Substituting expression (3.6.6) into (3.6.5), we obtain:

$$\sigma_\Omega = \frac{2I}{c \varepsilon_0 \mathscr{E}_0^2} r^2. \tag{3.6.7}$$

If the incident radiation is linearly polarized (i.e., the direction of its electric field vector remains parallel to a single straight line at all times), then according to the classical view, a single electron undergoing scattering exhibits a vibration intensity dependence on the scattering direction that is exactly the same as the angular dependence of the radiation intensity of a charge carrier moving harmonically along a straight line:

$$I = I_{\max} \sin^2 \eta. \tag{3.6.8}$$

Here η is the angle between the direction of the electron's vibration and the direction of observation (see Fig. 6), and the factor $I_{\max}$ is expressed by the formula:

$$I_{\max} = \frac{e^2 \omega^4 x_{\max}^2}{32 \pi^2 \varepsilon_0 c^3 r^2}, \tag{3.6.9}$$

where e is the electron charge, ω is the angular frequency of the radiation (and of the electron's vibration), $x_{\max}$ is the amplitude of the electron's forced vibration, and r is the distance from the scattering point to the observation point.

From Eq. (3.6.8) it follows that during linearly polarized radiation scattering, the angular distribution of the scattered radiation intensity is symmetric with respect to the polarization direction (see Fig. 6). When the scattered radiation is natural (unpolarized) light, during scattering, the direction of the electron's vibrations is perpendicular to the direction of radiation propagation, but otherwise completely random. This direction can be described by an angle ψ (see Fig. 7). Therefore, the angle θ measured with respect to a given direction must be expressed as an average value of expression (3.6.8) over all possible directions of the polarization vector. We will consider all values of the angle ψ from 0 to π to be equally probable. The average radiation intensity into a given angle θ must be defined as the average value of expression (3.6.8) with respect to the angle ψ. After calculating the integral of expression (3.6.8) from 0 to π with respect to the angle ψ and dividing it by π, we find that for any angle ψ, the integral over the interval from 0 to π with respect to the angle ψ requires an exact geometric relation (as shown in Fig. 7), yielding $\cos \eta = \sin \theta \cdot \cos \psi$. Therefore:

$$\begin{aligned} I &= \frac{I_{\max}}{\pi} \int_0^\pi \sin^2 \eta \, \mathrm{d}\psi = \frac{I_{\max}}{\pi} \int_0^\pi (1 - \cos^2 \eta) \, \mathrm{d}\psi \\ &= \frac{I_{\max}}{\pi} \int_0^\pi (1 - \sin^2 \theta \cdot \cos^2 \psi) \, \mathrm{d}\psi = \frac{1}{2} I_{\max} (1 + \cos^2 \theta), \end{aligned} \tag{3.6.10}$$

where $I_{\pi/2} = I_{\max}/2$ is the scattered radiation intensity in the direction $\theta = \pi/2$ (this direction is perpendicular to the initial radiation direction). Thus, for unpolarized radiation, the angular distribution of the scattered radiation intensity is rotationally symmetric with respect to the direction of incident radiation (see Fig. 8). This statement holds true not only for coherent scattering but also for Compton scattering. However,

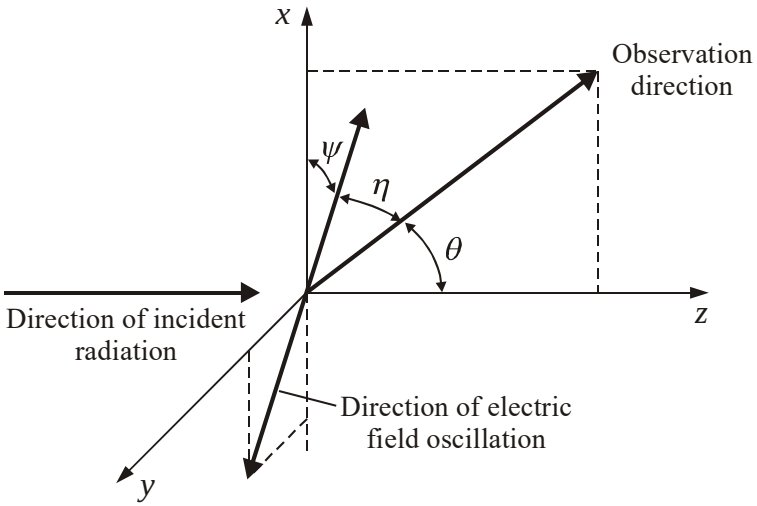


Fig. 7. Relations between angles θ, ψ, and η.

according to the classical model, the angular distribution has additional mirror symmetry with respect to the plane $\theta = \pi/2$ (see Fig. 8), resulting in equality of scattering intensity for opposite directions, which does not hold true for Compton scattering, as it will be shown in the next section.

Substituting the expression for $I_{\max}$ (3.6.9) into (3.6.10) and using Eq. (3.6.7), we obtain the classical expression for the differential scattering cross section:

$$\sigma_\Omega = \frac{e^2\omega^4 x_{\max}^2}{32\pi^2\varepsilon_0^2 c^4 \mathscr{E}_0^2}(1 + \cos^2\theta). \tag{3.6.11}$$

The final expression for this quantity is determined by the dependence of the vibration amplitude $x_{\max}$ on the frequency ω and the field strength amplitude $\mathscr{E}_0$.

First, let us assume that electromagnetic waves are scattered by atomic electrons (Rayleigh scattering). According to the classical model of electron motion in an atom, a forced vibration is induced under the influence of an external harmonic electric field—meaning that the motion is described as a one-dimensional harmonic oscillator. The equation of motion is as follows:

$$m\frac{\mathrm{d}^2x}{\mathrm{d}t^2} + a\frac{\mathrm{d}x}{\mathrm{d}t} + kx = -e\mathscr{E}(t), \tag{3.6.12}$$

where m is the electron mass, x is the displacement of the atomic electron from its equilibrium position, e is the modulus of the electron charge, and $\mathscr{E}$ is the electric field strength of the electromagnetic wave:

$$\mathscr{E}(t) = \mathscr{E}_0 \cos(\omega t), \tag{3.6.13}$$

a is the damping coefficient, which characterizes the spontaneous decrease of the vibration amplitude over time due to energy loss via radiation (or other mechanisms), and the constant k characterizes the restoring force $-kx$, which tends to return the electron to its equilibrium position. The coefficient k plays the same role as the spring stiffness coefficient, and the coefficient a acts as a friction coefficient (i.e., a force $-a \cdot (\mathrm{d}x/\mathrm{d}t)$ acting on a body moving with speed $\mathrm{d}x/\mathrm{d}t$). In Eq. (3.6.12), the right-hand side represents the force acting on the electron due to the electric field. When this field strength has the steady-state time dependence given

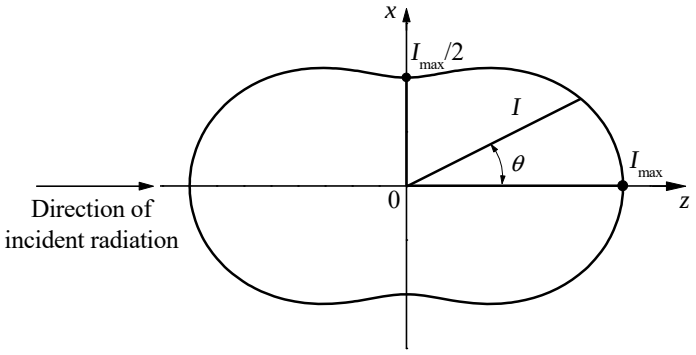


Fig. 8. Angular distribution of the intensity (I) of scattered unpolarized radiation: polar coordinates (θ, I) represent a plot where the length of the vector from the origin describes the intensity in the given direction. The spatial dependence is obtained by rotating the curve around the initial direction of radiation propagation.

by expression (3.6.13), the solution to the differential equation (3.6.12) is:

$$x(t) = \frac{e\mathscr{E}_0/m}{\sqrt{(\omega_0^2 - \omega^2)^2 + 4\beta^2\omega^2}} \cos(\omega t - \delta). \tag{3.6.14}$$

Here ω_0 is the natural angular frequency of the electron:

$$\omega_0 = \sqrt{\frac{k}{m}}, \tag{3.6.15}$$

while the constants β and δ are defined by the relations $\beta = \frac{a}{2m}$ and $\operatorname{tg}\delta = \frac{2\beta\omega}{\omega_0^2 - \omega^2}$. The factor multiplying the cosine in expression (3.6.14) is the forced vibration amplitude $x_{\max}$:

$$x_{\max} = \frac{e\mathscr{E}_0/m}{\sqrt{(\omega_0^2 - \omega^2)^2 + 4\beta^2\omega^2}}. \tag{3.6.16}$$

If the radiation angular frequency ω is much smaller than the electron's natural vibration angular frequency ω_0 (ω_0 is on the order of 10^{16}–10^{18} s^{-1}, and the radiation damping is sufficiently weak, meaning $\beta^2 \ll \omega_0^4/(4\omega^2)$), then from (3.6.16) it follows that the forced vibration amplitude $x_{\max}$ becomes almost independent of the radiation frequency and is approximately equal to:

$$x_{\max} \approx \frac{e\mathscr{E}_0}{m\omega_0^2}. \tag{3.6.17}$$

Therefore, as is evident from Eq. (3.6.11), the scattering cross section (and intensity of the scattered radiation) is proportional to the fourth power of the radiation frequency ω. This is why short-wavelength radiation scatters much more strongly. It is because of this frequency dependence that the sky appears blue: when unpolarized sunlight scatters in the atmosphere, the shorter-wavelength blue component dominates the scattered light.

Now let us assume that the electromagnetic waves are scattered by free electrons (Thomson scattering). In this case, there is no restoring force in the equation of motion, because the electron is not bound to a nucleus. If the electron's vibration damping is weak, the second term can also be neglected. We then obtain the following equation of motion for free electrons:

$$m\frac{\mathrm{d}^2x}{\mathrm{d}t^2} = -e\mathscr{E}(t). \tag{3.6.18}$$

From (3.6.18) it follows that in this case, when $\mathscr{E}$ has the form of expression (3.6.13):

$$x = x_{\max}\cos(\omega t), \tag{3.6.19}$$

where

$$x_{\max} = \frac{e\mathscr{E}_0}{m\omega^2}. \tag{3.6.20}$$

Thus, in this case, the electron's vibration amplitude is inversely proportional to the square of the radiation frequency. Substituting (3.6.20) into the differential scattering cross-section expression (3.6.11), we obtain the Thomson scattering differential cross section:

$$\sigma_{\Omega\mathrm{T}} = \frac{e^4}{32\pi^2\varepsilon_0^2c^4m^2}(1 + \cos^2\theta) \approx 4.0 \cdot 10^{-30}(1 + \cos^2\theta)\ [\mathrm{m}^2]. \tag{3.6.21}$$

We see that the Thomson scattering cross section does not depend on the radiation frequency.

The total Thomson scattering cross section is obtained by integrating expression (3.6.21) over the solid angle according to Eq. (3.4.12):

$$\sigma_{\mathrm{T}} = \frac{e^4}{6\pi\varepsilon_0^2c^4m^2} \approx 6.6 \cdot 10^{-29}\ \mathrm{m}^2. \tag{3.6.22}$$

Knowing the scattering cross section and assuming that scattering is the main interaction process with the material, the photon mean free path can be calculated in the given material using Eq. (3.4.4). For example, in water or biological tissues, the average electron concentration is $n \approx 3 \cdot 10^{29}$ m^{-3}. Substituting this value along with the scattering cross section (3.6.22) into the mean free path expression (3.4.4), we find that the "classical" mean free path in such a medium is $l \approx 5$ cm, i.e., a photon covers an average of 5 cm between collisions with electrons.

3.6.4. Compton scattering cross section

The cross section for Compton scattering depends on the photon energy, and the angular distribution of the scattered radiation intensity is not symmetric with respect to the $\theta = \pi/2$ plane (at small scattering angles, the probability is greater than at large scattering angles). In this respect, Compton scattering differs from classical scattering (see Section 3.6.3). According to the quantum theory of Compton scattering, which was developed in 1928 by Swedish physicist O. Klein and Japanese physicist Y. Nishina, the dependence of the differential scattering cross section on the scattering angle θ and the photon energy is described by the formula:

$$\sigma_{\Omega} = \frac{e^4}{32\pi^2\varepsilon_0^2 c^4 m_e^2} \frac{1+\cos^2\theta}{[1+\gamma(1-\cos\theta)]^2} \left\{ 1 + \frac{\gamma^2(1-\cos\theta)^2}{(1+\cos^2\theta)[1+\gamma(1-\cos\theta)]} \right\}, \tag{3.6.23}$$

where γ is the ratio of the initial photon energy $h\nu_0$ to the rest energy of the electron $m_e c^2 = 511$ keV[4]:

$$\gamma = \frac{h\nu_0}{m_e c^2}. \tag{3.6.24}$$

When $\gamma \ll 1$, the differential cross section for Compton scattering (3.6.23) coincides with the differential cross section for Thomson scattering (3.6.21). The angular distribution of the scattered radiation intensity for several values of γ is shown in Fig. 9. As the photon energy increases, the angular distribution of the scattered radiation intensity narrows and becomes increasingly stretched in the forward direction of the radiation propagation, while the total cross section decreases. The total cross section for Compton scattering by free electrons σ_C is obtained by integrating expression (3.6.23) over the solid angle according to Eq. (3.4.12):

$$\sigma_C = \frac{3}{4}\sigma_T \left\{ \frac{1+\gamma}{\gamma^2} \left[\frac{2(1+\gamma)}{1+2\gamma} - \frac{1}{\gamma}\ln(1+2\gamma) \right] + \frac{1}{2\gamma}\ln(1+2\gamma) - \frac{1+3\gamma}{(1+2\gamma)^2} \right\}, \tag{3.6.25}$$

where σ_T is the total Thomson scattering cross section (3.6.22). As the parameter γ decreases (i.e., as the initial photon energy $h\nu_0$ decreases), σ_C increases, approaching σ_T (see Fig. 10).

Limiting cases:

1. When $\gamma \ll 1$, $\sigma_C \approx \sigma_T(1-2\gamma)$. That is, as the photon energy decreases far below 0.5 MeV, the Compton scattering cross section decreases almost linearly with increasing photon energy.

2. When $\gamma \gg 1$, $\sigma_C \approx \frac{3}{8}\sigma_T \frac{1}{\gamma}\left(\frac{1}{2} + \ln 2\gamma\right)$. Consequently, when the photon energy is much greater than 0.5 MeV, the Compton scattering cross section is approximately inversely proportional to the photon energy.

Eq. (3.6.23) was derived using relativistic quantum mechanics methods and taking into account the interaction of the electron spin and its magnetic moment with the electromagnetic field (i.e., with γ quanta). The value calculated according to Eq. (3.6.25) represents the total cross section $\sigma \approx 2.5 \cdot 10^{-29}$ m^2, which is 2.6 times smaller than the total Thomson scattering cross section σ_T (3.6.22). Accordingly, the mean free path of such photons in a material medium is 2.6 times larger than that calculated by classical theory. For example, in water or biological tissue, it is equal to $l \approx 13$ cm, i.e., a 0.66 MeV energy photon covers an average distance of 13 cm between collisions with electrons in such a medium.

Up to this point, the scattering cross section has been defined for a single electron. However, in practice, the scattering cross section is usually defined for a single atom. Since, under standard conditions, the Compton effect involves the interaction of a photon with individual atomic electrons, the atomic cross section for Compton scattering (σ_A) is equal to the product of the electron scattering cross section (σ) and the atomic number of the element (Z):

$$\sigma_C = Z\sigma. \tag{3.6.26}$$

Thus, the atomic cross section for Compton scattering is directly proportional to the number of electrons in the atom. The calculation of σ_C dependency on energy is complex. As can be seen from Fig. 14a–16a,

[4] Sometimes, the "Compton scattering cross section" refers to the quantity $(\nu/\nu_0)\sigma_{\Omega}$, while the quantity $[1-(\nu/\nu_0)]\sigma_{\Omega}$ is called the "Compton absorption cross section" (here ν is the scattered photon frequency, and ν_0 is the incident photon frequency). In this text, these specific terms are not used.

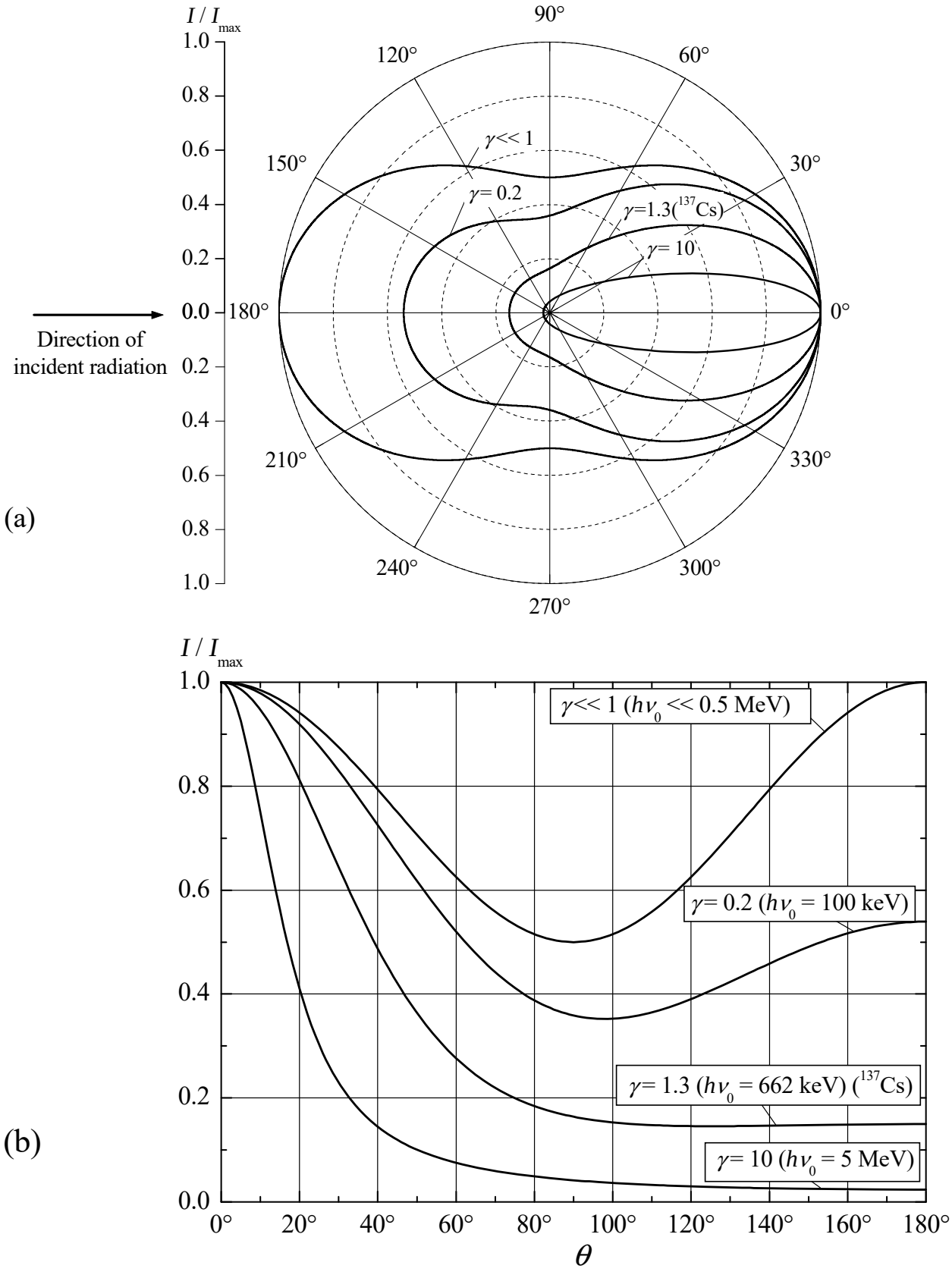


Fig. 9. Dependence of the relative intensity of Compton scattering (or relative differential cross section) on the scattering angle for several values of the initial photon energy, in polar (a) and rectangular (b) coordinates. The dependence calculated according to Eq. (3.6.23). γ is the ratio of the photon energy to the rest energy of the electron (511 keV). γ = 1.3 corresponds to the energy of photons emitted by the isotope ^{137}Cs (662 keV).

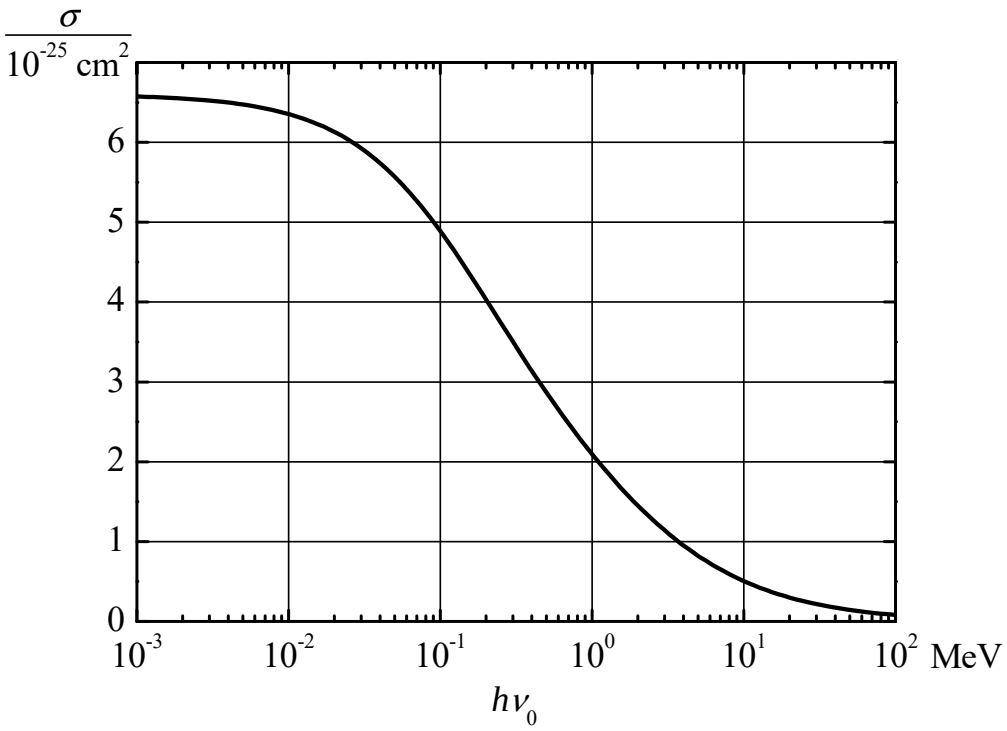


Fig. 10. Dependence of the Compton scattering cross section on the initial photon energy, calculated according to Eq. (3.6.25).

when the photon energy is low (much smaller than the electron rest energy $m_e c^2$), σ_C increases with energy, approaching a maximum value, and then decreases as the photon energy continues to increase toward the region of high energies, where σ_C decreases toward zero, as predicted by Eq. (3.6.25) (the decrease of the scattering cross section as energy approaches zero contradicts Eq. (3.6.25), which predics an *increase* up to the Thomson scattering cross section (3.6.22), and is related to the fact that for bound atomic electrons Eq. (3.6.25) becomes increasingly inaccurate when energy decreases below ~100 keV).

3.6.5. Photoelectric effect

The photoelectric effect or **photoelectric absorption** is an interaction of a photon with an atom whereby the atom absorbs the entire energy of the photon (i.e., the photon ceases to exist), and one of the atomic electrons is ejected out of the atom. The electron ejected from the atom is called a **photoelectron**. This phenomenon is sometimes called the **internal photoelectric effect** or **atomic photoelectric effect** to emphasize that the photoelectron usually remains inside the material (the "external" photoelectric effect was described in Section 3.2). Thus, the primary difference between the atomic photoelectric effect and Compton scattering is that during Compton scattering, the photon loses only a fraction of its energy, whereas during the photoelectric effect, the photon is completely absorbed[5]. From the law of conservation of energy, the kinetic energy of the photoelectron is expressed as:

$$E_{ph} = h\nu - \varepsilon_b, \tag{3.6.27}$$

where ε_b is the binding energy of the corresponding electron shell.

Based on the laws of conservation of energy and momentum (3.3.2a,b), it can be proven that free electrons cannot absorb a photon, meaning they cannot undergo the photoelectric effect. To verify this, it is sufficient to eliminate the first terms on the right-hand sides of Eqs. (3.3.2a,b) (which corresponds to the assumption of complete photon absorption). The resulting system of two equations (with unknowns v and $v \equiv |\mathbf{v}|$) has no solution.

According to Eq. (3.6.27), the photoelectric effect is possible only when $h\nu > \varepsilon_b$. Therefore, the dependence of the photoelectric effect cross section on the photon energy is characterized by sharp jumps (**absorption edges**), which correspond to the binding energies of the individual electron shells (K, L, …)

[5] Sometimes, all processes where a photon releases an electron from an atom (including ionization via Compton scattering) are called the "atomic photoelectric effect". However, here this term is used in its conventional (narrower) sense.

(see Fig. 14a–16a). The last (highest energy) jump corresponds to the liberation of an electron from the innermost (K) electron shell. Such processes constitute roughly 80% of all photoelectric effect events if the photon energy $h\nu$ is greater than the binding energy of the K-shell electrons. When $h\nu$ is on the order of the electron rest energy $m_e c^2$ (i.e., when $h\nu$ is on the order of several hundred keV), the cross section of the photoelectric effect from the K shell (m^2) is approximately equal to:

$$(\sigma_{ph})_K \approx 10^{-37} Z^5 / (h\nu)^{7/2}, \tag{3.6.28}$$

where the photon energy $h\nu$ is expressed in MeV. As can be seen, the photoelectric effect cross section decreases very rapidly with increasing photon energy and with decreasing nuclear charge. When $h\nu \gg m_e c^2$, the photoelectric effect cross section is inversely proportional to the photon energy (i.e., the cross section decreases more slowly with increasing photon energy), but it remains proportional to Z^5. Therefore, for heavy elements (e.g., lead), the photoelectric effect manifests itself even when the photon energy is around 5 MeV.

The rapid decrease of the photoelectric effect cross section with increasing photon energy can be explained as follows. As the difference between the photon energy and the electron binding energy grows, the fraction of the photon energy that is converted into the kinetic energy of the electron E_{ph} during the photoelectric effect increases, while the fraction spent on breaking the electron's bond with the atom decreases (see 3.6.27). That is, as the photon energy increases, the atomic electron becomes increasingly similar to a free electron from the photon's perspective. However, as mentioned, a free electron cannot absorb a photon. Therefore, the photoelectric effect cross section decreases and becomes much smaller in the high-energy region than the Compton scattering cross section, which decreases much more slowly with increasing photon energy (see Fig. 14a–16a). Analogously, one can explain the increase in the photoelectric effect cross section as Z increases: as the nuclear charge increases, the electron binding energy in the atom grows, thereby decreasing the difference between the photon energy and the electron binding energy. The mathematical form of the dependence of the photoelectric effect and Compton scattering cross sections on the photon energy can only be explained using the methods of quantum electrodynamics. Thus, a simple explanation does not exist.

During the photoelectric effect, the vacancy created in the inner electron shell is filled by an electron from a higher electron shell. During this quantum transition, the released energy is emitted either in the form of characteristic X-ray radiation or is spent on liberating another electron from the same atom (**Auger effect**). The vast majority of those characteristic X-ray photons and secondary electrons are absorbed in the material where the photoelectric effect occurs.

3.6.6. Electron and positron pair production

In the electric field of a nucleus or an electron, a photon can cease to exist, giving rise to an electron and positron pair. Writing the law of conservation of energy for such a process occurring in the electric field of a nucleus, we must take into account the recoil energy of the nucleus E_r:

$$h\nu = m_+ c^2 + m_- c^2 + E_r, \tag{3.6.29}$$

where $m_+ c^2$ and $m_- c^2$ are the total relativistic energies of the positron and electron, and m_+ and m_- are the relativistic masses of the positron and electron. Since m_+ and m_- cannot be smaller than the electron rest mass m_e, and E_r cannot be negative, such a process is possible only when the photon energy $h\nu$ is greater than the sum of the rest energies of the electron and positron, $2m_e c^2 \approx 1.02$ MeV.

Let us verify that an electron-positron pair cannot be created in a vacuum. If a pair were created in a vacuum, the recoil energy would be zero ($E_r = 0$), so the energy conservation law would take the form: $h\nu = m_+ c^2 + m_- c^2$. If the positron and electron move in the same direction that the photon was moving, the momentum conservation law would yield:

$$h\nu / c = p_+ + p_- = m_+ v_+ + m_- v_-, \tag{3.6.30}$$

where p_+ and p_- are the momenta of the positron and electron, and v_+ and v_- are their speeds. these two equations are compatible with the relation $h\nu = m_+ c^2 + m_- c^2$ only when $v_+ = v_- = c$. However, as is well known from the theory of relativity, particles with a non-zero rest mass can never move at the speed of light

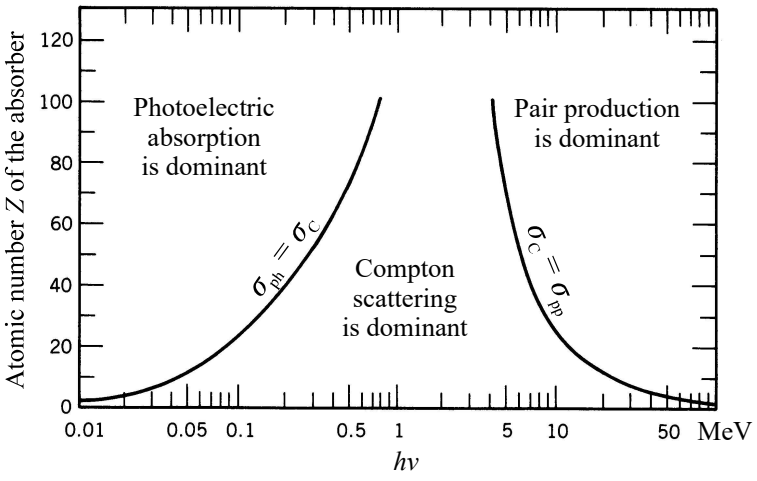


Fig. 11. Relative importance of the three major types of γ-ray interactions. The curves correspond to values of Z and $h\nu$ for which the Compton scattering cross section is equal to the photoelectric effect or pair production cross section (from [1]).

(as this would require an infinite kinetic energy). This means that an electron and a positron pair cannot be created in a vacuum.

Since the recoil energy of the nucleus is relatively small, the threshold value for pair production in the field of a nucleus is taken to be $2m_ec^2 \approx 1.02$ MeV, and in the energy balance, the recoil energy of the nucleus can be neglected. Then the total kinetic energy of the electron and positron is equal to:

$$E_{pp} = h\nu - 2m_ec^2. \tag{3.6.31}$$

The threshold for pair production in the field of an electron is twice as large ($4m_ec^2$). This is because the recoil energy is much larger due to the much smaller mass of the electron, and its contribution cannot be neglected.

The general shape of the dependence of the pair production cross section on energy is evident from Fig. 14a–16a: when the photon energy exceeds 1.02 MeV, the pair production cross section initially increases rapidly, and then this increase slows down and reaches saturation. At high photon energies, where the inequality $h\nu \gg 137m_ec^2Z^{-1/3}$ holds, the cross section value is approximately equal to:

$$(\sigma_{pp})_{max} \approx 1.9 \cdot 10^{-31}Z^2 \ln(183Z^{-1/3}) \text{ [m}^2\text{]}. \tag{3.6.32}$$

When the photon energy exceeds 10 MeV, pair production becomes the dominant mechanism of gamma radiation interaction with matter.

3.6.7. Attenuation coefficients

According to Eq. (3.4.2), the total cross section for a photon's interaction with an atom is equal to:

$$\sigma = \sigma_C + \sigma_{ph} + \sigma_{pp}, \tag{3.6.33}$$

where σ_C, σ_{ph}, and σ_{pp} are the atomic cross sections for Compton scattering, the photoelectric effect, and pair production, respectively. Depending on the photon energy and the material, one of these three cross sections can be significantly larger than the other two. Thus, the corresponding interaction process is the dominant one. Fig. 11 illustrates the intervals of photon energy $h\nu$ and material atomic number Z within which each of these three processes dominates. As can be seen, when the photon energy ($h\nu$) is small, the photoelectric effect dominates; when the photon energy is intermediate, Compton scattering dominates; and when the photon energy is large, pair production dominates. The intervals of photon energy where Compton scattering dominates widen as the atomic number Z of the material decreases.

Based on the general expression for the probability of an interaction (3.4.1), one can express the dependence of the gamma radiation intensity I on the thickness x of the material layer (or "absorber"). Suppose a narrow, parallel beam of monochromatic gamma radiation with initial intensity I_0 falls on a flat layer of material of thickness x (see Fig. 12). In practice, such a narrow, parallel beam is formed using a narrow channel made of a high-density material, which is called a **collimator**. The formation process itself is called **collimation**. Collimation is used to ensure that only unscattered gamma radiation photons reach the detector and are recorded. As shown in Fig. 12, photons that undergo a photoelectric effect or pair production are

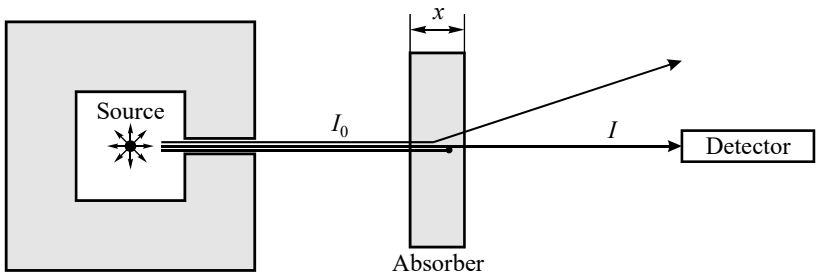


Fig. 12. Experimental schematic for studying gamma radiation attenuation in matter. A narrow parallel beam of radiation falls from a source on a layer of absorber of thickness x. Only those photons that pass through the medium without interacting reach the detector.

absorbed (the photon disappears), or due to Compton scattering, they are deflected away from the detector (such photons bypass the detector, provided it is far enough from the scattering region). Photons that reach the detector are those that passed through the medium without interacting with its atoms. The interaction of a single photon with an atom in a layer of thickness dx is described by the probability dP given by Eq. (3.4.1). Since the intensity of the gamma radiation is proportional to the number of photons per unit time, and the decrease in intensity is proportional to the number of interacting photons, the relative decrease in intensity ($-\mathrm{d}I/I$) must be equated to the interaction probability dP, writing the number of interactions with a minus sign ($-\mathrm{d}I$, over which the thickness increases by dx). Thus, the left side of Eq. (3.4.1) can be replaced by the relative decrease ($-\mathrm{d}I/I$) over a thickness dx:

$$-\frac{\mathrm{d}I}{I} = \sigma \cdot n_\mathrm{a} \cdot \mathrm{d}x, \tag{3.6.34}$$

where n_a is the number of atoms per unit volume. Integrating the differential equation (3.6.34), we obtain:

$$I(x) = I_0 e^{-\sigma n_\mathrm{a} x}, \tag{3.6.35}$$

where I_0 is the initial intensity. This relationship can be written in the following form:

$$I(x) = I_0 e^{-\mu x}, \tag{3.6.36}$$

where μ is the **linear attenuation coefficient**:

$$\mu = \sigma \cdot n_\mathrm{a}. \tag{3.6.37}$$

Thus, the intensity of a narrow beam of gamma radiation decreases exponentially with increasing material thickness (see Fig. 13).

Since the total cross section σ is equal to the sum of three distinct processes (3.6.33), the total linear attenuation coefficient μ is also equal to the sum of three components, each of which represents a specific type of interaction—Compton scattering, the photoelectric effect, and pair production:

$$\mu = \mu_\mathrm{C} + \mu_\mathrm{ph} + \mu_\mathrm{pp}. \tag{3.6.38}$$

The expressions of the coefficients μ_C, μ_ph, and μ_pp are obtained by substituting the correspondimg cross section into Eq. (3.6.37).

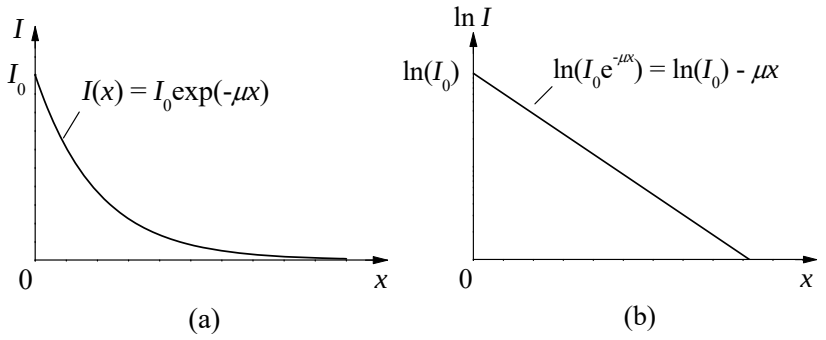


Fig. 13. Dependence of the gamma radiation intensity (a) and its logarithm (b) on the thickness of the material layer.

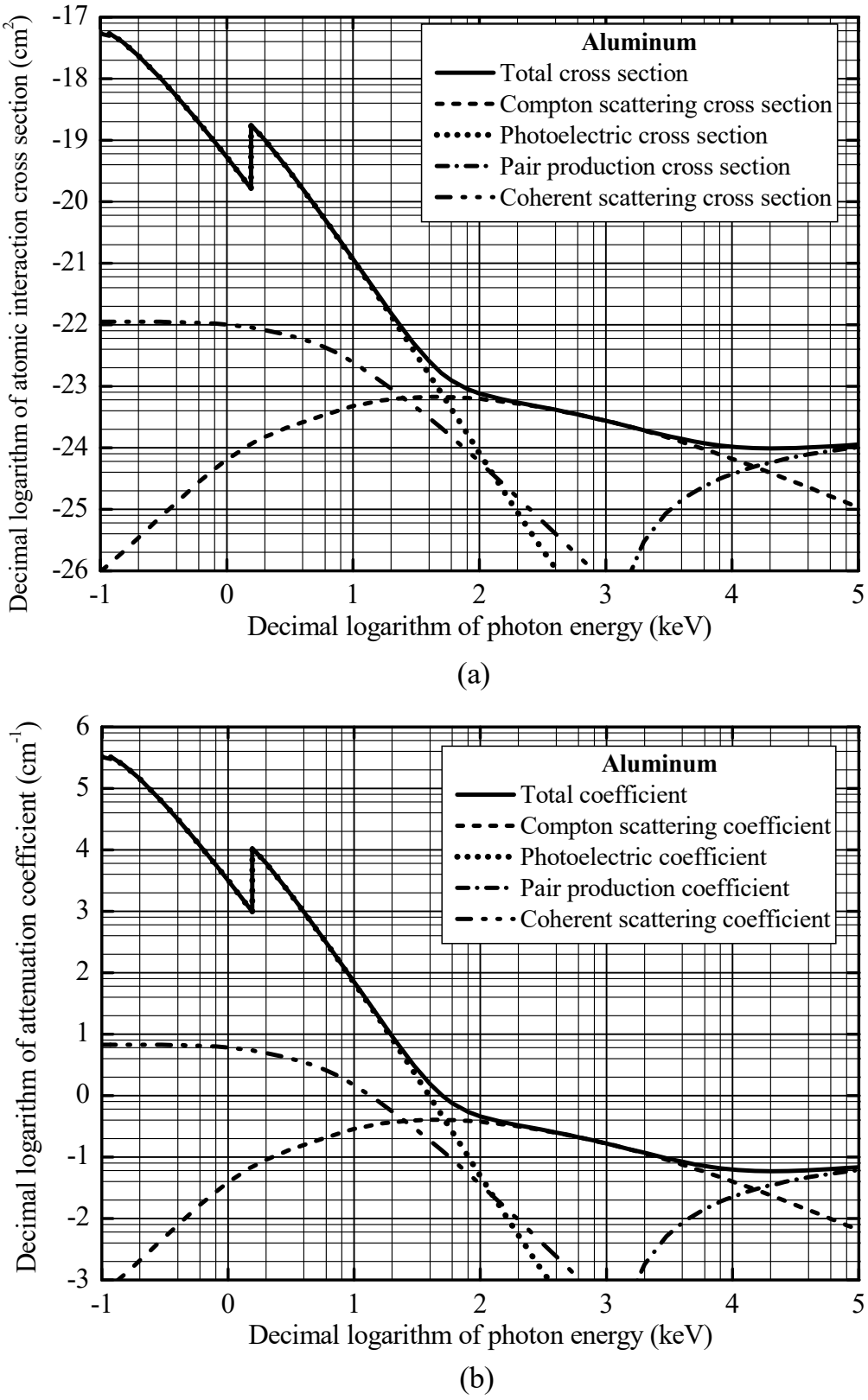


Fig. 14. Dependence of the atomic interaction cross section (a) and attenuation coefficient (b) in aluminum on the logarithm of the photon energy (from [4]).

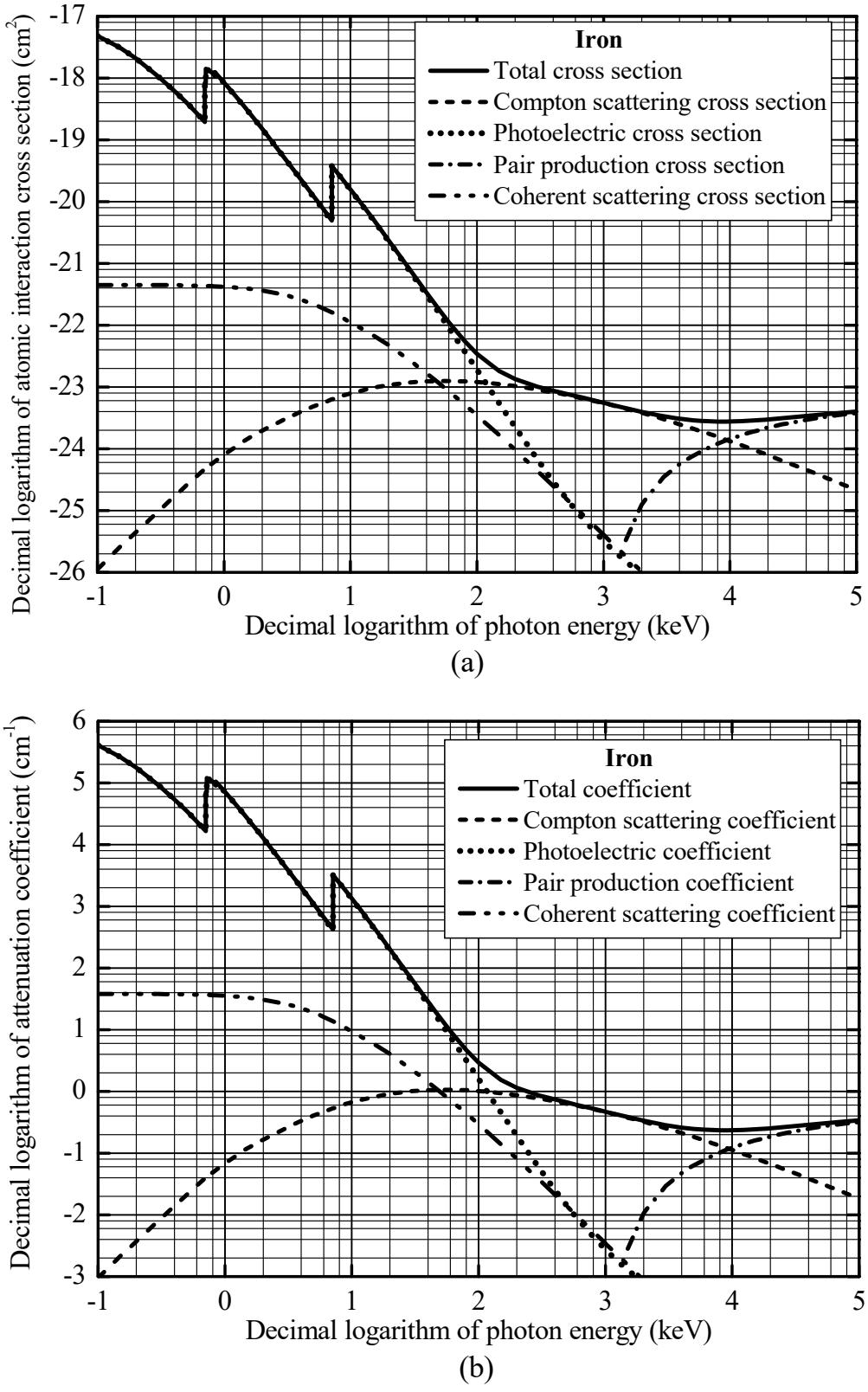


Fig. 15. Dependence of the atomic interaction cross section (a) and attenuation coefficient (b) in iron on the logarithm of the photon energy (from [4])

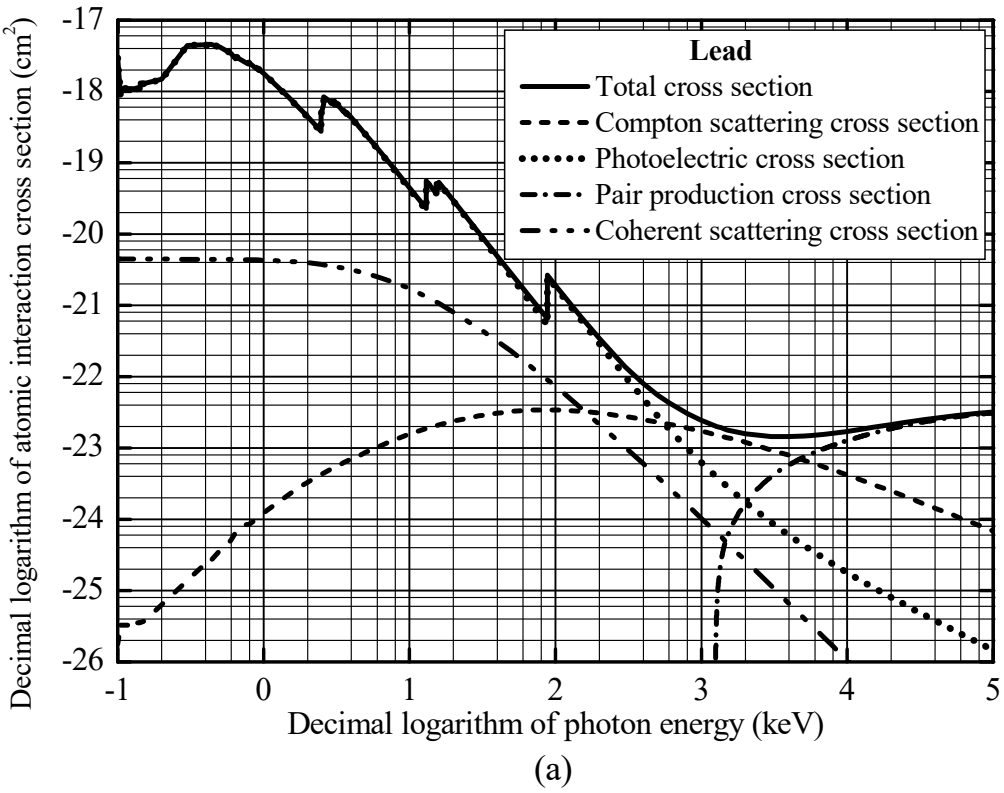


Fig. 16. Dependence of the atomic interaction cross section (a) and attenuation coefficient (b) in lead on the logarithm of the photon energy (from [4])

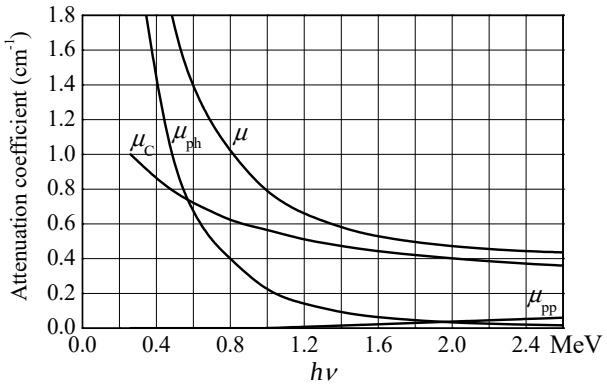


Fig. 17. Dependence of different components of the linear attenuation coefficient of lead on the quantum energy.

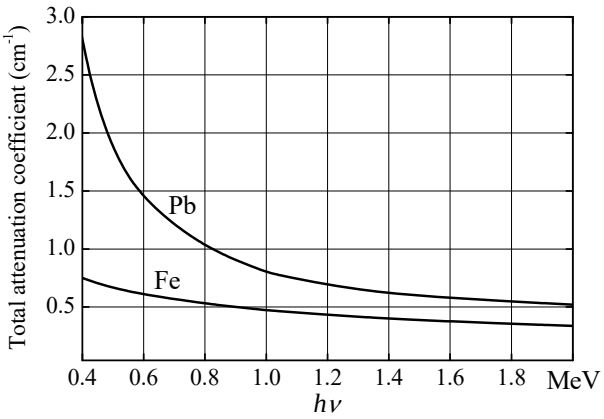


Fig. 18. Dependence of the total linear attenuation coefficient of lead and iron on the gamma quantum energy.

The attenuation coefficient μ is proportional to the interaction cross section, so the attenuation coefficient's dependence on the quantum energy reflects the corresponding cross-section dependencies (see Fig. 14–16). Energy dependences of the coefficients μ_C, μ_{ph}, and μ_{pp}, as well as of the total linear attenuation coefficient μ for lead are shown in Fig. 17. As can be seen, in the low-energy region (when $h\nu < 0.5$ MeV), the photoelectric effect is the primary interaction mechanism. The attenuation coefficient μ depends strongly not only on the quantum energy but also on the elemental composition of the absorber. The baseline reason for this dependence is the strong dependence of the photoelectric cross section σ on the atomic number Z (which is equal to the number of electrons in an atom). As mentioned in Sections 3.6.4–3.6.6, the atomic Compton scattering cross section is proportional to Z, the photoelectric cross section is proportional to Z^5, and the pair production cross section is proportional to Z^2. Therefore, as the atomic number increases, the linear attenuation coefficient increases. This is illustrated in Fig. 18, where the values of μ for lead and iron are compared. Furthermore, the relative weight of photoelectric absorption events in the total number of interaction events for lead is much greater than in materials composed of light elements, such as iron or aluminum (compare Fig. 14a and Fig. 16a).

4. Scintillation Detectors

4.1. Introduction

A **scintillation detector** is a detector of ionizing radiation whose output signal is produced by detecting flashes of visible light (*scintillations*) caused in the detector material by ionizing radiation. Thus, a characteristic property of a scintillation detector is that the electrons that cause the output pulse of the detector voltage are not the same electrons that were created by the ionizing action of the radiation. In this respect, scintillation detectors fundamentally differ from gas-filled and semiconductor detectors. In gas-filled and semiconductor detectors, the output signal is formed by those same charge carriers that the detected radiation liberated from atoms. In a scintillation detector, an intermediate step between the charge carriers created during ionization and the charge carriers forming the output pulse is visible light. This solves the conflicting requirements for the active material of a solid-state detector: on one hand, a high mobility of charge carriers is required (to achieve high speed) and a low ionization energy (to increase the number of charge carriers); on the other hand, a high resistivity is necessary (to reduce the effect of leakage current on the output signal). The first requirement is best met by materials whose electrical conductivity is high, whereas the second is best met by insulators. Since the output signal in a scintillation detector is formed outside the active material boundaries, and the occurrence of a scintillation within this material does not require charge transport over long distances, high resistivity and charge carrier mobility are not as critical parameters as they are in a semiconductor detector (in a scintillation detector, it is more important for the active material to be transparent to visible light).

Material emission excited by various types of energy within the material is called **luminescence**. Luminescence can be caused by light, heating, mechanical stresses, chemical reactions, or the action of ionizing particles on the material. Luminescence materials used in scintillation detectors are often called **scintillating materials** or **scintillators**, while the flashes of light induced in them by ionizing radiation are called **scintillations**.

The scintillation method is currently one of the most widely used methods for detecting radioactive radiation. Scintillation detectors are widely used in nuclear physics to study the radiation energy spectra of radioactive isotopes, to measure the lifetimes of excited nuclear states, and to investigate cosmic radiation.

The advantages of scintillation detectors are:

1. high detection efficiency (a scintillation detector with a NaI(Tl) crystal of typical dimensions registers 40–60% of all incident γ quanta with an energy of 662 keV, whereas the efficiency of a gas detector under the same conditions is only 1–4%); furthermore, when the energy of γ quanta is greater than 40 keV, the peak efficiency of scintillation detectors is greater than the peak efficiency of semiconductor detectors of the same dimensions;
2. short dead time (10^{-7}–10^{-9} s, while the dead time of a Geiger-Müller counter is 10^{-4}–10^{-2} s);
3. ability to measure particle energy with an accuracy of a few percent;
4. relatively simple recording equipment.

The disadvantages of scintillation detectors are:

1. energy measurement error (5–10% when the energy of γ quanta is 662 keV) is roughly an order of magnitude larger than that of semiconductor detectors;
2. the sensitivity of the main practical scintillator—sodium iodide NaI(Tl)—to moisture (when exposed to moisture, NaI(Tl) turns yellow and becomes opaque to scintillation light);
3. the photomultiplier tube of the scintillation detector requires a highly stable power supply voltage ($\approx$ 1 kV).

4.2. The elementary process of scintillation in an inorganic scintillator

The scintillator most frequently used in scintillation detectors is a sodium iodide (NaI) crystal activated with a thallium (Tl) impurity. Other inorganic scintillators are also used (e.g., halides CsF, CsI, etc.). All these

inorganic crystals are dielectrics, i.e., the width of their energy gap is several times larger than that of a typical semiconductor energy gap. For example, the energy gap width of NaI is 5.9 eV. Therefore, under normal conditions, there are practically no free charge carriers in dielectrics. Free charge carriers appear in these crystals only due to the action of ionizing radiation. The process of charge carrier formation in an inorganic scintillator is very similar to that occurring in a semiconductor detector. Under the influence of ionizing radiation, electrons of the crystal transition from filled energy bands (i.e., the valence band and lower bands) to the unfilled conduction band and higher bands. Consequently, vacancies are created in the filled bands. Vacancies that appear in the valence band behave as positive charge carriers (+e) with a certain mass and kinetic energy. These "quasiparticles" are called **holes**. Vacancies that appear in deeper bands are quickly filled due to electron transitions from higher energy bands, which generates photons that can be absorbed in the material, producing new electron-hole pairs. In addition, the free electrons and holes lose a part of their energy by creating new electron-hole pairs due to impact ionization. Thus, the process of slowing down of fast secondary charge carriers (electrons and holes) in the material is accompanied by an increase of their number. Within approximately 10^{-12} s, all electrons in the conduction band slow down and drop to the bottom of the conduction band, while holes float to the top edge of the valence band.

Subsequently, electrons and holes recombine. For a scintillation detector to operate, it is crucial that this recombination process yields visible light photons (**radiative recombination**) that are not reabsorbed by the scintillator itself. Pure crystals cannot fulfill this role well due to two reasons: 1) in a pure crystal, radiative recombination is relatively slow; 2) in a pure crystal, the emitted photons can easily be reabsorbed, since their energy is greater than or equal to the width of the energy gap, which matches the energy required to excite an electron from the valence band to the conduction band.

To increase the probability of radiative recombination and reduce the reabsorption of the resulting light, small amounts of impurities, called **activators**, are introduced into the crystal. For example, a sodium iodide crystal is activated with thallium (NaI(Tl)), and a ZnS crystal is activated with silver (ZnS(Ag)), etc. Activators create discrete energy levels in the energy gap (see Fig. 19). Since these states are localized near the activator atoms, we will call these energy levels "activator levels" (but one must keep in mind that energy levels of an activator atom in a solid material are quite different from energy levels of an isolated activator atom). Activator atoms introduced into the scintillator matrix create **luminescence centers**. The stages of electron and hole recombination are shown in Fig. 19. Initially, the scintillator is in a quiet state with an empty conduction band and a completely filled valence band. When ionizing radiation strikes the crystal, it abruptly generates a large population of non-equilibrium electron-hole pairs. The free holes in the valence band are rapidly thermalized and begin migrating through the lattice. Because the activator atoms have a high capture cross section for holes compared to other lattice defects, the rate of hole trapping at the activator

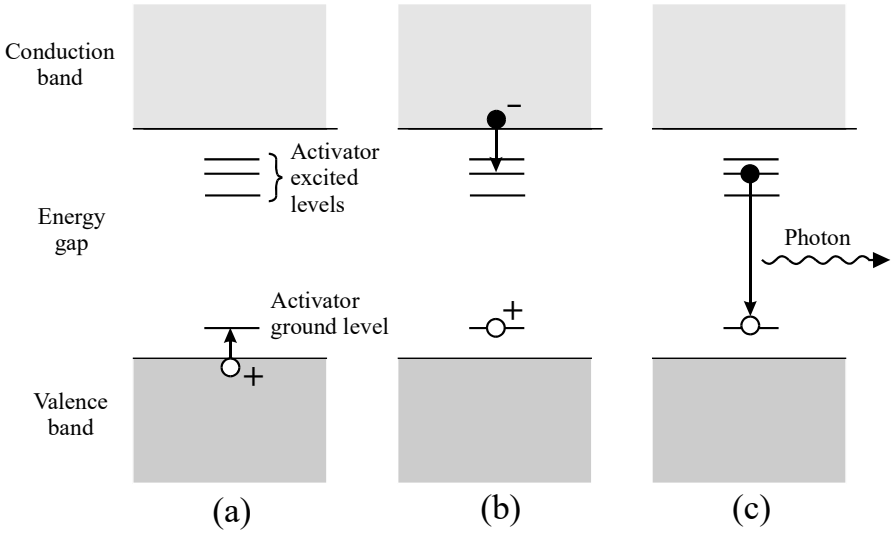


Fig. 19. Stages of the recombination process in an activated inorganic scintillator: (a) ionization of an activator center resulting in a positive ion (occurring within approximately 10^{-12} s after the appearance of free electrons and holes); (b) electron capture resulting in a neutral excited activator atom (occurring within approximately 10^{-12} s after electron capture); (c) quantum transition of the activator atom from the excited level to the ground energy level accompanied by emission of a visible light photon (occurring within $(5–50) \cdot 10^{-8}$ s after electron capture).

centers vastly outpaces any detrapping or loss mechanisms. As a result, the majority of the radiation-induced holes are swiftly localized at the activator sites, ionizing them (see Fig. 19a). The generation of a high density of ionized activator sites creates localized positive point charges, attracting non-equilibrium conduction electrons via long-range Coulomb forces. Subsequent electron capture by these ionized centers neutralizes the defect, placing the activator into an excited electronic state (see Fig. 19b). Finally, each excited activator center undergoes a radiative transition back to its electronic ground state, emitting a characteristic optical photon. (see Fig. 19c).

Another mechanism of energy transfer to the activator involves an electron-hole bound state known as an **exciton**. In this case, the electron and hole remain bound to one another, but the exciton can move freely through the crystal until it encounters a neutral activator atom, transferring its energy to it and exciting the activator center.

As can be seen from Fig. 19c, the energy of the emitted photons is less than the width of the energy gap, so they are not reabsorbed by the crystal. For various scintillators, the scintillation wavelength range matches the interval of 200–600 nm (energy from 2 eV to 6 eV), and the emission spectrum width is close to 100 nm. The median scintillation wavelength for NaI(Tl) crystals is close to 410 nm (this corresponds to approximately 3 eV photon energy), and the maxima of the absorption spectrum are at 293 nm and 234 nm. As a result, the transparency of the crystal to its own emission is almost 100%.

An important characteristic of a scintillator is the scintillation duration. Both the time of themalization of nonequilibrium holes and electrons and the time required for activator atoms to become ionized and capture electrons is of the order of 10^{-12} s. By comparison, the average lifetime of an excided activator atom is much longer - of the order of $10^{-8} - 10^{-6}$ s. For example, the average lifetime of excited Tl atoms in a NaI(Tl) crystal at a room temperature is $2.3 \cdot 10^{-7}$ s. This duration determines the scintillation intensity decay over time. That is to say, the average duration of a scintillation (a single flash) is approximately equal to the average lifetime of the excited state of the activator atoms.

4.3. Structure of a Scintillation Detector

The formation of the output signal of a scintillation detector becomes clear from its schematic diagram, which is illustrated in Fig. 20. The detected particle (e.g., a γ quantum) enters the scintillator (1) and causes a flash. The scintillation photons hit the photocathode (3) of the photomultiplier tube, to which a high negative voltage U_0 (≈ -1 kV) is connected relative to the grounded anode (7). In some scintillation detectors (including the one used for this experiment), the photocathode is grounded, and a high positive voltage is connected to the anode (7). The scintillator is surrounded by a reflective screen, so almost all scintillation photons reach the photocathode. These photons, upon reaching the photocathode, knock photoelectrons out of it. The electric field existing inside the photomultiplier tube focuses these electrons and directs them onto an intermediate electrode called a **dynode**. The material of the dynode is selected such that intense secondary electron emission occurs within it. Each electron hitting a dynode knocks out roughly 3 to 10 new electrons from it (this number is called the **secondary emission coefficient**). From the first dynode, the electron flow hits the second dynode, and so on. In total, there are usually about 10–20 dynodes (5) in a photomultiplier tube. Therefore, the electron flow is amplified $10^5 - 10^8$ times by the time it strikes the last dynode. An important property of a photomultiplier tube is the high linearity of its amplification. From the

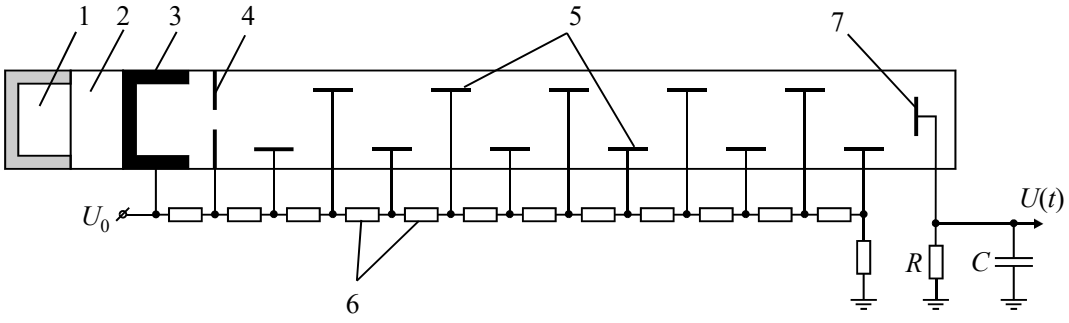


Fig. 20. Schematic diagram of a scintillation detector: 1 – scintillator, 2 – light guide, which couples the scintillator to the photomultiplier tube, 3 – photocathode, 4 – focusing electrode, 5 – dynodes, 6 – voltage dividers, 7 – anode, R – load resistance, C – anode capacitance.

last dynode, the amplified electron flow hits the anode (7), creating a voltage pulse across the load resistor *R*, which is transmitted to the electronic recording equipment (an amplitude analyzer, a counting device, etc.). The electron multiplication process in a photomultiplier tube is illustrated in Fig. 21.

The photomultiplier tube sends to the recording equipment not only the pulses caused by the flashes, but also background pulses, which are caused by thermoelectronic emission from the photocathode and dynodes, leakage currents across the anode and dynode insulation, and other parasitic electronic processes occurring within the photomultiplier tube.

The number of photons emitted during each scintillation is proportional to the final number of the secondary particles (excited activator atoms in an inorganic scintillator or excited molecules in an organic scintillator) that were created by the action of the ionizing radiation. Since the final number of secondary particles is proportional to the energy loss of the incident particles in the material, the number of scintillation photons is also proportional to the energy loss of the incident particles in the material. On the other hand, the amplitude of the output pulse of the photomultiplier tube is proportional to the number of scintillation photons. Therefore, the amplitude of the output pulse is proportional to the energy loss of the incident particles in the material.

Thus, these five processes determine the output signal of a scintillation detector, and their quantitative expressions are directly proportional to one another:

1. the loss of energy of the incident radiation and the creation of fast electrons in the scintillator (quantitative expression – the deposited energy);

2. the slowing down of the fast electrons (and the increase in their number) leading to the formation of "secondary particles" – electrons, holes, and excited activator atoms in inorganic crystals, or excited molecules in organic scintillators (quantitative expression – the number of secondary particles);

3. the recombination and deexcitation of secondary particles and the emission of visible light scintillation photons (quantitative expression – the number of photons per unit time);

4. the liberation of photoelectrons from the photocathode when the scintillation photons strike it (quantitative expression – the number of photoelectrons per unit time);

5. secondary electron emission from the dynodes of the photomultiplier tube and the electron flow towards the anode of the photomultiplier tube (quantitative expression – the instantaneous anode current, i.e., the instantaneous detector current).

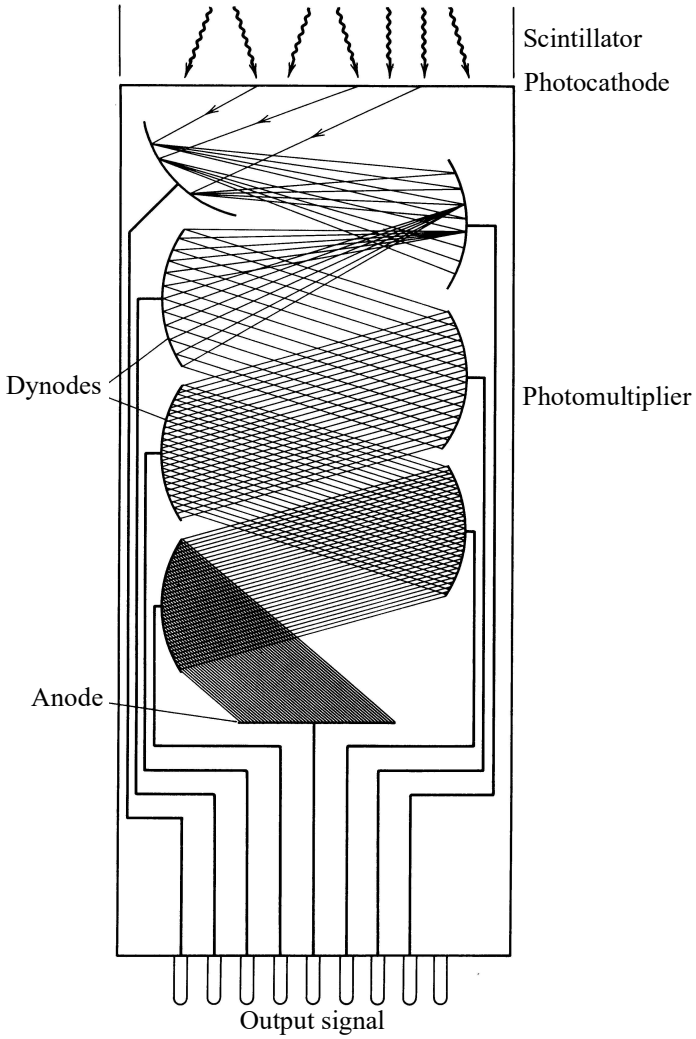


Fig. 21. Operating principle of a photomultiplier tube. Photoelectrons that were liberated from the photocathode are attracted to the first dynode, and during the subsequent secondary electron emission from the dynode, the number of electrons increases. The potential of each successive dynode is higher than the potential of the previous dynode; typically, a photomultiplier tube has from 10 to 20 dynodes. After interacting with each successive dynode, the number of electrons is multiplied several times.

5. Gamma Spectroscopy Using Scintillation Detectors

5.1. Pulse Height Spectra

A detector can operate in either pulse mode or current mode. **Pulse mode** measuring instruments connected to the detector are designed to separately record *each* current pulse caused by an interaction event in the detector. Individual particles interacting with the detector are recorded in this manner. When measuring the energy of individual particles (radiation spectroscopy), pulse mode is always used. In this case, the integral of each current pulse is measured:

$$\int_0^{t_c} i(t)\,\mathrm{d}t = Q = HC, \tag{5.1.1}$$

where Q is the absolute value of the total charge of the electrons forming the current pulse, which is proportional to the energy loss of the particle in the detector, H is the amplitude of the voltage pulse created across the detector's load resistor (the symbol H originates from the word "height"), and C is the effective capacitance of the detector (the word "effective" indicates that this capacitance also includes the capacitance of the external circuit). In **current mode**, only the average current over a time interval much longer than the interval between interaction events is measured (such a mode is used, for example, in dosimetry, when only the total absorbed energy over a long period is important). Only pulse mode will be discussed further below.

In pulse mode, the detector's current pulse is converted into a voltage pulse, which is then amplified and recorded or analyzed. Many detectors incorporate a special device that converts the detector's current pulse into a voltage pulse. This device is called a **preamplifier** (this name reflects the fact that the amplitude of the preamplifier's voltage pulse is often too small to be analyzed directly, so the pulse is subsequently further amplified). In pulse mode, the amplitude of each pulse is proportional to the charge created in the detector during the corresponding interaction event (see Eq. (5.1.1)). Having measured a large number of such pulses, one would notice that their amplitudes are not identical. The pulse height distribution can reflect both the energy spectrum of the incident particles and fluctuations in the detector's response to particles of a definite energy. Therefore, the pulse height distribution is frequently used when studying incident radiation or the operation of the detector itself.

The most commonly used method of representing a pulse height distribution is the so-called **differential pulse height spectrum**. An example of such a spectrum is shown in Fig. 22a.

The pulse height (expressed in volts, V) is plotted along the horizontal axis. The ratio $\mathrm{d}N/\mathrm{d}H$ of the number of pulses $\mathrm{d}N$ whose amplitudes belong to an infinitesimally narrow interval to the width of that interval $\mathrm{d}H$ (units: reciprocal volts, V^{-1}) is plotted along the vertical axis. The number of pulses $N(H_1 < H < H_2)$ whose amplitudes belong to the interval from H_1 to H_2 is determined by integrating the differential pulse height spectrum from H_1 to H_2:

$$N(H_1 < H < H_2) = \int_{H_1}^{H_2} \frac{\mathrm{d}N}{\mathrm{d}H}\,\mathrm{d}H. \tag{5.1.2}$$

This integral is represented by the hatched area in Fig. 22a. The total number of pulses N_0 is determined by integrating the entire spectrum:

$$N_0 = \int_0^{\infty} \frac{\mathrm{d}N}{\mathrm{d}H}\,\mathrm{d}H. \tag{5.1.3}$$

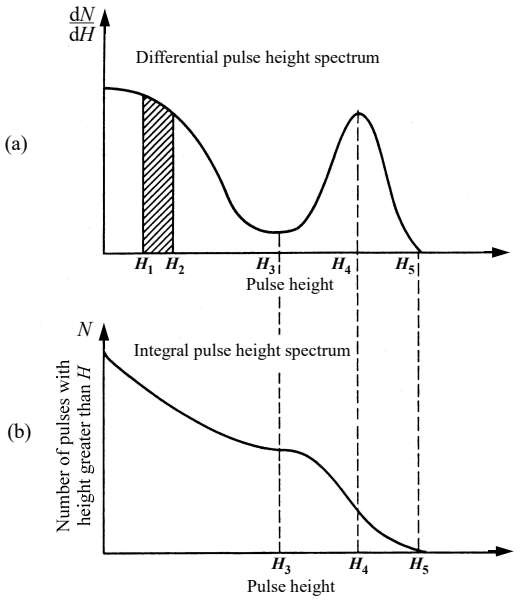


Fig. 22. Examples of differential (a) and integral (b) pulse height spectra.

The maximum pulse height is indicated by the abscissa of the point at which the spectrum drops to zero (e.g., in Fig. 22a, the maximum amplitude is H_5). The maxima of the spectrum (e.g., at point H_4) correspond to the most probable amplitudes, i.e., amplitudes that are recorded particularly frequently. The minima of the spectrum (e.g., at point H_3) correspond to the least probable amplitudes, i.e., amplitudes that are recorded particularly rarely. Any physical interpretation

of a pulse height spectrum is related to calculating the integrals (i.e., areas) of the spectrum. The ordinate ($\mathrm{d}N/\mathrm{d}H$) acquires physical meaning only after multiplying it by a small change in the abscissa (ΔH): $(\mathrm{d}N/\mathrm{d}H) \cdot \Delta H \approx \Delta N$, where ΔN is the number of pulses with amplitudes between H and $H + \Delta H$.

The same information conveyed by a differential pulse height spectrum can be expressed using a so-called **integral pulse height spectrum**. The integral pulse height spectrum corresponding to the differential spectrum shown in Fig. 22a is presented in Fig. 22b. When constructing an integral spectrum, the pulse height is likewise plotted along the abscissa axis, while the number of pulses whose amplitude is greater than a given value (abscissa) is plotted along the ordinate axis:

$$N(H) = \int_{H}^{\infty} \frac{\mathrm{d}N}{\mathrm{d}H}\,\mathrm{d}H. \tag{5.1.4}$$

$N(H)$ is a monotonically decreasing function because, if $H_2 > H_1$, then the number of pulses with amplitudes greater than H_2 is always smaller than the number of pulses with amplitudes greater than H_1. The value of the integral spectrum at the point $H = 0$ gives the total number of pulses N_0. The integral pulse height spectrum becomes zero at the point corresponding to the maximum amplitude (in Fig. 22b, at point $H = H_5$).

Differential and integral pulse height spectra provide identical information about the amplitude distribution and are uniquely related to one another. The value of the differential spectrum corresponding to any amplitude H is equal to the absolute value of the derivative (slope) of the integral spectrum corresponding to the same amplitude H. Maxima of the differential spectrum correspond to the steepest slope of the integral spectrum (Fig. 22, point H_4). Minima of the differential spectrum correspond to the shallowest slope of the integral spectrum (in the case of Fig. 22, point H_3). Small changes in a spectrum are easier to observe using a differential spectrum; therefore, in practice, the differential spectrum is used more frequently than the integral one.

5.2. Detector Energy Resolution

Radiation detectors are frequently used to measure the energy spectrum of radiation. Such measurements belong to **radiation spectroscopy**. In this section, we will discuss some general characteristics of detectors that are important in the field of radiation spectroscopy.

5.2.1. Pulse height response function and pulse height resolution

From the standpoint of radiation spectroscopy, the most important characteristic of a detector is its response to monoenergetic radiation (i.e., a flux of particles with equal energy). The differential pulse height spectrum obtained under conditions of monoenergetic radiation is called the detector's **pulse height response function** (or simply "response function") for a given energy of incident particles. We will denote the response function corresponding to a given particle energy E_0 as $G(H; E_0)$. The pulse height H is the argument of the response function, while the radiation particle energy E_0 is a parameter of the function. Fig. 23 shows two response functions corresponding to the same radiation energy. Since the energy is identical, both response functions have maxima at the same point H_0 (which indicates the average pulse height). If an equal number of pulses was recorded in both cases, then the *areas* (integrals) of both peaks are also equal. However, it is obvious that the *widths* of the peaks are different. A larger peak width corresponds to poorer **energy resolution**. A large peak width means that the fluctuations in pulse height were large, even though the exact same amount of energy was transferred to the detector's active medium during each interaction event. As these fluctuations decrease, the width of the response function narrows and the response function approaches a Dirac δ-function. Evidently, as the width of the response function decreases, it becomes easier to distinguish fine details in the radiation energy spectrum.

Before presenting the exact definition of energy resolution, it is useful to define another "intermediate" concept—pulse height resolution. A detector's **pulse height resolution** R_H is the ratio of the width of the detector's pulse height response function, measured at half of its maximum height ("full width at half maximum", "FWHM"), to the position of the peak center H_0[6] (see Fig. 24a):

$$R_H = \frac{\mathrm{FWHM}_H}{H_0}. \tag{5.2.1}$$

[6] If there is a background (i.e., an extraneous term included in the measured response function), then that background must be subtracted before calculating the pulse height resolution.

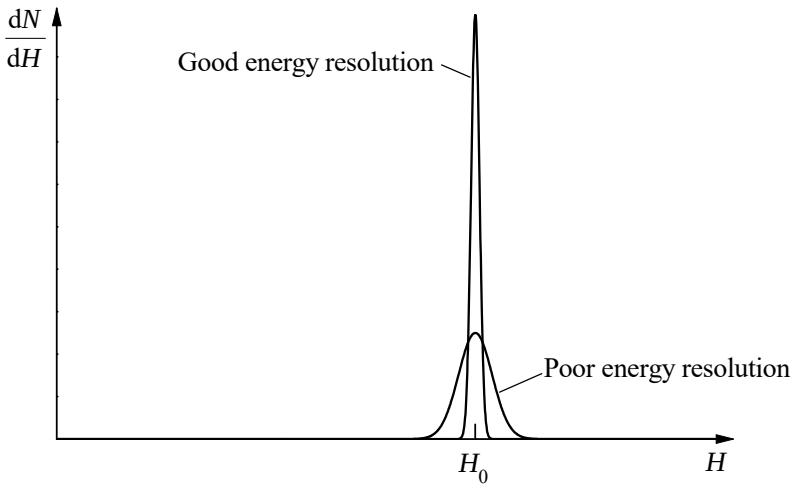


Fig. 23. Examples of detector response functions. In one case, the detector's energy resolution is relatively good, while in the other case it is poor.

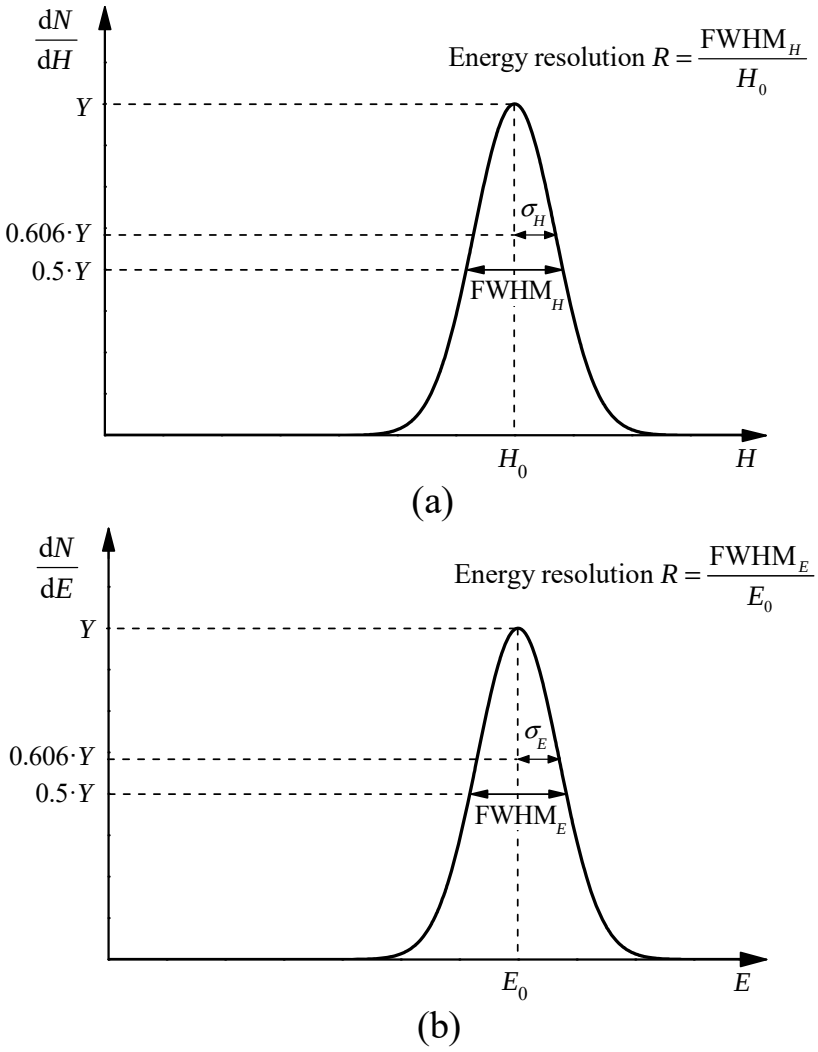


Fig. 24. Definition of detector energy resolution. (a) Pulse height response function; σ_H is the standard deviation of the amplitude; FWHM_H is the width of the pulse height response function at half maximum of the peak (for a Gaussian-shaped peak, $\mathrm{FWHM}_H = 2.35, \sigma_H$). (b) Energy response function; σ_E is the standard deviation of the energy calculated from the amplitude; FWHM_E is the width of the energy response function at half maximum of the peak (for a Gaussian-shaped peak, $\mathrm{FWHM}_E = 2.35, \sigma_E$).

5.2.2. Energy response function and energy resolution

The average signal amplitude H_0 is a function of the particle energy:

$$H_0 = f(E_0). \tag{5.2.2}$$

We will denote the inverse function by $h(H_0)$:

$$E_0 = h(H_0). \tag{5.2.3}$$

The *true* particle energy E_0 of monoenergetic radiation is indicated by only a single value (5.2.3). However, using the function $h(H)$, a certain energy E can be assigned to *each* pulse height H (including those that

differ from the average amplitude H_0):

$$E = h(H). \tag{5.2.4}$$

Therefore, the differential pulse height spectrum $\mathrm{d}N/\mathrm{d}H$ can be transformed into a **differential energy spectrum** $\mathrm{d}N/\mathrm{d}E$. To do this, we express the energy increment $\mathrm{d}E$ by differentiating Eq. (5.2.4):

$$\mathrm{d}E = h'(H), \mathrm{d}H \equiv \frac{1}{f'(E)}, \mathrm{d}H. \tag{5.2.5}$$

Hence,

$$\frac{\mathrm{d}N}{\mathrm{d}E} = f'(E)\frac{\mathrm{d}N}{\mathrm{d}H}. \tag{5.2.6}$$

Thus, to convert a differential pulse height spectrum into a differential energy spectrum, the abscissas H of all points must be replaced with the corresponding energies $E = h(H)$, and the ordinates must be multiplied by $f'(E)$. If this spectrum is obtained under monoenergetic radiation, it is then called the **energy response function** for the given energy of incident particles. We will denote this function as $G(E; E_0)$. The true particle energy E_0 is a parameter of this function, while the energy E calculated from the pulse height (5.2.4) is the argument of the function. Once the energy response function is available, energy resolution can be defined in the exact same manner as pulse height resolution is defined from the pulse height response function. Thus, a detector's **energy resolution** R is the ratio of the width FWHM_E of the detector's energy response function, measured at half of its maximum height, to the position of the peak center E_0 (see Fig. 24b):

$$R = \frac{\mathrm{FWHM}_E}{E_0}. \tag{5.2.7}$$

In detectors designed to study radiation spectra, the ratio of the average amplitude H_0 to the particle energy E_0 must be constant:

$$H_0 = \mathrm{const} \cdot E_0. \tag{5.2.8}$$

Let us verify that in this case, the energy resolution is equal to the pulse height resolution. Let us assume that the energy and pulse height widths of the spectrum peak, FWHM_E and FWHM_H, are small, so they are related in the same way as differentials (see (5.2.5)):

$$\mathrm{FWHM}_E = \frac{1}{f'(E_0)}, \mathrm{FWHM}_H. \tag{5.2.9}$$

Substituting (5.2.9) into (5.2.7) and taking into account that $f'(E_0) = \mathrm{const}$ (see (5.2.8)), we conclude that

$$\frac{\mathrm{FWHM}_E}{E_0} = \frac{\mathrm{FWHM}_H}{H_0}, \tag{5.2.10}$$

i.e., $R = R_H$. Therefore, in practice, pulse height resolution is often referred to as "energy resolution". Hereafter, these two concepts will not be distinguished from one another.

Energy resolution is most frequently expressed as a percentage. The energy resolution of semiconductor detectors is less than 1 %. For scintillation detectors used in the field of γ-radiation spectroscopy, the energy resolution is 5–10 % when the photon energy is (0.5–2) MeV. The smaller the energy resolution, the easier it is for the detector to resolve two closely spaced spectral lines of radiation. If the radiation consists of particles of two energies, then the smallest difference between their energies at which it is still possible to separate the two peaks in the measured spectrum is approximately equal to the width of the energy response function at half maximum, i.e., FWHM_E or RE_0, where E_0 is the average of the two energies.

5.3. Gamma Radiation Spectrum. Gamma Spectrometer. Secondary Electrons

A device designed to measure a γ-radiation spectrum is called a **gamma spectrometer** (γ-spectrometer). A **γ-radiation spectrum** is described by an energy function equal to the number of γ-quanta corresponding to a unit energy interval, i.e., $\mathrm{d}N/\mathrm{d}E$ (here N is the number of γ-quanta, and E is the energy of a γ-quantum). Characterizing a spectrum by the energy function $\mathrm{d}N/\mathrm{d}E$ is the most convenient because, in its meaning, this function is closest to the function measured directly by spectroscopic measurements—the differential pulse height spectrum (see Section 5.1).

As we can see, the definition of a radiation spectrum is similar to the definition of a detector's energy response function (see Section 5.2.2), yet there are differences: 1) in the definition of the detector's energy response function, N denotes the number of detector *pulses* (and not the number of γ-quanta); 2) in the definition of the detector's energy response function, E denotes not the true energy of the γ-quantum, but the *energy calculated from the pulse height* using the proportionality relation (5.2.8). The first difference is not fundamental, because the number of output pulses is easily related to the number of γ-quanta striking the detector: these two numbers are equal or at least proportional to each other. However, relating the pulse height to the true energy of the γ-quantum is more complicated. This is due to two reasons—the finite energy resolution of the detector and the fact that γ-radiation is indirectly ionizing. The latter property of γ-radiation means that the vast majority of ionization events in a medium are caused by the interaction of atoms not with the photons of the incident radiation (γ-quanta), but with fast electrons (or, when the energy of the γ-quanta is sufficiently high, with positrons) that can be produced due to the interaction of γ-radiation with matter. We will call these electrons **secondary electrons**[7].

Since γ-quanta are practically "invisible" to the detector, information about the incident γ-radiation is provided by the secondary electrons. Electrons lose energy by ionizing and exciting atoms of the medium or through bremsstrahlung.

Thus, in order for a detector to be used as a γ-radiation spectrometer, it must perform two functions. First, it must "convert" the energy of the γ-quantum into the energy of one or several fast electrons. Second, it must detect those electrons. This is the operating principle of scintillation and semiconductor γ-radiation spectrometers (only such γ-spectrometers will be discussed further below). If the detector is sufficiently large, the escape of secondary electrons (and their bremsstrahlung) from the detector is unlikely. Only those electrons that are produced within a distance from the detector surface smaller than their range can escape from the detector. Consequently, in order for the majority of secondary electrons to remain inside the detector, the dimensions of the detector must be much larger than the range of the highest-energy secondary electrons in the medium. The maximum energy of the electrons is close to the energy of the γ quantum. The range of an electron with an energy of several MeV in a solid is on the order of several millimeters. The mean free path of bremsstrahlung photons is usually even smaller. Consequently, in order for the entire energy of the secondary electrons to be absorbed in the detector, its dimensions must be larger than 1 cm.

At typical γ quantum energies (> 0.1 MeV), gas-filled detectors do not meet the requirements of a γ spectrometer mentioned earlier. First, the range of a 1 MeV electron in gases at normal atmospheric pressure is several meters, so conventional gas-filled detectors cannot absorb the entire energy of the secondary electrons. Second, γ quanta interact much more frequently with the outer shell (cathode) of the detector. The electrons produced during this interaction that reach the active region of the detector (the gas) lose part of their energy in the cathode material. Since this portion of energy can vary and is unknown in practice, there is no possibility of relating the energy of the secondary electrons to the energy of the incident γ quanta.

5.4. Energy spectrum of secondary electrons

Based on what was stated in Section 5.3, it can be asserted that a detector used as a γ radiation spectrometer is, in reality, a secondary electron spectrometer. Therefore, the shape of the γ spectrometer's response function approximately reflects the shape of the secondary electron energy spectrum (the general definition of the detector's response function was given in Sections 5.2.1 and 5.2.2). As shown in Fig. 11, the photoelectric effect dominates at low γ quantum energies (up to several hundred keV), Compton scattering dominates at intermediate energies (from several hundred keV to several MeV), and electron-positron pair production dominates at high γ quantum energies (above 5–10 MeV). Furthermore, the relative probability of each of these three processes (with respect to the probabilities of the other two processes) depends on the atomic number Z of the material. The photoelectric effect cross section depends most strongly on Z, being approximately proportional to Z^5 (see Eq. (3.6.28)). As we will see later, in γ spectroscopy it is desirable to have as high a probability of the photoelectric effect as possible; therefore, detectors made of high atomic number materials are best suited for γ spectroscopy.

Let us examine the influence of the three processes mentioned above on the energy spectrum of secondary electrons. During the photoelectric effect, a γ quantum disappears and an electron (photoelectron) is created,

[7] The transfer of energy from fast positrons to matter occurs essentially in the same way as the transfer of energy from fast electrons to matter. Therefore, positrons that can be produced if the gamma-quantum energy is sufficiently high will not be distinguished from electrons, except in the context of positron-specific processes, such as positron-electron annihilation.

whose energy is equal to

$$E_{\text{ph}} = h\nu_0 - \varepsilon_{\text{b}}; \tag{5.4.1}$$

here $h\nu_0$ is the γ quantum energy, and ε_{b} is the binding energy of the liberated electron in the atom. At typical γ quantum energies, the photoelectron is most often liberated from the K shell, whose binding energy ε_{b} ranges from a few keV for low-Z materials to several tens of keV for high-Z materials. The resulting vacancy is filled by an electron from a higher electron shell. During this process, a characteristic X-ray photon or an Auger electron is emitted. For example, out of 100 iodine atoms that have a vacancy in the K shell, on average 88 atoms emit a characteristic X-ray photon (the remaining ones emit an Auger electron). The range of Auger electrons is very short (due to their low energy), so they practically never escape from the detector. A characteristic X-ray photon can travel a distance of roughly 1 mm or less in the material before being absorbed. These photons are absorbed via the photoelectric effect (during this photoelectric effect, electrons are liberated not from the K shell, but from higher shells whose binding energy is less than the energy of the X-ray photon). We will assume that characteristic X-ray photons also do not escape from the detector.

Thus, the consequence of the photoelectric effect is the liberation of a photoelectron whose energy is equal to the major part of the γ quantum's energy (more precisely, smaller than the latter by the amount ε_{b}), and one or more lower-energy electrons whose total energy is equal to the binding energy ε_{b} of the first electron. If none of these electrons escape from the detector, then the total energy of all secondary electrons remaining in the detector is equal to the energy of the γ quantum. Therefore, the photoelectric effect is ideally suited for measuring the energy of γ quanta: if monoenergetic γ radiation falls on the detector, the total kinetic energy distribution of all secondary electrons appearing after each photoelectric effect event has the shape of a delta function (see Fig. 25a). The maximum ("peak") is at the energy $h\nu_0$ of the incident γ quanta. The energy response function would have this shape if the photoelectric effect were the sole interaction process of γ radiation with matter and if the energy resolution of the detector were equal to zero.

The consequence of Compton scattering is the appearance of a Compton recoil electron with energy E_{C} and a scattered γ radiation photon with energy $h\nu$. The sum of both of their energies is equal to the initial photon energy $h\nu_0$, i.e.,

$$E_{\text{C}} = h\nu_0 - h\nu. \tag{5.4.2}$$

The energy $h\nu$ of the scattered photon (and the energy E_{C} of the Compton recoil electron) depends on the scattering angle θ (see Eqs. (3.6.1)). Since this angle can take all values from 0 to π, the energy of the Compton recoil electron can take all values from 0 (when $\theta = 0$, i.e., when there is practically no scattering) to the maximum energy

$$E_{\text{C max}} = \frac{h\nu_0}{1 + \dfrac{m_{\text{e}}c^2}{2h\nu_0}}, \tag{5.4.3}$$

which is reached when $\theta = \pi$, i.e., when the collision is head-on and the photon reverses its direction of motion, while the recoil electron moves in the same direction in which the photon was moving prior to the collision. Thus, the energy spectrum of Compton recoil electrons is continuous. According to the theoretical expression for the differential cross section of Compton scattering (3.6.23), the recoil electron energy spectrum should be approximately of the shape shown in Fig. 25b. The detector's energy response function would have this shape if Compton scattering were the sole interaction process of γ radiation with

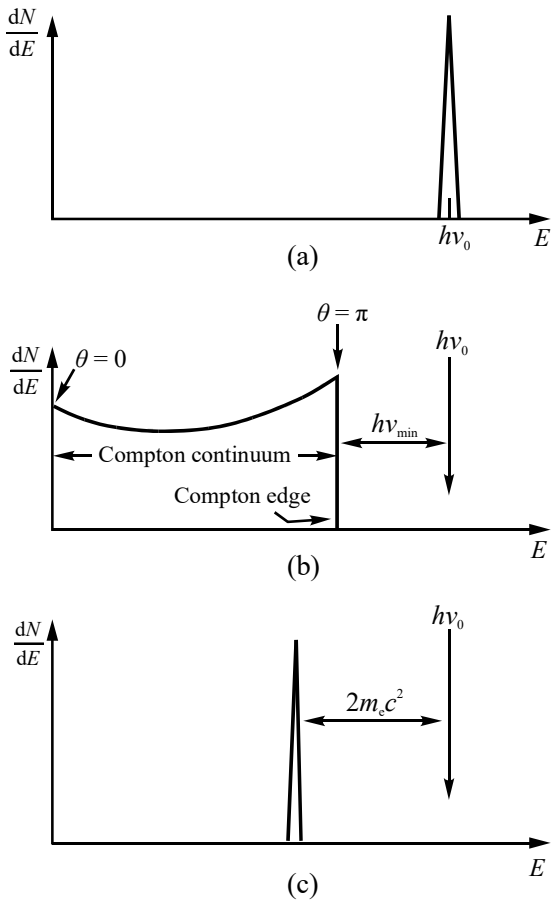


Fig. 25. Energy spectra of secondary electrons produced after various processes: (a) after the photoelectric effect; (b) after single Compton scattering; (c) after electron-positron pair production and the escape of both annihilation photons.

matter and if each γ quantum were scattered only once in the detector material. According to (5.4.2), the difference between the initial energy $h\nu_0$ of the γ quanta and the maximum energy $E_{\mathrm{C\,max}}$ of the Compton recoil electron is equal to the minimum energy of the scattered γ quantum:

$$h\nu_{\min} = h\nu_0 - E_{\mathrm{C\,max}} = \frac{h\nu_0}{1 + \dfrac{2h\nu_0}{m_e c^2}}. \tag{5.4.4}$$

When the initial energy of the γ quanta is much greater than the rest energy of the electron ($h\nu_0 \gg m_e c^2$), this energy difference tends to a constant value

$$h\nu_{\min} = m_e c^2/2 \quad (= 0.256\ \mathrm{MeV}). \tag{5.4.5}$$

The energy spectrum of Compton recoil electrons is sometimes called the **Compton continuum**, and its edge on the high-energy side is called the **Compton edge**.

Since most electrons belong to atoms (are not free), the analysis of Compton scattering presented earlier is accurate only when the energy of the γ quanta is much greater than the binding energy of an electron in the atom. At low energies of incident γ quanta, the electron binding energy can influence the shape of the Compton continuum. This manifests itself by "rounding off" the sharp corner in the high-energy region (see Fig. 25b), and the drop of the Compton edge becomes less steep. This is because at low γ quantum energy, the uncertainty of the electron's momentum in the atom can no longer be neglected. That is, it cannot be stated that the electron is stationary prior to the interaction. Then the energies of the scattered γ quantum and the recoil electron, after scattering by a given angle θ, can be either greater or smaller than the values given by Eq. (3.6.1), depending on the initial direction and speed of the electron's motion. However, in practice, this effect is often difficult to observe due to the finite energy resolution of the detector, which can manifest itself as a "rounding off" of sharp corners.

The consequence of electron-positron pair production is that in the electric field of an atomic nucleus, a γ quantum disappears and an electron-positron pair is created. This process becomes possible only when the γ quantum energy $h\nu_0$ becomes greater than $2m_e c^2 = 1.02$ MeV. Then the sum of the kinetic energies of the created electron and positron is smaller than the γ quantum energy by the amount $2m_e c^2$:

$$E_+ + E_- = h\nu_0 - 2m_e c^2, \tag{5.4.6}$$

where E_- is the energy of the electron, and E_+ is the energy of the positron. Thus, in this case, just as in the case of the photoelectric effect, the entire energy of the secondary electrons absorbed in the detector is strictly defined. Therefore, the total kinetic energy distribution of all secondary electrons appearing after each pair production event also has the shape of a delta function, as shown in Fig. 25c. The peak is at the total energy of the electron and positron, which is given by expression (5.4.6). The detector's energy response function would have the shape shown in Fig. 25c if electron-positron pair production were the sole consequence of γ radiation interaction with matter and if the detector's energy resolution were equal to zero.

However, the lifetime of a positron in a material is finite: when the positron's energy decreases to thermal energy, the positron reacts with an electron of the material. Then both of them disappear ("annihilate"), and in their place two photons moving in opposite directions appear, each having an energy equal to $m_e c^2 = 0.511$ MeV (**annihilation radiation** or **annihilation photons**). Since the slowing-down time of a positron is short, annihilation radiation appears practically at the same instant as the electron-positron pair. In order for pair production to manifest itself only as a single peak, which is illustrated in Fig. 25c, both annihilation photons would have to escape from the detector without losing energy in it. Therefore, the peak in the detector's energy response function whose energy is smaller by the amount $2m_e c^2 = 1.02$ MeV than the energy of the incident γ quanta is called the **double escape peak**.

5.5. Shapes of response functions for detectors of various sizes

In two of the three previously mentioned processes of γ radiation interaction with matter—during Compton scattering and during electron-positron pair production—**secondary γ radiation** is produced. The secondary radiation during Compton scattering is the scattered γ radiation, and the secondary radiation during electron-positron pair production is the annihilation radiation. The shape of the detector's response function depends on how much energy these secondary γ quanta lose in the detector material. The energy losses of secondary

γ quanta depend on the dimensions of the detector. We will examine three cases—a "small" detector, a large detector, and an intermediate-sized detector.

First, we will examine the limiting case where the dimensions of the detector are small compared to the mean free path of the secondary γ quanta. Since the mean free path of secondary γ quanta in a solid is usually on the order of several centimeters, the "smallness" condition means that the dimensions of the detector must be (1–2) cm or smaller. Then the energy response function of the detector is a superposition of the spectra shown in Fig. 25 (if we neglect peak broadening due to the finite energy resolution of the detector). If the γ quantum energy $h\nu_0$ is less than $2m_ec^2$, then the response function consists of the Compton continuum and the **full-energy peak**, i.e., the peak corresponding to photoelectric absorption events, which manifest themselves by the fact that the *entire* energy of the primary photon is transferred to the active material of the detector (see Fig. 26b). In a small detector, the ratio of the areas under the full-energy peak and the Compton continuum is equal to the ratio of the photoelectric effect and Compton scattering cross sections. If the γ quantum energy is much greater than $2m_ec^2$, then a double escape peak may also be present, as shown in Fig. 26c.

The opposite limiting case is as follows. Suppose that γ quanta enter the very center of a large detector, e.g., using a measurement geometry such as that shown in Fig. 27a. The dimensions of the detector are so large that all secondary γ quanta also interact with the active volume of the detector and none of them escape from the detector. For this to be the case at typical γ quantum energies (500 keV – 5 MeV), the dimensions of the detector must exceed several tens of centimeters. Some possible sequences of γ quantum interaction processes with the detector are shown in Fig. 27a. For example, if the first interaction process is Compton scattering, then the scattered γ quantum later interacts with the detector material at another point. This interaction process can also be Compton scattering. In this case, another secondary γ quantum appears, whose energy is even smaller. Eventually, the photoelectric effect occurs and this sequence of processes ends.

It is important to keep in mind that this entire sequence of processes takes a very short time. Incident

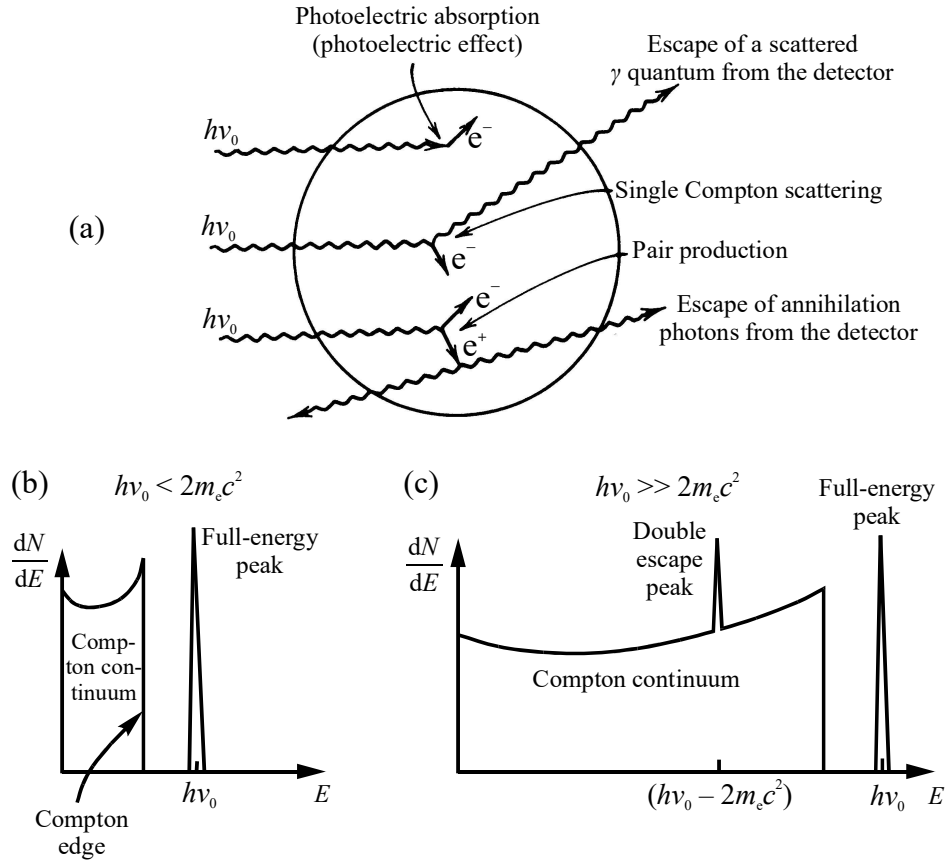


Fig. 26. "Small detector" limiting case in γ spectroscopy. (a) Interaction processes occurring in a small detector; (b) response function when secondary electrons are produced due to Compton scattering and the photoelectric effect; (c) response function when electron-positron pair production also occurs alongside Compton scattering and the photoelectric effect.

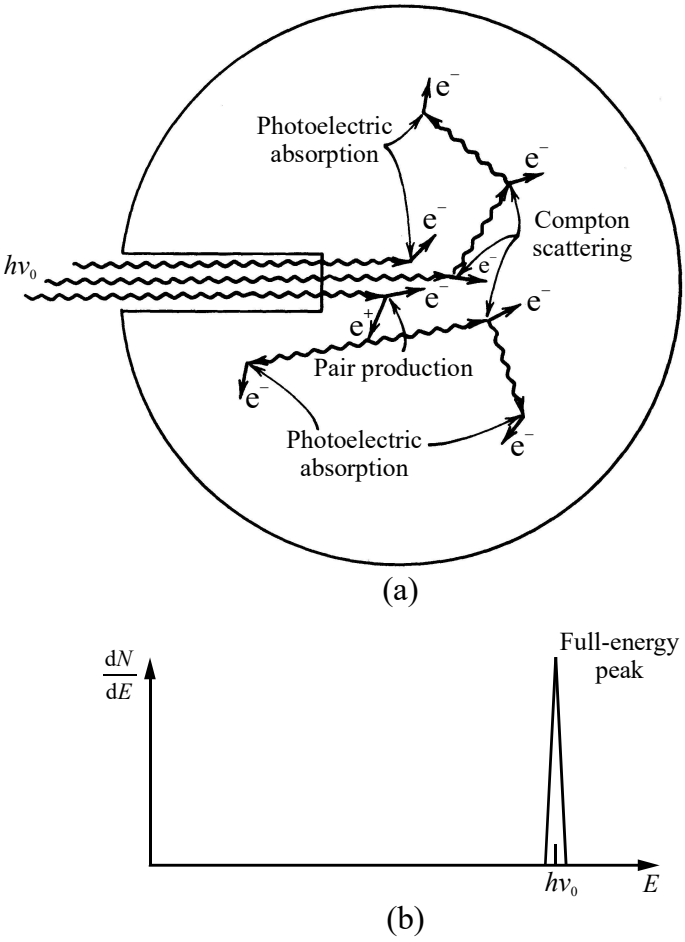


Fig. 27. "Large detector" limiting case in γ spectroscopy. (a) Some sequences of γ quantum interaction processes with a large detector. All γ quanta, regardless of how complex their interaction history with the detector was, transfer all of their energy $h\nu_0$ to the detector material. (b) Response function of a large detector.

and secondary γ quanta move at the speed of light. If the average path of secondary γ quanta in the detector material is on the order of 10 cm, then the entire time from the entry of the primary γ quantum into the detector until the absorption of the last secondary γ quantum is less than 10^{-9} s. This time is much shorter than the response duration of all γ radiation detectors used in practice. Therefore, it can be assumed that all Compton recoil electrons and the final photoelectron appear practically at the same instant. Thus, the output pulse of the detector is the sum of the pulses that would be caused by each secondary electron of the given sequence of events. If the detector's response to a single electron is proportional to the energy of that electron, then the total pulse amplitude is proportional to the *total* energy of all secondary electrons. Since we state that the entire energy of the primary γ quantum remains in the detector, the total energy of the secondary electrons is equal to the energy of the primary γ quantum, regardless of how complex the history of its energy transfer to the detector material may be.

This same conclusion also applies to a sequence of interaction events in which an electron-positron pair is created. Two annihilation photons interact with the detector material via Compton scattering or the photoelectric effect. If the detector is sufficiently large, then the sum of the kinetic energies of the electron-positron pair and all subsequently produced Compton recoil electrons and two photoelectrons is equal to the energy of the primary γ quantum. Thus, the detector's response is again proportional to the energy of the primary γ quantum.

Consequently, if the detector is sufficiently large and if its response function is proportional to the kinetic energy of the electron, then the pulse amplitude is identical for all primary γ quanta of the same energy, regardless of their interaction history with the detector material. This means that the detector's response function consists of a single peak—the full-energy peak (see Fig. 27b). Thus, the response function of a large detector is much simpler than that of a small one (compare Fig. 26b and 26c). Complex γ spectra consisting of many different energies are much easier to investigate when the response function consists of a single sharp peak. Therefore, a large detector is better suited for γ spectroscopy than a small one.

The dimensions of practical detectors used in γ spectroscopy lie between the two limiting cases examined earlier. Moreover, under standard conditions, γ quanta fall onto the outer surface of the detector (and not into the center of the detector volume, as in Fig. 27a). Therefore, even in the case of a very large detector,

some Compton scattering or electron-positron pair production events occur near the surface of the detector, and some secondary γ quanta escape from the detector. For these reasons, in real detectors, only part of the energy of some secondary γ quanta is absorbed, while the other part leaves the detector. Correspondingly, the response function of real detectors has several new features that are related to the *partial* absorption of the energy of secondary γ quanta. Some sequences of interaction events that reflect the properties of intermediate-sized detectors and the corresponding response functions are shown in Fig. 28.

As we can see in Fig. 28b, if electron-positron pair production is not significant, then the main regions of the response function of an intermediate-sized detector are the same as those of a small-sized detector: namely, the full-energy absorption peak and the Compton continuum. However, compared to the case of Fig. 26b, it is obvious that the ratio of the area under the full-energy absorption peak to the area under the Compton continuum is larger. This is because the full-energy absorption peak now reflects not only those γ quanta whose interaction with the detector manifested as a single photoelectric effect event, but also those γ quanta that were scattered one or more times prior to the photoelectric effect. Another feature of the response function shown in Fig. 28b is that the gap between the Compton edge and the full-energy absorption peak is partially "filled in." This is because the total energy of two or more Compton recoil electrons can be greater than the maximum possible energy $E_{\mathrm{C\,max}}$ of a single recoil electron, which is defined by expression (5.4.3). Therefore, if a γ quantum was scattered two or more times and then left the detector without interacting further, then the total energy of the secondary electrons can fall between the value $E_{\mathrm{C\,max}}$ and $h\nu_0$.

If the energy of the primary γ quantum is so high that the probability of electron-positron pair production is large, then in an intermediate-sized detector the annihilation photons can either be completely absorbed

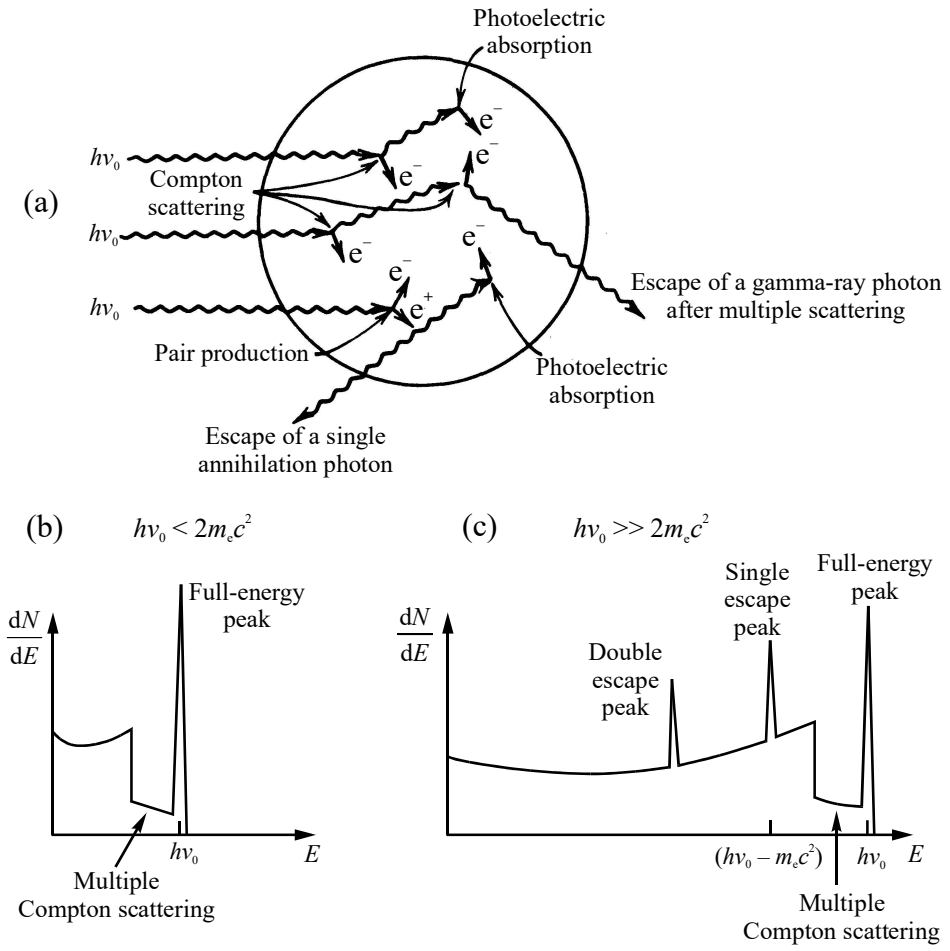


Fig. 28. Intermediate-sized detector case in γ spectroscopy. (a) Some sequences of γ quantum interaction processes with the detector. A characteristic property of an intermediate-sized detector is the *partial* absorption of secondary γ quantum energy (i.e., multiple Compton scattering after which the γ quantum escapes from the detector, or Compton scattering of annihilation γ quanta after which they escape from the detector, or absorption of only one of the two annihilation γ quanta). (b) Response function when secondary electrons are produced only due to Compton scattering and the photoelectric effect; (c) response function when electron-positron pair production is also important alongside Compton scattering and the photoelectric effect.

(as in a large detector), or partially absorbed, or not interact with the detector material at all (as in a small detector). If they do not interact with the detector, then, as in the case of a small detector, a double-escape peak appears (see Fig. 28c). If one or both annihilation photons are scattered, and then one of them or both leave the detector, then the total energy of the secondary electrons lies between the full-energy absorption peak and the two-annihilation-photon escape peak. If one annihilation photon is completely absorbed while the other leaves the detector without interacting with its material, a "single-escape peak" appears. The position of this peak in the spectrum is at an energy that is lower by $m_e c^2 = 0.511$ MeV than the γ-quantum energy $h\nu_0$ (see Fig. 28c).

5.6. Structure and Main Parameters of a Gamma Spectrometer

To measure the energy of γ quanta, the proportionality of the detector's output pulse amplitude to the energy loss of the γ quantum in the material is used. The γ-quantum energy is determined from the pulse amplitude corresponding to the full-energy absorption peak. Thus, a γ spectrometer directly measures not the energy spectrum, but the pulse-height spectrum (see Section 5.1). The pulse-height spectrum is measured with special instruments—**pulse-height analyzers**, also called **multichannel analyzers** (MCA). A multichannel analyzer can be imagined as a set of counters with a common input, each of which counts only those pulses whose amplitudes belong to a certain narrow interval called a **channel**. The channels have equal width, do not overlap with one another, and there are no gaps between them. Therefore, when a voltage pulse whose amplitude lies between the lower edge of the first channel (i.e., the minimum voltage that the analyzer can record) and the upper edge of the last channel (i.e., the maximum voltage) arrives at the input of the multichannel analyzer, that amplitude necessarily belongs to one (and *only* one) channel. That is, such a pulse is recorded by one of the above-mentioned counters. Thus, a multichannel analyzer sorts pulses according to their amplitudes. In this way, the **pulse-height spectrum** is measured—the amplitude function $\delta N/\delta H$, where δN is the number of pulses corresponding to each channel, and δH is the channel width. It is convenient to choose the unit of amplitude measurement equal to the channel width. Then $\delta H = 1$, $\delta N/\delta H = \delta N$, and the amplitude H is equal to the channel number.

The block diagram of the simplest γ spectrometer is shown in Fig. 29. The detector output signal is first fed to a **preamplifier**, which converts the detector current pulse into a voltage pulse. The preamplifier output signal is fed to an **amplifier**, which increases the amplitude of the voltage pulse from a few millivolts to a few volts so that the pulse can be processed more conveniently. The detector, preamplifier, and amplifier may be housed in a single casing. The amplifier must be **linear**, i.e., its output pulse amplitude must be directly proportional to the input pulse amplitude. The amplifier signal is fed to a multichannel analyzer, which displays the measurement data in the form of a pulse-height histogram. An example of a γ spectrum measured with such a spectrometer is presented in Fig. 30.

The purpose of spectroscopic measurements of γ radiation (and other types of radiation) is to determine the energy and intensity of the radiation. The energy of γ quanta is determined from the **centroid** of the full-energy absorption peak—the position of the center of that peak on the horizontal axis. For example, in Fig. 30, the centroid corresponds to channel No. 3100 or an energy of 662 keV. It is often difficult to determine the centroid by eye, because a peak may consist of only a few points, and moreover, the peak may sit on

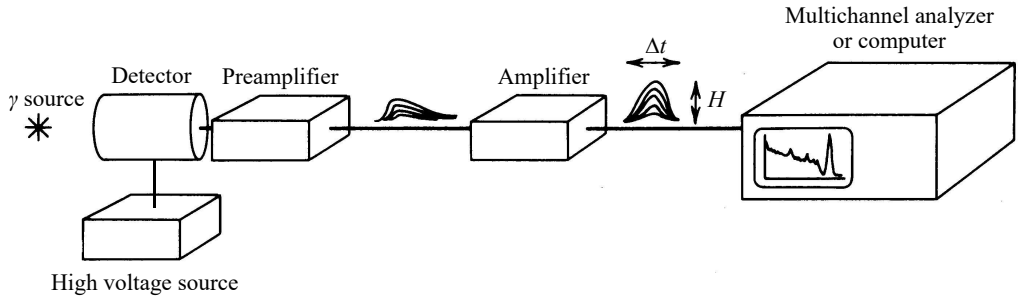


Fig. 29. Structure of the simplest γ spectrometer. The output pulses of the preamplifier usually have a fast leading edge (on the order of 10^{-9} s), a slow trailing edge (duration of $(5–10) \cdot 10^{-5}$ s), and a small amplitude (on the order of a few millivolts). The output pulses of the amplifier are more symmetric; their duration (Δt) is on the order of 10^{-6} s, and their amplitude (H) is on the order of a few volts.

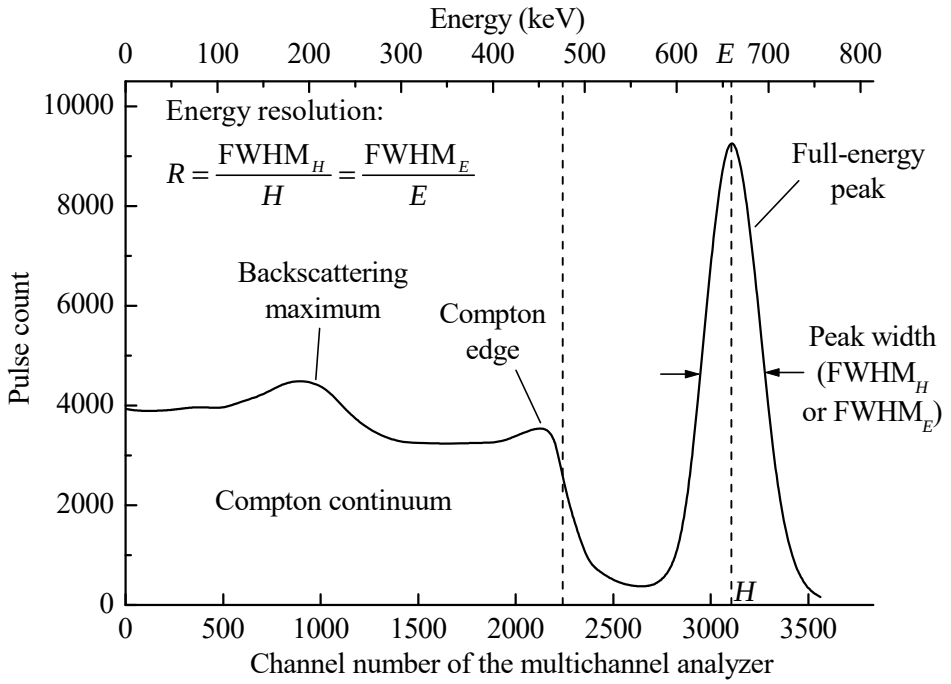


Fig. 30. Pulse-height spectrum of a NaI(Tl) scintillation spectrometer when detecting γ radiation from the cesium isotope ^{137}Cs, and calculation of the energy resolution R. The two vertical dashed lines mark the γ-quantum energy (662 keV) and the Compton edge energy (478 keV, according to Eq. (5.4.3)).

top of an extraneous continuous spectrum—the so-called "background"—in the energy region. For example, the background can be caused by extraneous radiation sources, the Compton continuum, or bremsstrahlung in the casing of the radioactive source under study. The background component associated with extraneous radiation sources is measured after removing the radiation source under study. That component must then be subtracted from the total (raw) spectrum. The result of this subtraction is a "cleaner" spectrum in which the peak under study is seen more clearly than in the raw spectrum. The remaining part of the background arises from *partial* absorption of the radiation from the source under study (e.g., due to multiple Compton scattering events in the active material of the detector, after which the photon escapes from the detector). This background component can be calculated approximately based on certain assumptions about its dependence on the channel number (i.e., on energy). If a given peak is clearly pronounced and does not overlap with other spectral maxima (as in Fig. 31), then the background component corresponding to each channel belonging to the peak region can sometimes be calculated approximately based on the assumption that its dependence on the channel number is linear. That is, linear interpolation can be performed between two background points, one of which corresponds to a lower energy and the other to a higher energy compared to the peak energy (see Fig. 31). Having calculated the coefficients of that straight line, one can compute the background component for each channel corresponding to the peak and subtract that component from the total number of counts corresponding to the given peak. In this way, we obtain the corrected count numbers

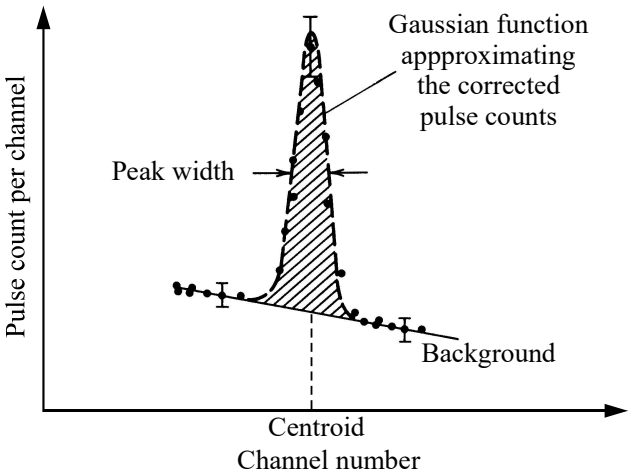


Fig. 31. The peak integral ("area") can be calculated by subtracting a linear dependence of the background on energy and then summing the corrected counts, or by performing a nonlinear fit with a Gaussian function. The error (standard deviation) of the count number in each channel is equal to the square root of that number.

y_i (where i is the channel number). Then the total number of counts in the peak region (the peak "integral" or "area") S and the peak centroid H_0 can be calculated using the following formulas:

$$S = \sum_i y_i, \tag{5.6.1}$$

$$H_0 = \frac{\sum_i H_i y_i}{\sum_i y_i}; \tag{5.6.2}$$

here H_i is the channel number of the i-th channel. For brevity, we will henceforth refer to the total number of counts S in the peak region as the "peak integral." However, it should be borne in mind that in general this quantity does not correspond to the mathematically exact definition of the term "integral," because integration would introduce an additional extraneous factor equal to the difference between the abscissas (i.e., X values) of adjacent points (in other words, the channel width). The peak integral (5.6.1) defines the total number of interaction events of a given type (in gamma spectroscopy, the number of full-energy absorption events of photons of a given energy). This number is proportional to the cross section of that type of interaction and to the flux density of γ quanta. If a given peak is the full-energy absorption peak of γ quanta of a certain energy, then from its integral one can calculate the number n_0 of γ quanta of that energy that struck the detector during the measurement time. To do this, one needs to know the photopeak efficiency of the detector. The **photopeak efficiency** (or **photoefficiency**) ε_{ph} of a γ detector is the ratio of the number of counts S_1 corresponding to the full-energy absorption peak of the response function to the total number n_0 of γ quanta of the same energy that struck the detector during the same time:

$$\varepsilon_{\text{ph}} = S_1 / n_0 \tag{5.6.3}$$

or

$$n_0 = S_1 / \varepsilon_{\text{ph}}. \tag{5.6.4}$$

S_1 is the integral of the part of the pulse-height spectrum corresponding to the given full-energy absorption peak (it must be calculated using Eq. (5.6.1)). The photopeak efficiency ε_{ph} is the probability that a γ quantum entering the detector will be completely absorbed, i.e., will lose all of its energy in it. The energy dependences of the photopeak efficiencies of NaI(Tl) and germanium (Ge) detectors are shown in Fig. 32. It should be borne in mind that the photopeak efficiency depends on the detector dimensions, shape, and position in space; for NaI(Tl) and Ge detectors of different geometry, the photopeak efficiency values may differ from those given in Fig. 32. However, the general shape of the energy dependence remains the same in any case: the photopeak efficiency decreases rapidly as the γ-quantum energy increases.

The **intrinsic efficiency** ε of a detector (also called the **total intrinsic efficiency**) is the ratio of the number n of recorded γ quanta to the total number n_0 of γ quanta that entered the detector during the same time:

$$\varepsilon = n / n_0, \tag{5.6.5}$$

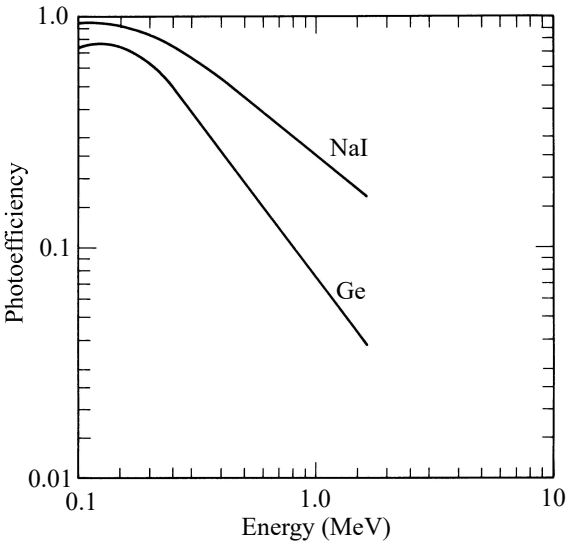


Fig. 32. Intrinsic photopeak efficiency of NaI and Ge detectors. These curves correspond to a NaI scintillator with a diameter and height equal to 7.62 cm, and a Ge semiconductor detector with a diameter and height equal to 4.2 cm.

where n is calculated simply by summing the counts corresponding to all channels (i.e., n is the integral of the entire measured spectrum). Hereafter we will omit the word "intrinsic." The total efficiency ε thus defined is the probability that a γ quantum entering the detector will produce an output pulse from the detector. Since a pulse is produced by any interaction event (photoelectric effect, Compton scattering, and pair production), the total efficiency can be defined as the probability that a γ quantum entering the detector will interact with at least one atom.

If the energy spectrum of the detected γ radiation is complex (consisting of several lines), then the full-energy absorption peaks of lower-energy γ quanta may fall into the Compton continuum region of higher-energy γ quanta. This makes it more difficult to measure the spectrum of lower-energy γ radiation. Therefore, it is desirable that the Compton continuum be as weak as possible, and the full-energy absorption peak as prominent as possible. This property of the response function of a γ spectrometer is described by the **photofraction** of the spectrum—the ratio of the number of counts S_1 corresponding to the full-energy absorption peak to the total number of counts $n = S_1 + S_2$ recorded during the same time:

$$P = \frac{S_1}{n} = \frac{S_1}{S_1 + S_2}. \tag{5.6.6a}$$

S_2 is the integral of the part of the response function that does not belong to the full-energy absorption peak. From Eqs. (5.6.5) and (5.6.6a), it follows that the photofraction is equal to the ratio of the detector's photopeak efficiency to its total efficiency:

$$P = \frac{\varepsilon_{\text{ph}}}{\varepsilon}. \tag{5.6.6b}$$

The higher the values of the parameters ε, ε_{ph}, and P, the better suited the detector is for γ spectroscopy. To increase the values of the parameters ε_{ph} and P, the Compton continuum must be reduced. Since the Compton continuum arises due to the escape of scattered γ quanta from the detector (see Sections 5.4 and 5.5), the simplest ways to increase the photopeak efficiency ε_{ph} and the photofraction P are as follows:

(a) to increase the share of photoelectric effect events in the total number of interaction events of γ quanta with the material (this reduces photon scattering and the probability of their escape from the detector),

(b) to increase the number of collisions of each γ quantum with the atoms of the active detector material, i.e., the total interaction probability (during each Compton scattering event, part of the photon's energy is transferred to the active detector material and the probability increases that the next interaction event will be the photoelectric effect, i.e., that the photon will be absorbed).

The probability of the photoelectric effect during an interaction and the total interaction probability increase with increasing detector dimensions and average atomic number Z. Therefore, in scintillation γ spectrometers, inorganic scintillators (e.g., NaI(Tl)) are preferable to organic ones (e.g., anthracene, stilbene), because the Z of inorganic scintillators is relatively high (e.g., iodine atom $Z = 53$). For the same reason, semiconductor γ spectrometers are made from germanium ($Z = 32$) rather than silicon ($Z = 14$). Another way to reduce the probability of a γ quantum escaping from the crystal is to increase the crystal dimensions (see Section 5.5). There are also other methods for reducing the Compton continuum (some of which are based on the use of coincidence or anti-coincidence devices).

If the detector thickness x is much smaller than the mean free path $1/\mu$ of a γ quantum (where μ is the attenuation coefficient of γ radiation), then the probability of multiple scattering of a γ quantum is small, so analytical expressions for the previously mentioned parameters can be derived. When there is a parallel beam of monoenergetic γ quanta, the total intrinsic efficiency of the detector is expressed by the formula

$$\varepsilon = 1 - \exp(-\mu x). \tag{5.6.7}$$

If electron-positron pairs are not formed (i.e., if the γ-quantum energy is less than 1.02 MeV), then the photopeak efficiency is expressed by the formula

$$\varepsilon_{\text{ph}} \approx 1 - \exp(-\mu_{\text{ph}} x); \tag{5.6.8}$$

here μ_{ph} is the **photoelectric absorption coefficient**—the part of the total attenuation coefficient μ that is due to the photoelectric effect. Substituting the theoretical expressions (5.6.7) and (5.6.8) for efficiency and photopeak efficiency into (5.6.6b), we find the theoretical expression for the photofraction:

$$P = \frac{\varepsilon_{\text{ph}}}{\varepsilon} \approx \frac{1 - \exp(-\mu_{\text{ph}} x)}{1 - \exp(-\mu x)}. \tag{5.6.9}$$

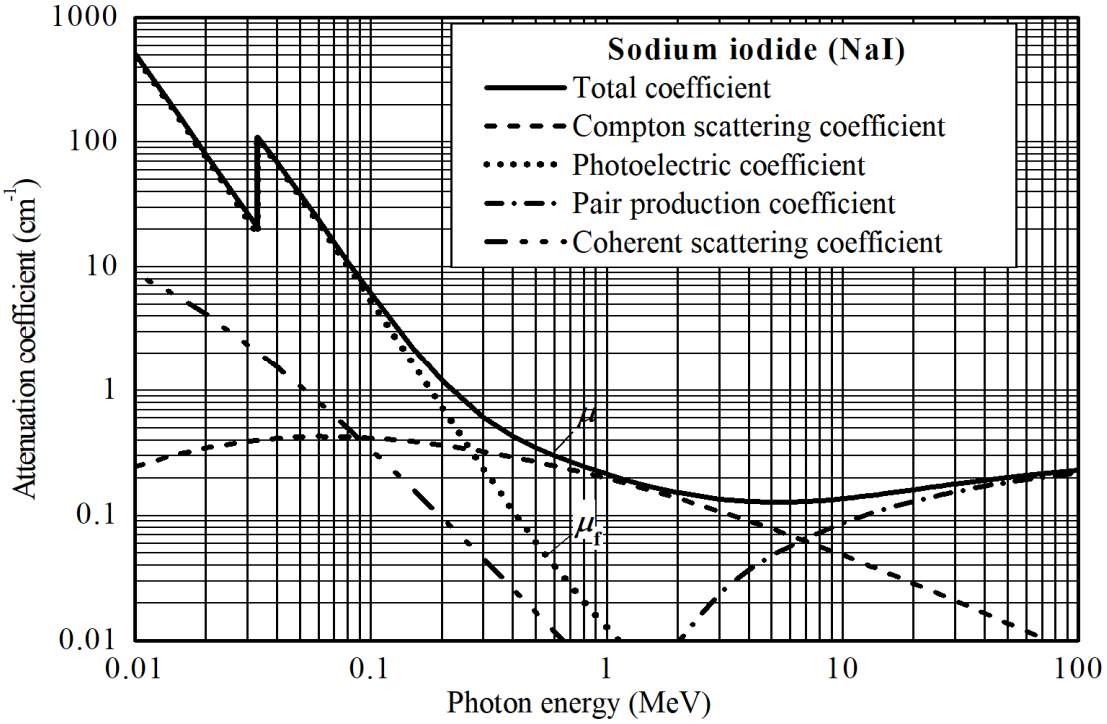


Fig. 33. Dependences of the attenuation coefficient of sodium iodide and its components on photon energy, using a logarithmic scale.

The dependences of the NaI(Tl) coefficients μ_{ph} and μ on the γ-quantum energy are shown in Fig. 33.

If the probability of interaction of a γ quantum with the detector material is high (in large-sized detectors), then the true values of the photopeak efficiency and photofraction are greater than those predicted by the theoretical Eqs. (5.6.8) and (5.6.9) (see Section 5.5). However, the total efficiency can be calculated using the formula $\varepsilon = 1 - \exp(-\mu x)$ regardless of the thickness x of the active region of the detector, because the total efficiency defines the probability of *at least one* interaction event, which is equal to $1 - \exp(-\mu x)$.

5.7. Energy Calibration of a Spectrometer

To determine the energy of γ quanta, it is not enough simply to measure the pulse-height spectrum and find the channel H_0 that corresponds to the full-energy absorption peak. One must also **calibrate** the spectrometer, i.e., assign a certain energy E to each channel H. The graph of the function $H(E)$ or $E(H)$ is called the **calibration curve**. For most spectrometers, the average pulse amplitude H is directly proportional to the energy loss E of the γ quantum in the detector, i.e.,

$$H \approx aE. \tag{5.7.1}$$

Thus, in the ideal case, the calibration curve is a straight line with intercept equal to zero. In such a case, the proportionality coefficient a can be determined using a single γ-radiation source of known energy (E_0): it suffices to measure the corresponding pulse-height spectrum and then divide H_0, the centroid of the full-energy absorption peak corresponding to energy E_0, by E_0:

$$a = \frac{H_0}{E_0}. \tag{5.7.2}$$

Substituting (5.7.2) into (5.7.1) and solving for E, we obtain:

$$E = \frac{E_0}{H_0} \cdot H. \tag{5.7.3}$$

6. Measurement methodology

6.1. Theory of the measurement method

6.1.1. Measurement schematic

The schematic diagram for studying Compton scattering is shown in Fig. 34. A radioactive cesium isotope ^{137}Cs serves as the source of photons (γ quanta). The radioactive material is enclosed in a steel capsule of dimensions 0.6 cm × 1 cm, which is placed inside a lead container of dimensions 7 cm × 8 cm with a narrow channel (collimator). The collimator forms a narrow beam of radiation that strikes a steel rod (radiation scatterer). Part of the photons are scattered in the steel rod. The scattered photons are detected by a scintillation detector.

The source can be positioned at various angles θ relative to the line connecting the scatterer and the detector, thereby "selecting" only γ quanta scattered at that specific angle. To reduce the influence of natural background, the detector is housed inside a cylindrical lead shield. To narrow the angular interval of the recorded scattered photons, a collimator is mounted in front of the detector and screwed into the lead shield.

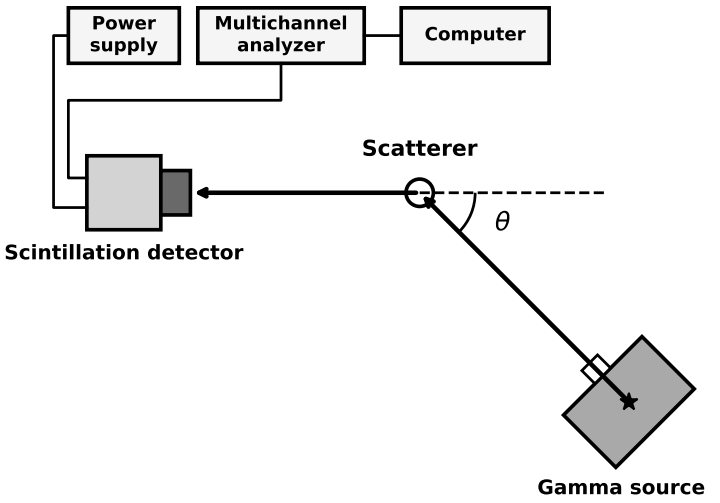


Fig. 34. Structural schematic of the experimental setup for studying Compton scattering.

In this work, the increase in the wavelength of scattered radiation (the Compton effect) is investigated at various scattering angles. The wavelength is determined from the position of the full-energy absorption peak in the spectrum of the scattered radiation. As the Compton scattering angle θ increases, the energy transfer to the Compton recoil electron increases (see the second equation of system (3.6.1)); therefore, the energy of the scattered photon decreases, i.e., its wavelength increases. This manifests itself as a shift of the full-energy absorption peak toward lower channel numbers (see Fig. 30).

Since the collimation is not ideal and the detector is located relatively close to the source (the maximum distance between the detector and the source is approximately 15 cm, and the dimensions of the scintillator are 3.8 cm × 5 cm), direct radiation from the gamma source also enters the detector along with the scattered radiation. This effect is particularly pronounced when the scattering angle θ is small, because then the thickness of the lead layer separating the source and the scintillator—measured along the lines connecting the radioactive sample capsule with various points on the scintillator surface—is smaller, and consequently the attenuation of primary radiation propagating in those directions in the lead shield is reduced. Although this phenomenon hinders the investigation of scattering at angles smaller than 40°, it is useful in another respect: the detector can be calibrated using the full-energy absorption peak of the primary radiation (see Section 5.7), since the energy of the photons emitted by ^{137}Cs is known (661.7 keV). In this work, the calibration spectrum is measured with the scatterer removed and the source placed at the smallest reachable angle, which is equal to 25°.

6.1.2. Calculation of the full-energy peak centroid by non-linear least squares fitting

To accurately determine the centroid of the full-energy absorption peak, a non-linear least squares fit must be performed using the sum of a Gaussian function and a background term. In the simplest case, the background term is a linear function (see Fig. 31); however, such an approximation is insufficiently accurate and severely limits the number of points that can be used in the fit. For example, if the experimental spectrum is like the one shown by a scatter plot in Fig. 35, then a fit consisting of the sum of a Gaussian function and a straight line could only be used between channel numbers 2600 and 3000, i.e., in the peak region, because elsewhere the spectrum is nearly constant and cannot be approximated by a decreasing straight line. A more flexible

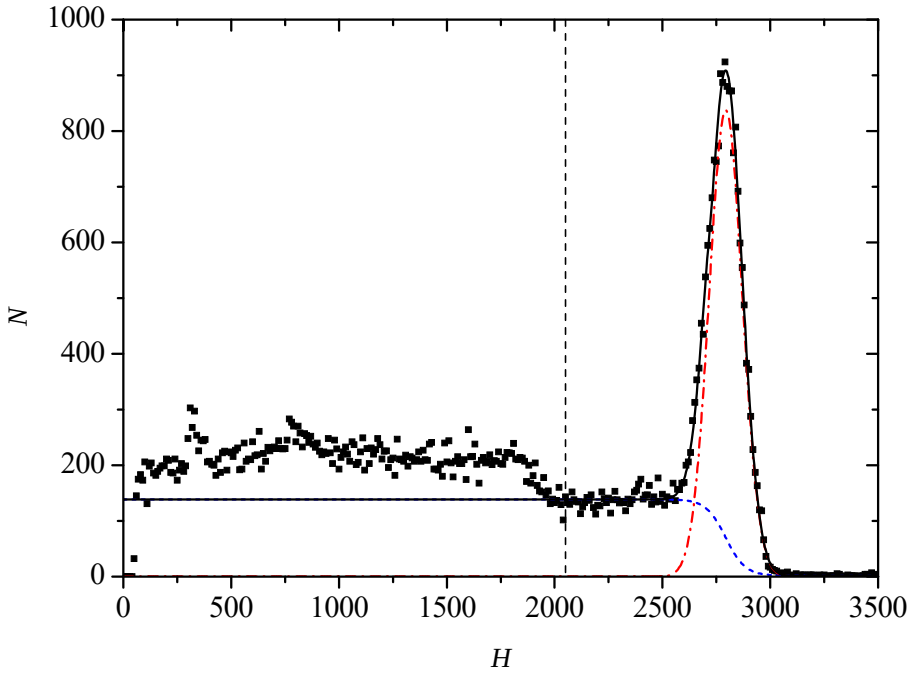


Fig. 35. Example of a calibration ^{137}Cs spectrum (individual points) and its fit by the sum of a Gaussian function and a sigmoid (solid line). The blue dashed line and the red dash-dotted line represent the two components of the fit: the sigmoid and the Gaussian function, respectively. The fit is performed over the interval $2050 \leq H \leq 3540$ (the left boundary of this interval is marked by the vertical dashed line), with a channel width equal to 10.

approximation for the background term is a sigmoid, which is defined as follows:

$$s(x) = \text{lower} + \frac{\text{upper} - \text{lower}}{1 + \exp\left(-\dfrac{x - \text{xmid}}{\text{wsig}}\right)}, \tag{6.1.1}$$

where the same notation for the four sigmoid parameters is used here as in the non-linear curve-fitting program "Fityk". As shown in Fig. 36, the parameters "upper" and "lower" are equal to the maximum and minimum values that the sigmoid approaches asymptotically as $x \to \pm\infty$, the parameter "xmid" is equal to the abscissa of the sigmoid's inflection point, and the parameter "wsig" determines how rapidly the sigmoid varies near its inflection point: in the interval xmid – |wsig| < x < xmid + |wsig|, the second term of the

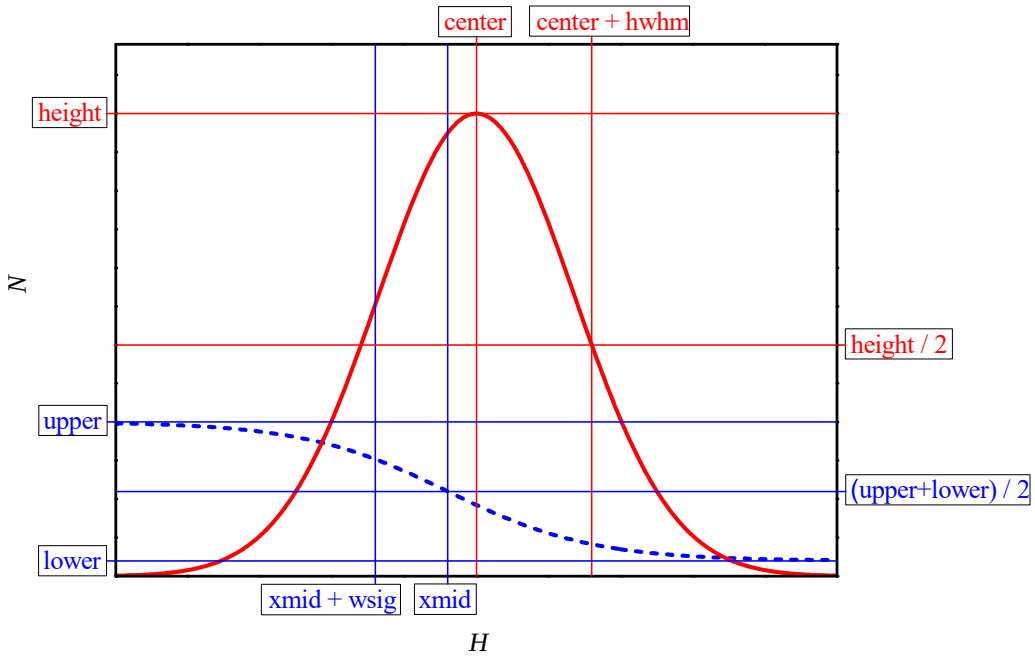


Fig. 36. Gaussian function (solid red line) and sigmoid (dashed blue line) along with their parameters.

sigmoid (the fraction in expression (6.1.1)) changes from $1/(1+\mathrm{e}) = 26.89\ \%$ of its maximum value (which is equal to upper – lower) to $1/(1+\mathrm{e}^{-1}) = 73.11\ \%$ of its maximum value. The direction of variation of the sigmoid is indicated by the sign of the parameter wsig: if wsig > 0, the sigmoid is increasing, whereas if wsig < 0, the sigmoid is decreasing. It is obvious that in the case of Fig. 35, the sigmoid must be decreasing (because the background value to the left of the peak is greater than to the right of it), and the region of steepest decrease must lie within the full-energy absorption peak region (because the background values on both sides of that peak are nearly independent of the channel number).

The definition of the Gaussian function (using the same parameter notation as in the program "Fityk") is:

$$g(x) = \text{height} \cdot \exp\left(-\ln(2) \cdot \left(\frac{x - \text{center}}{\text{hwhm}} \right)^2 \right). \tag{6.1.2}$$

The meaning of the three parameters of this function—"height", "center", and "hwhm"—is evident from Fig. 36: "height" is the height of the Gaussian peak, "center" is its centroid, and "hwhm" is the half-width of the peak at half maximum (the name of the latter parameter is an acronym standing for "*half width at half maximum*").

For this experiment, the most important parameter is "center", because it is proportional to the average energy of the photons incident on the detector. This parameter (as well as the other six parameters mentioned above) is calculated by fitting the measurement data (the pulse-height spectrum) with the sum of functions (6.1.1) and (6.1.2):

$$f(x) = s(x) + g(x) = \text{lower} + \frac{\text{upper} - \text{lower}}{1 + \exp\left(-\dfrac{x - \text{xmid}}{\text{wsig}} \right)} + \text{height} \cdot \exp\left(-\ln(2) \cdot \left(\frac{x - \text{center}}{\text{hwhm}} \right)^2 \right). \tag{6.1.3}$$

During this non-linear fitting, the minimum of the weighted sum of squared residuals ("SSR") is found with respect to the unknown parameters. Its definition is as follows:

$$\text{SSR} = \sum_{i=1}^{M} \left(\frac{f(x_i) - y_i}{\sigma_i} \right)^2, \tag{6.1.4}$$

where M is the number of data points (channels) used in the fit ($i = 1, 2, \ldots, M$), x_i are their x-values (abscissas of the channel centers), y_i are the corresponding Y-values (numbers of detector pulses, i.e., recorded photon counts), and σ_i are the standard deviations of those Y-values. If y_i are directly measured pulse counts N_i (as in Fig. 35), then

$$\sigma_i = \sqrt{y_i} = \sqrt{N_i} \tag{6.1.5}$$

(this is a property of the Poisson distribution). In this work, the scattered photon counts are measured by subtracting the photon counts b_i, measured without the scatterer, from the photon counts N_i, measured with the scatterer:

$$y_i = N_i - b_i. \tag{6.1.6}$$

According to the rules of mathematical statistics, the standard deviation of the difference of two random numbers is equal to the square root of the sum of the squares of the standard deviations of those two numbers. In this case, both counts follow a Poisson distribution, so the squares of their standard deviations are equal to N_i and b_i, respectively. Consequently, the standard deviation of the difference (6.1.6) is equal to

$$\sigma_i = \sqrt{N_i + b_i}. \tag{6.1.7}$$

During the fit, not only are the "optimal" parameter values (i.e., their values corresponding to the minimum of SSR) found, but also their standard deviations. In general, we will denote the parameters by p_j ($j = 1, 2, \ldots, J$, where J is the number of unknown parameters), and their standard deviations by δp_j. The standard method for calculating δp_j (e.g., see [5]) uses the matrix of second partial derivatives of SSR, whose elements are equal to

$$G_{jk} = \frac{1}{2} \frac{\partial^2 \text{SSR}}{\partial p_j \partial p_k}\bigg|_{\mathbf{p}=\mathbf{p}_0}, \tag{6.1.8}$$

where $\mathbf{p}$ is the set of unknown parameter values (a "parameter vector" having J components). The derivatives (6.1.8) are evaluated at the optimal parameter values ($\mathbf{p} = \mathbf{p}_0$), where SSR is at its minimum. If the theoretical

model is correct and if the residuals are independent and normally distributed, then the distributions of the parameter estimates are also Gaussian, and the standard deviation estimate for parameter No. j is

$$\delta p_j = \sqrt{[G^{-1}]_{jj}\,\mathrm{SSR}/(M-J)} \qquad (j = 1, 2, \ldots, J), \tag{6.1.9}$$

where G^{-1} is the matrix inverse to the matrix defined by equation (6.1.8) (the matrix G^{-1} is called the variance-covariance matrix).

Note: The presence of the factor $\mathrm{SSR}/(M-J)$ under the square root in expression (6.1.9) corresponds to the assumption that the statistical distributions of the deviations of the measured data from the fitted theoretical dependence (i.e., the differences $y_i - f(x_i)$) coincide with the error distributions of the experimental y-values. Then the weighting factors $(1/\sigma_i)^2$ in expression (6.1.4) determine only the *relative* weight of the i-th point, so δp_j does not change when all σ_i are multiplied by the same factor. Some programs that perform weighted fitting (i.e., minimizing expression (6.1.4)) calculate the parameter standard deviations δp_j without the factor $\mathrm{SSR}/(M-J)$. Then, multiplying all σ_i by the same factor changes all δp_j by the exact same factor.

During the nonlinear fitting, the sigmoid parameter "xmid" must be bounded from above so that it does not exceed the Gaussian function's centroid "center", because the Gaussian function is associated with the *full-energy* absorption of direct ^{137}Cs source photons in the scintillator, whereas the sigmoid reflects *partial* energy absorption of those photons. In the case of partial absorption, the amount of energy transferred to the scintillator is always smaller than in the case of full-energy absorption, and therefore the detector pulse amplitude must also be smaller (random deviations from this regularity are possible due to detector imperfection, i.e., due to the random component of pulse amplitudes, which manifests itself as finite energy resolution). In addition, the width of the transition region of the sigmoid ("width of the sigmoid" in short) cannot become less than the width of the Gaussian function, whereas the right edge of the sigmoid must approximately coincide with the right edge of the Gaussian, corresponding to decrease of the Gaussian term by half relative to its maximum value (as in Fig. 36). The sigmoid width corresponds to the interval of x values where the second term of the sigmoid (6.1.1) changes from 10 % to 90 % of its maximum value. The sigmoid width defined in this way is approximately equal to $4 \cdot |\mathrm{wsig}|$. Since the Gaussian width is equal to $2 \cdot \mathrm{hwhm}$, the following inequality must be satisfied: $|\mathrm{wsig}| \geq \mathrm{hwhm}/2$. However, the "Fityk" program allows defining bounds only in constant form (e.g., "wsig ≤ -100"). Therefore, the parameter "wsig" must be replaced with parameter "wsig_incr", whose meaning is the difference $|\mathrm{wsig}| - \mathrm{hwhm}/2$, and a lower bound equal to 0 must be defined for that parameter. In addition, the latter parameter must also be related to the Gaussian centroid, because, as mentioned, the right edge of the centroid must always coincide with the right edge of the Gaussian. In such a case, the equality $|\mathrm{wsig}| - \mathrm{hwhm}/2 = 0$ is equivalent to the equality xmid = center (i.e., when wsig_incr = 0, the abscissa of the sigmoid inflection point coincides with the Gaussian centroid). In other words, $2 \cdot$ wsig_incr is equal to the offset of the sigmoid inflection point to the left with respect to the Gaussian centroid. Thus, the two unknown parameters "wsig" and "xmid" must be replaced during the least squares fitting with a single non-negative parameter "wsig_incr", which is related to parameters "wsig" and "xmid" as follows:

$$\mathrm{wsig} = -(\mathrm{hwhm}/2 + \mathrm{wsig_incr}), \tag{6.1.10a}$$

$$\mathrm{xmid} = \mathrm{center} - 2 \cdot \mathrm{wsig_incr}. \tag{6.1.10b}$$

Because of those constraints, the total number of unknown parameters is reduced from 7 to 6.

6.1.3. Calculation of the confidence interval for the experimental wavelength

The energy E and standard deviation δE of radiation photons scattered at a given angle θ can be calculated once the centroid H and its standard uncertainty δH of the corresponding pulse-height spectrum peak are known. As mentioned in Section 6.1.2, these quantities are determined by least squares fitting (H is the parameter "center" of the Gaussian function (6.1.2)). To calculate E from H, the detector must be calibrated (see Section 5.7). Then E is calculated using formula (5.7.3). If the calibration spectrum centroid H_0 were known without error, then δE could be calculated in the same way as E, using δH instead of H, i.e., according to the formula $\delta E = (E_0/H_0)\delta H$. However, H_0 is also measured with a certain random error; therefore, δE must be calculated according to the rule for calculating the standard deviation of a function of several

random variables, whose general formulation is as follows: if a quantity f is a function of n independent arguments $x_1, x_2, \dots, x_n$, then the standard deviation (uncertainty) of the quantity f is equal to

$$\Delta f = \sqrt{\left(\frac{\partial f}{\partial x_1}\right)^2 (\Delta x_1)^2 + \left(\frac{\partial f}{\partial x_2}\right)^2 (\Delta x_2)^2 + \dots + \left(\frac{\partial f}{\partial x_n}\right)^2 (\Delta x_n)^2}, \tag{6.1.11}$$

where $\Delta x_1, \Delta x_2, \dots, \Delta x_n$ are the standard deviations (uncertainties) of the quantities $x_1, x_2, \dots, x_n$. In this case, "f" is E, and the arguments ("x_1" and "x_2") are H and H_0; therefore, from the general formula (6.1.11) and from the energy expression (5.7.3), the following expression for the standard deviation of the energy follows:

$$\delta E = E\sqrt{\left(\frac{\delta H}{H}\right)^2 + \left(\frac{\delta H_0}{H_0}\right)^2}, \tag{6.1.12}$$

where δH_0 is the standard uncertainty of the calibration spectrum centroid.

Knowing the standard deviation δE, one can calculate the **confidence interval**, i.e., an interval of E values centered at the experimental value E whose width is such that the true energy value would belong to that interval with a given probability α, provided the theoretical model used for fitting is valid (in other words, if the deviations of the fitted theoretical Y-values from the corresponding true values are purely random rather than systematic). The half-width ΔE of the confidence interval is equal to the product of the standard deviation δE and the Student's t-coefficient corresponding to the given confidence level α and the given number of degrees of freedom. The standard confidence level is 95 %, and the number of degrees of freedom is equal to the difference between the number of data points used in the fit and the number of unknown parameters. As the number of degrees of freedom increases, the Student's t-coefficient corresponding to a 95 % confidence level decreases, approaching 1.96. When the number of degrees of freedom is greater than 20, this Student's t-coefficient is approximately equal to 2. Since more than 30 points are used in the fits in this work (e.g., see Fig. 35), and the number of parameters of the fitting function (6.1.3) is 7, the number of degrees of freedom is greater than $30 - 7 = 23$. Consequently, the half-width of the 95 % confidence interval is approximately equal to twice the standard deviation:

$$\Delta E \approx 2\,\delta E. \tag{6.1.13}$$

The half-width of the confidence interval is called the **margin of error** (or **error bound**).

The wavelength of gamma radiation is related to the speed of light c and the radiation frequency ν by the relation:

$$\lambda = \frac{c}{\nu} = \frac{hc}{h\nu} = \frac{hc}{E}, \tag{6.1.14}$$

where h is Planck's constant. Therefore, the wavelength margin of error (according to the general formula (6.1.11)) is equal to

$$\Delta\lambda = \left|\frac{\mathrm{d}\lambda}{\mathrm{d}E}\right| \Delta E = \lambda\frac{\Delta E}{E}. \tag{6.1.15}$$

In other words, the relative wavelength error $\Delta\lambda/\lambda$ is equal to the relative photon energy error $\Delta E/E$.

6.2. Equipment and measurement procedure

This experiment uses a teaching equipment set manufactured by the German company "Phywe Systeme". A general view of the measurement setup is shown in Fig. 37. The equipment consists of:

1) a Scionix 38B51/2-X2 scintillation detector with a NaI(Tl) scintillator (scintillator crystal diameter 38.1 mm, height 50.8 mm), with a grounded cathode and a positively biased anode (unlike in Fig. 20),

2) a high-voltage power supply connected to the detector,

3) a multichannel analyzer connected to the detector and to a computer,

4) a ^{137}Cs gamma source whose activity in 1979 was 12.8 MBq $= 1.28 \cdot 10^7$ decays/s (the half-life of ^{137}Cs is equal to 30.04 years),

5) a computer with installed software for analyzing data from the multichannel analyzer.



Fig. 37. General view of the measurement setup.

The radioactive material is enclosed in a steel capsule of dimensions 0.6 cm × 1 cm, which is placed inside a lead container of dimensions 7 cm × 8 cm with a 12 mm diameter channel (collimator) into which a steel tube with an inner diameter of 5 mm is inserted.

The detector is housed inside a lead hood designed to reduce the influence of natural gamma background (emitted, e.g., by building materials in the walls of the room) and to absorb direct (unscattered) radiation coming from the gamma source. A collimator with a narrow slot is screwed onto the end of the hood (see Fig. 38). When measuring scattered radiation, this slot must be vertical (as in Fig. 38a), because then the uncertainty of the scattering angle θ is smallest. When measuring the calibration spectrum (see the last paragraph of Section 6.1.1), the collimator must be rotated by 90° so that the slot is horizontal (see Fig. 38b), because then the total thickness of the lead layer that photons traveling from the gamma source toward the scintillator must traverse is reduced, and therefore their absorption is decreased and the count rate increases.

Measurement procedure:

1. Turn on the computer to which the multichannel analyzer is connected.
2. Turn on the multichannel analyzer.
3. Turn on the high-voltage power supply. For the first few seconds, its display shows the device firmware version number, and then the last set voltage value appears. Immediately after turning it on, the indicator below the “HV on/off” button is unlit, and the decimal point on the display blinks. This means that the voltage value shown by the power supply is not yet connected to its output (i.e., to the detector). At this time, the voltage value can be changed using the “▲” and “▼” buttons in steps of 1 V. If the displayed value is not equal to 0.760 kV, set the voltage to 0.760 kV using those buttons.
4. Press the “HV on/off” button. The mentioned indicator lights up green. This means that the supply voltage is now connected to the detector (at this time, the voltage value cannot be changed using the “▲” and “▼” buttons).
5. Uncover the radioactive source container and place it on the holder, aiming the source collimator opening at the scatterer.
6. Launch the “Measure” program, which will record the pulse-height spectra of the detector.
7. By rotating the swivel arm (rotating platform) on which the gamma source holder is mounted, set the source to the position corresponding to the scattering angle $\theta = 25°$ (this is the smallest reachable scattering angle). The scattering angle is read from the scale on the arc-shaped brass strip attached to the base of the stand (see Fig. 37).

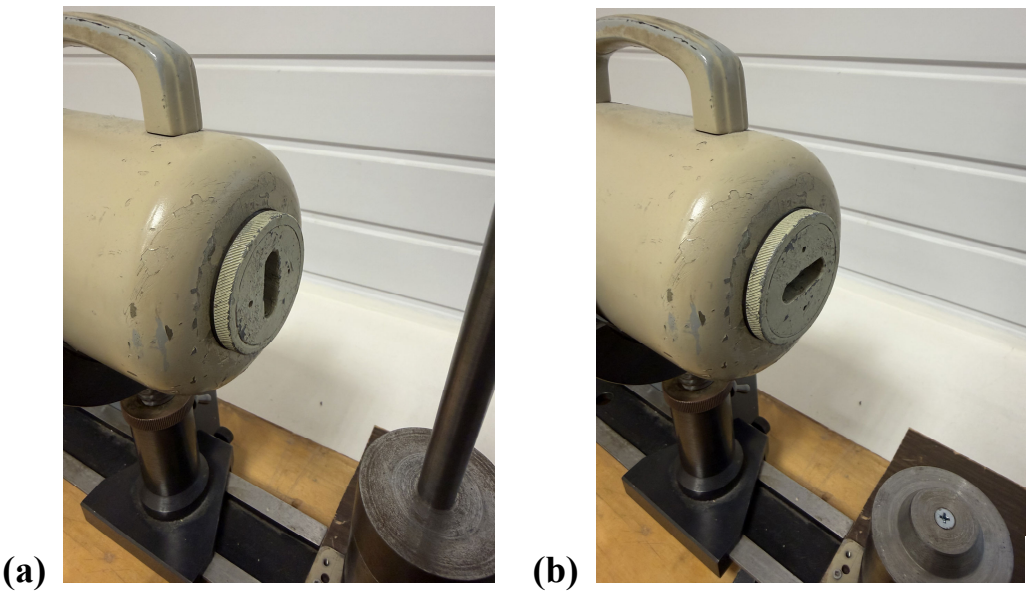


Fig. 38. Detector collimator: (a) collimator position when measuring scattered radiation (the steel rod used as the radiation scatterer is visible on the right); (b) collimator position when measuring direct (unscattered) radiation (for detector calibration). During this measurement, the scatterer is removed from the radiation beam.

8. Remove the scatterer (steel rod) from the radiation beam. Rotate the detector collimator so that the slot is horizontal (see Fig. 38b).

9. In the "Measure" program, set the amplification gain to 2 ("Gain level 2"), the channel width to 10 ("Interval width [channels]"), and the measurement duration to 300 s.

10. Measure the calibration gamma-ray spectrum for 5 min.

11. Once the calibration spectrum measurement is complete, click the "Accept data" button. The plot (histogram) of the calibration spectrum then appears in the main window of the "Measure" program.

12. Save the calibration spectrum data to a "Measure" data file (`*.msr`), which will be needed later for measurement data analysis. To do this, select the menu command "*File > Save measurement...*". *Note:* Lithuanian characters must not be used in file names (or in the names of folders containing those files), because otherwise the "Measure" program will not be able to open those files.

13. Rotate the detector collimator by 90° so that the slot is vertical (see Fig. 38a).

14. Rotate the swivel arm to the position corresponding to the scattering angle $\theta = 45°$. In the "Measure" program, set the channel width to 50.

15. Measure the spectrum for 5 min. Since there is no scatterer during this measurement, the measurement result is the "unwanted" spectrum component that will later need to be subtracted from the spectrum measured with the scatterer. This component consists of natural ambient background, direct (unscattered) source radiation, and source radiation scattered in all other objects (other than the steel rod), e.g., in the walls of the room and in the components of the experimental setup. For brevity, this unwanted spectrum component will henceforth be referred to as the "background".

16. Once the background spectrum measurement is complete, click the "Accept data" button. The plot of the background spectrum then appears in the main window of the "Measure" program. Since in the next step this spectrum will be combined with another plot, modify the plot format (to make it easier to visually distinguish the two spectra that will be displayed in a single graph window): **(a)** select the menu command "*Measurement > Display options...*" (or press the "F2" key), **(b)** in the dialog box that opens, select the "Channels" tab, **(c)** in the "Title:" text box, enter the spectrum name "Background_45deg" (or similar), **(d)** in the "Interpolation:" list box, select the "straight lines" item, **(e)** click the "OK" button.

17. Save the background spectrum data to a "Measure" data file (`*.msr`), which will be needed later for measurement data analysis. To do this, select the menu command "*File > Save measurement...*".

18. Place the scatterer in front of the detector. Measure the total spectrum (the sum of the background and scattered radiation spectra) for 5 min.

19. Once the total spectrum measurement is complete, repeat step 16 with the following three modifications: **(a)** the spectrum name must be "Total_45deg" or similar, **(b)** change the line width (so that the total and background spectra are plotted with lines of different thickness), i.e., in the "Line width:" list box, select the second line plot from the top (then the total spectrum will be plotted with a thicker line than the background spectrum), **(c)** change the line color (so that the total and background spectra are plotted with lines of different colors), i.e., click the "..." button located in the "Display options" dialog box next to the "Color:" label, then in the "Color" dialog box that opens, click on the black rectangle and click "OK" (then the total spectrum will be plotted with a black line, while the background will be plotted with the default color line, i.e., red).

20. Load the background spectrum into the same window that contains the total spectrum: **(a)** select the menu command "*Measurement > Adopt channel...*", **(b)** in the "Channel:" list box of the dialog box that opens, select the background spectrum name that was entered in step 16c ("Background_45deg"), **(c)** click the "OK" button. The second spectrum then appears in the current window. It is important to note that in the "Measure" program, the *Y*-axis is associated with only *one* spectrum. If a graph window contains more than one spectrum, then the *Y*-axis limits of all spectra must be defined separately for each spectrum so that the *Y*-axis range is identical for all spectra. If this is not done, all spectra will be automatically displayed such that the minimum and maximum *Y*-values of the curve representing the spectrum correspond to the bottom and top edges of the plotting area, *even if the displayed Y-axis limits do not match the actual limits of that spectrum*. After loading the background spectrum data, the displayed *Y*-axis limits automatically become equal to the boundary values of the background, i.e., they change, whereas the curve representing the total spectrum does not change and no longer corresponds to the numbers written at the *Y*-axis tick marks. To ensure that those numbers apply equally to both the total spectrum and the background spectrum, perform the following actions: **(d)** select the menu command "*Measurement > Display options...*" (or press the "F2" key), **(e)** in the dialog box that opens, select the "Channels" tab, **(f)** in the two fields located next to the "Displayed area:" label, enter the minimum and maximum *Y*-axis values, which *must be identical for both spectra* (the spectrum is selected in the top "Channels" list). The optimal upper *Y*-axis limit is the maximum *Y*-value of the total spectrum, and the optimal lower limit is 0. That is, copy the number from the maximum field of the total spectrum's *Y*-axis into the corresponding field of the background spectrum, and enter the number 0 into the minimum field of both spectra. Then click the "OK" button.

21. Save the data of the total and background spectra to a "Measure" data file (`*.msr`), which will be needed later for measurement data analysis. To do this, select the menu command "*File > Save measurement...*" (the file can be named, e.g., "45deg.msr"). After performing this action, the file with the background spectrum data that was created in step 17 is no longer needed (since those same data have already been transferred to another file), so the file with the background spectrum data can be deleted (before doing so, the corresponding graph window must be closed).

22. Repeat the measurements of the background spectrum (without the scatterer) and the total spectrum (with the scatterer) (i.e., steps 15–21) for six more scattering angles, increasing the angle in 15° increments. That is, these measurements must be performed for a total of seven angles: 45°, 60°, 75°, 90°, 105°, 120°, and 135°. For the last four angles (from 90° to 135°), reduce the channel width from 50 to 20. *Note:* After changing the angle, the background must be measured anew, because, as mentioned, one of the background components is source radiation (direct or scattered in surrounding objects), whose spectrum depends on the position of the source.

23. Once the measurements are finished, remove the radioactive source container from the holder and cover it. Turn off the high voltage (i.e., press the "HV on/off" button on the power supply so that the indicator below it turns off), then turn off the power supply and the multichannel analyzer from the mains.

24. Save all eight `*.msr` files that were created while performing steps 12 and 21 to a USB flash drive or store them in online storage (e.g., via e-mail, etc.). In addition, save each plot to an "Enhanced Metafile" format file (`*.emf`): **(a)** select the "Measure" program menu command "*Measurement* > *Export data*", **(b)** in the "Export data" dialog box that opens, check the "Save to file" and "Export as metafile" radio buttons and click the "OK" button, **(c)** in the "Save As" dialog box that opens, type the file name (including the extension ".emf") and click the "Save" button. Insert the latter files into a single Word file (2–4 plots per page). Print that file (you may use the printer located in the laboratory). The laboratory supervisor or teaching assistant signs the sheets with the printed plots.

25. At the beginning of data analysis, it will be necessary to calculate the difference between the total and background spectra as well as its standard deviation, which is equal to the square root of the sum of the total and background spectra (see formula (6.1.7)). Since the data are saved in `*.msr` format, the "Measure" program will be needed at this stage. This program is free (its download link is at the beginning of the next section). However, if you do not intend to install the "Measure" program on your computer, you can save those data in text files (`*.txt`) now. How to do this is explained below. If you intend to install the "Measure" program on your computer later, then this step can be skipped, because the `*.txt` files can be generated later using menu commands of the "Measure" program (all the data analysis instructions are given in the next section). **(a)** In the main window of the "Measure" program, select the menu command "*Measurement* > *Export data*", **(b)** in the "Export data" dialog box that opens, check the "Save to file" and "Export as numbers" radio buttons and click the "OK" button, **(c)** in the "Save As" dialog box that opens, type the file name (including the extension ".txt") and click the "Save" button. A text file with three columns will then be created: the first column contains the X-coordinates of the center of each histogram interval ("channel"), and the other two columns contain the corresponding pulse counts of the total and background spectra. In the case of the calibration spectrum, there will be only two columns: the channel center and the pulse count. Save all eight `*.txt` files with the spectrum data to a USB flash drive or store them in online storage (e.g., via e-mail, etc.) for further analysis.

A separate description of the measurement procedure, which is much more detailed than the one presented here, is located next to the measurement equipment. That description should be used only during the measurement. After finishing the measurements, it must be left next to the measurement equipment. When preparing for the lab work, it is not necessary to know all the details of the measurement procedure. If the measurement procedure instructions presented earlier do not match the instructions given in the detailed description, then the detailed description must be followed during the measurement.

6.3. Analysis of measurement data

Before fitting the spectra (see Section 6.1.2), text files must be created in which the spectrum data are presented in columns: the first column contains the X-coordinates of the centers of all histogram bins (channels), the second column contains the pulse counts (for the calibration spectrum) or the difference between the total and background pulse counts (for the scattered radiation spectra), and the third column contains the standard deviation of the difference mentioned above, i.e., the square root of the sum of the total and background pulse counts (the third column is required only for the scattered radiation spectra). If the data are saved in `*.msr` format, then this data transformation can be performed using the capabilities of the "Measure" program. This program can be downloaded from the website of the German company "PHYWE" (link: https://phywe-itemservice.s3.eu-central-1.amazonaws.com/sites/DMS-Phywe/PROD/de-DE/item/phy_itemsoftware/14/14452-61/SETUPM.EXE). After installing the "Measure" program, a "measure activation assistant" window appears, in which you must click the "Exit" button. Subsequent steps are described in the next subsection. If the measurement data are already saved in text files (see step 25 of the previous section), then the difference between the two spectra and the square root of their sum can be calculated by loading those files into any other data analysis program (e.g., Excel) and using its capabilities. In that case, Section 6.3.1 can be skipped, and you can proceed directly to Section 6.3.2.

6.3.1. Generation of the text file with initial approximation data in “Measure”

To generate a text file (`*.txt`) from the calibration spectrum `*.msr` file, it suffices to open the latter file using the “Measure” program menu command “*File > Open measurement...*” and execute the menu command “*Measurement > Export data...*”, as explained in step 25 of the previous section. Below is a description of how to generate the text files required for fitting from the `*.msr` files containing the scattered radiation spectrum measurement data:

1. Open the initial file (created while performing step 21 of the previous section) using the “Measure” program menu command “*File > Open measurement...*”.
2. Select the menu command “*Analysis > Channel modification...*”. The “Channel modification” dialog box then opens, whose initial appearance is shown in Fig. 39a. At the top are the definitions of the variables that can be used in arithmetic operations. For example, in the case of Fig. 39a, the symbol “Imp2” denotes the background pulse count. In the next list box (which initially contains the word “[off]”), select the other spectrum contained in the same file, i.e., “Total_45deg”. The dialog box then takes the appearance shown in Fig. 39b.
3. Check the radio button located next to the label “f :=”, and in the text field to the right of it, type the arithmetic operation “Imp1-Imp2” (see Fig. 39c).
4. Check the “add new y-channel” radio button, and in the “Title:” field, type the name of the new spectrum (e.g., “Difference_45deg”, as shown in Fig. 39c).
5. Click the “Calculate” button. A new (third) curve representing the difference of the spectra then appears in the graph window.



Fig. 39. The “Channel modification” dialog box of the “Measure” program: (a) initial appearance of the window (only one operand “Imp2” is defined); (b) appearance of the window after defining the second operand (“Imp1”); (c) final appearance of the window before calculating the difference between the total and background spectra; (d) final appearance of the window before calculating the standard deviation of the difference, i.e., the square root of the sum of the total and background spectra.

6. Select the menu command "*Analysis* > *Channel modification...*" again. Now, at the top of the "Channel modification" dialog box, you may see a new variable symbol "Imp3" corresponding to the calculated difference of the two spectra; however, since no operations will be performed with it, select one of the two initial spectra instead, and in the second list box select the other initial spectrum. Since you now need to calculate the standard deviation of the difference between the total and background spectra, which is equal to the square root of the sum of those two spectra, type the text "sqrt(Imp1+Imp2)" in the "f :=" field. The name of the new dependence can be, e.g., "Error_45deg" (see Fig. 39d).

7. Click the "Calculate" button. A new (fourth) curve representing the standard deviation of the spectrum difference then appears in the plot window.

8. Since only *all* data in the plot can be exported to a text file at once, and only the two calculated dependences (the difference of the spectra and the square root of their sum) are needed, the two initial spectra must be deleted. To do this, select the menu command "*Measurement* > *Delete channel...*", highlight one of the two spectra ("Total_45deg" or "Background_45deg") in the list, and click "OK", then select "*Measurement* > *Delete channel...*" again to delete the second initial spectrum in the exact same way.

9. Export the plot data to a text file as explained in step 25 of the previous section. To avoid losing the data of the two initial spectra, close the plot window without saving changes or select the menu command "*File* > *Save measurement as...*" and save the `*.msr` file under a different name. Do not select the menu command "*File* > *Save measurement...*", because then all changes would be written into the existing file, the data of the two initial spectra would be lost, and it would no longer be possible to repeat the calculations (e.g., if a mistake were noticed later).

6.3.2. Calculation of the calibration spectrum peak centroid by non-linear least squares fitting

Curve fitting can be performed using various data analysis programs that provide non-linear fitting capabilities. Below is a description of how to perform the fit using the data analysis program "Fityk". This program is free and can be downloaded from the website https://fityk.nieto.pl/.

1. Launch the "Fityk" program and select the menu command "*Data* > *Quick Load File*". A file selection dialog box then opens, an example of which is shown in Fig. 40. At the bottom of the window, the check box "data weighting: $\sigma = \max(\sqrt{y}, 1)$" (see Fig. 40) must be checked, which enables calculation of the standard deviation according to Eq. (6.1.5).

2. In that dialog box, select the text file containing the calibration spectrum data and click the "Open" button (see Fig. 40).

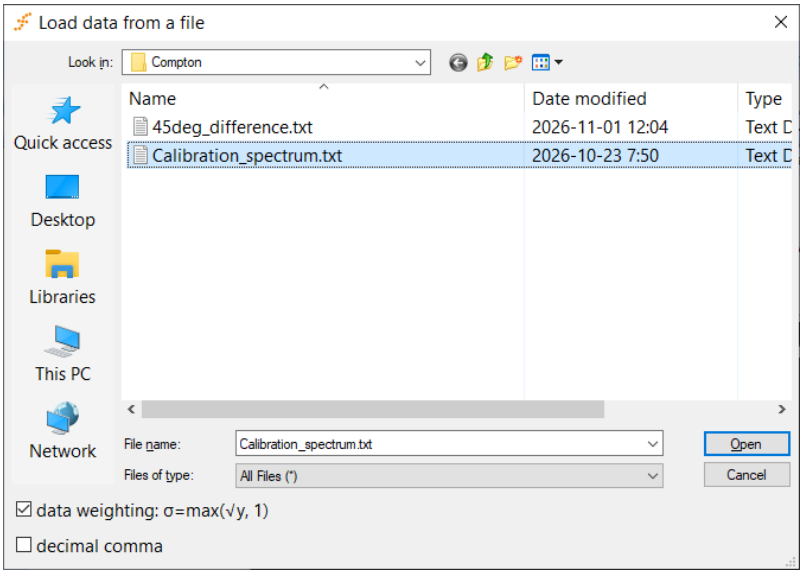


Fig. 40. Data file selection dialog box of the "Fityk" program.

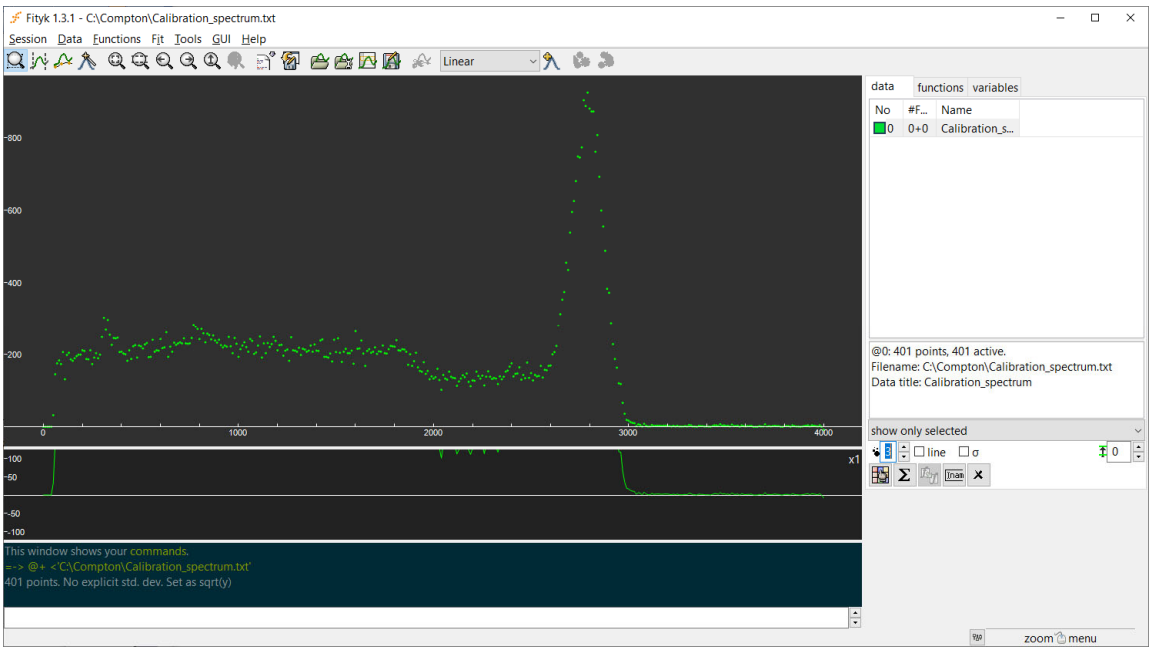


Fig. 41. Main window of the "Fityk" program after loading the calibration spectrum data.

3. Once the data plot window opens (e.g., see Fig. 41), you can change the size of the data points using the spin control located in the lower-right part of the window (in Fig. 41, the selected point size is 3). This spin control is visible only when the "data" tab is selected in the upper-right corner (see Fig. 41).

4. Set the *X*-axis fitting interval. To do this, click the second toolbar button "" (see Fig. 41). Then drag the mouse across the plot window while holding down the right mouse button. Points whose *X*-values the mouse passes over will be excluded from the fitting region (those points turn gray in the plot). To restore points back into the fitting region, drag the mouse while holding down the left mouse button. In this way, define a fitting interval that encompasses the entire peak located at the right edge of the spectrum, plus another 50–60 points on both sides of that peak (the latter points must be chosen such that their *Y*-values are approximately equal, apart from random variations). In Fig. 41, the optimal fitting interval is approximately $2000 < x < 3500$. The selected interval is displayed on the right side of the main window after the words "Active data range" (in Fig. 42, that interval is $2050 \le x \le 3540$).

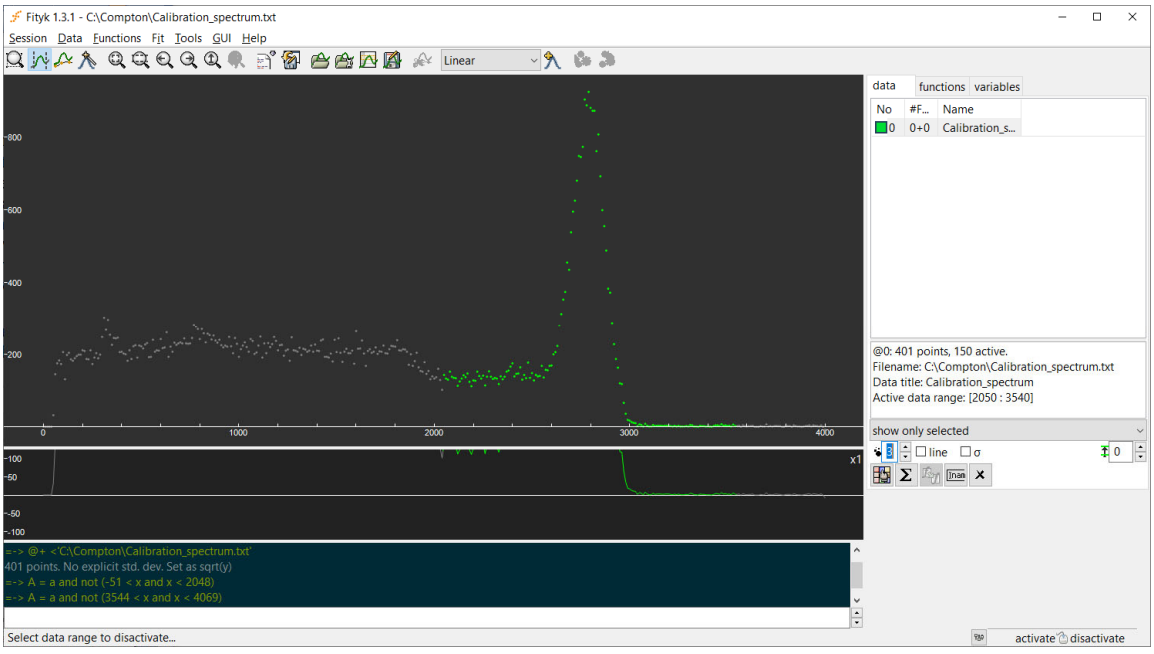


Fig. 42. Main window of the "Fityk" program after marking the points to be used in the fit.

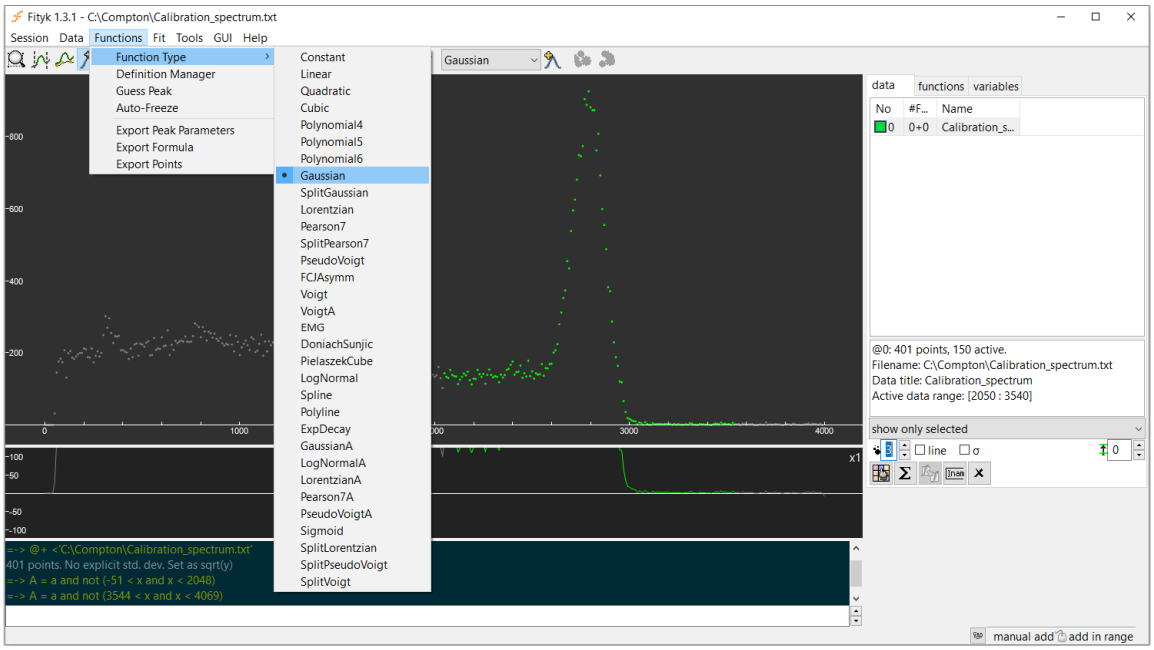


Fig. 43. Fitting function selection menu of the "Fityk" program.

5. Define the fitting function. To do this, click the fourth toolbar button "" and select the "Gaussian" function from the function list that opens when selecting the menu command "*Functions* > *Function Type*" (see Fig. 43). Next, set the initial parameter values of the Gaussian function. To do this, place the mouse cursor near the top of the peak, press and hold the left mouse button, and drag the mouse to the left or right by a distance approximately equal to the half-width at half maximum of the peak. Then release the left mouse button. A yellow line representing the initial Gaussian function appears in the plot (see Fig. 44). Three fields with the initial parameter values of the Gaussian function (6.1.2) appear in the lower-right corner of the window (see Fig. 44).

6. Since the fitting function is the sum of a Gaussian function and a sigmoid (6.1.3), you must also define the second term of the fitting function—the sigmoid (6.1.1). To do this, select the menu command "*Functions* > *Function Type*" again, but this time click "Sigmoid" in the function list (in Fig. 43, it is the fourth item from the bottom). Next, set the initial parameter values of the sigmoid. To do this,

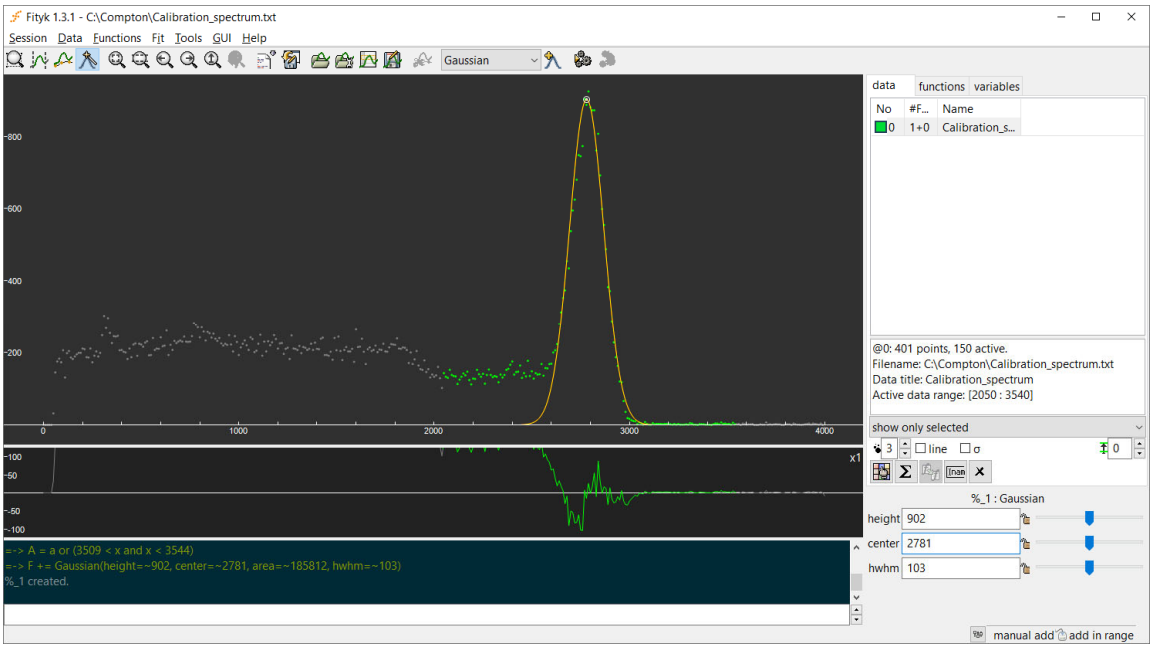


Fig. 44. Main window of the "Fityk" program after defining the initial parameter values of the Gaussian function.

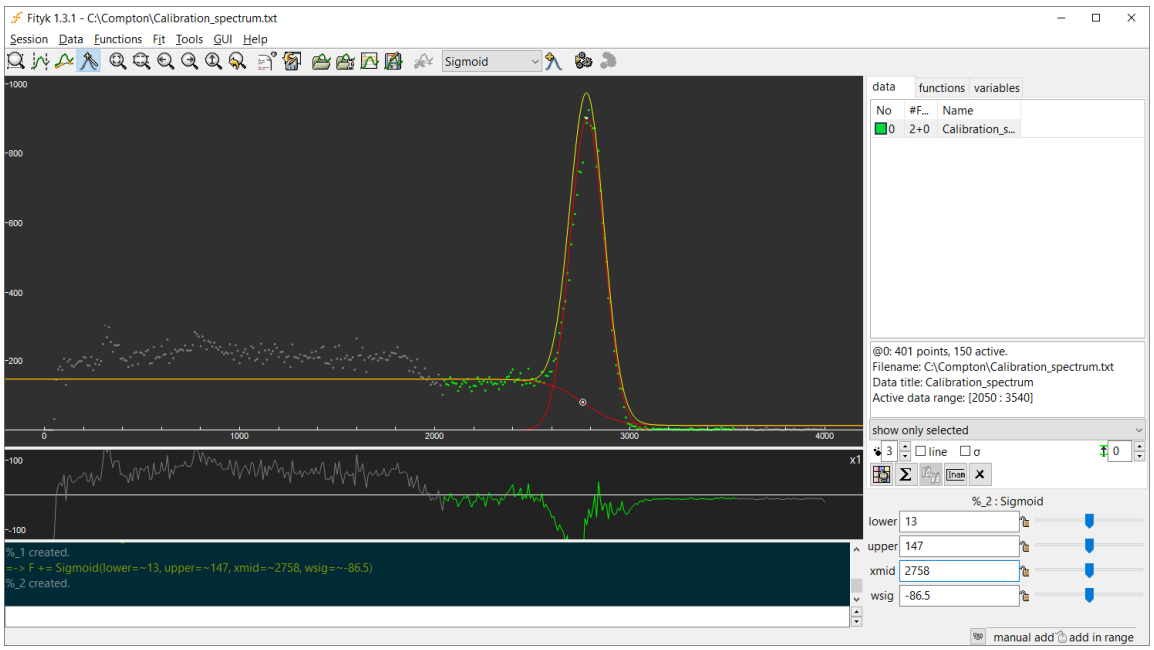


Fig. 45. Main window of the "Fityk" program after defining the initial parameter values of the sigmoid.

place the mouse cursor near the inflection point of the sigmoid (in the region of the Gaussian peak, near the base of the peak) and, while holding down the left mouse button, drag the mouse to the right and downward to the minimum of the sigmoid (in the sigmoid expression (6.1.1), the minimum is equal to the parameter "lower", which in this case should be close to zero). After releasing the left mouse button, three lines are visible in the plot: the two red lines correspond to the Gaussian function and the sigmoid, while the yellow line corresponds to their sum (see Fig. 45). Four fields with the initial parameter values of the sigmoid (6.1.1) appear in the lower-right corner of the window (see Fig. 45).

7. As explained at the end of Section 6.1.2, two parameters "wsig" and "xmid" must be replaced by a single non-negative parameter "wsig_incr", which couples the sigmoid's shape (position and width) to the Gaussian function's position and width according to Eqs. (6.1.10a) and (6.1.10b). This is done using the command line of the "Fityk" program (at the bottom of the main window): **(a)** in the command line, type the command "`$wsig_incr = ~20 [0:2000]`" and press the "Enter" key ("`$wsig_incr`" is the name of the above-mentioned new parameter, the symbol "`~`" means that the parameter "`$wsig_incr`" must be one of the unknown parameters whose values are calculated during the fit, "20" is its initial value, and the text "`[0:2000]`" sets its domain interval—from 0 to 2000), **(b)** in the upper-right corner of the main window, select the "functions" tab so that the identifiers of both functions used (the Gaussian function and the sigmoid) are visible (as shown in Fig. 46, the function identifiers are listed in the "Name" column, and in this example they are "`_1`" and "`_2`", respectively, but they may be different depending on how many times and in what order fitting functions were selected or removed), **(c)** in the command line, type "`%_2.wsig = -(%_1.hwhm / 2 + $wsig_incr)`" (here "`_2`" and "`_1`" are the identifiers of the sigmoid and Gaussian functions) and press the "Enter" key (this command sets the calculation method for the sigmoid's parameter "wsig": wsig $= -(\text{hwhm}/2 + \$\text{wsig_incr})$), **(d)** in the command line, type the command "`%_2.xmid = %_1.center - 2 * $wsig_incr`" and press the "Enter" key (this command sets the calculation method for the sigmoid's parameter "xmid": xmid $=$ center $- 2 \cdot \$\text{wsig_incr}$). The value of the parameters "wsig" and "xmid" visible in the lower-right corner of the window then change (e.g., in the case of Fig. 46, they become equal to $-(103/2 + 20) = -71.5$ and $2781 - 2 \cdot 20 = 2741$). Moreover, it is no longer possible to change those values manually (the background of the corresponding text fields turns gray).

8. The final step before fitting is changing the fitting method. To do this, select the menu command "*Fit > Method > Lev-Mar (from MPFIT)*" (see Fig. 46). The default method of the "Fityk" program is the first one in the list ("Lev-Mar (own)"), but it has been observed that it does not always work properly when parameters "wsig" and "xmid" are constrained (see the previous step). The second method in the list has been tested without any issues, so it is advisable to select this method, as shown in Fig. 46.

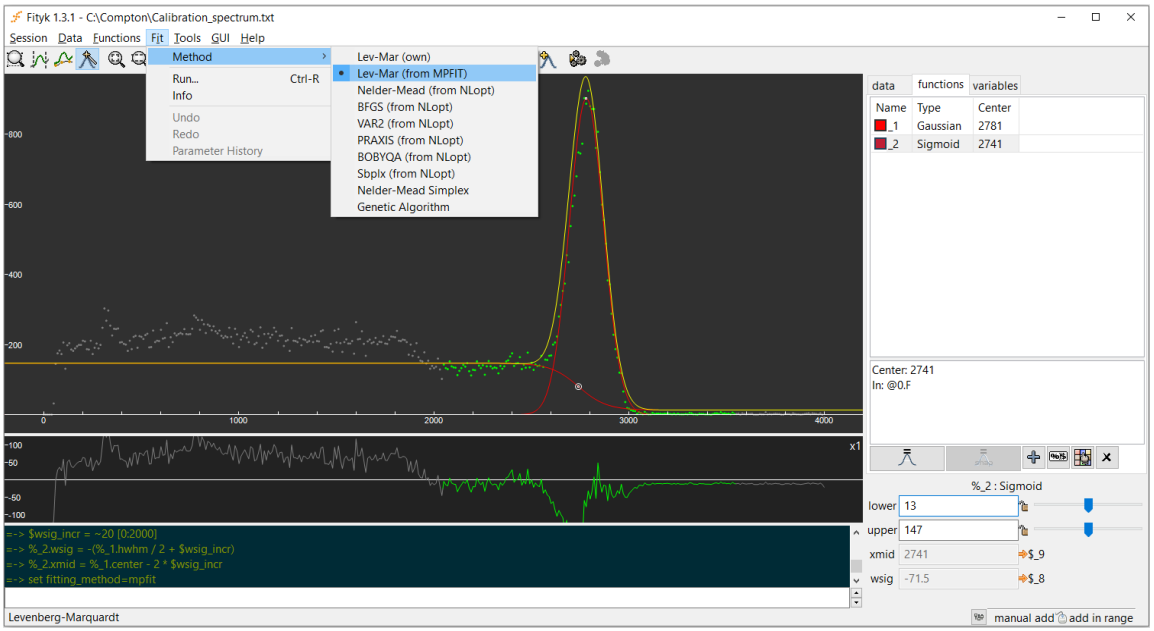


Fig. 46. Selection of the fitting method in the "Fityk" program.

9. Fitting is started by clicking the next-to-last toolbar button "". After one click, several iterations are performed, the parameter values change, and the curves displayed in the plot window change accordingly (see Fig. 47a). Usually this is sufficient; however, to ensure that the program has found the minimum of the sum of squared residuals, you may click the same button "" a few more times until a message appears at the bottom of the program window stating that the parameters did not change because the sum of squared residuals could not be reduced any further (see Fig. 47b).

10. Once the fit is complete, write down its most important results—the centroid of the Gaussian function and its standard deviation. To do this, select the menu command "*Fit* > *Info*". The "Fit Info" window then opens, containing the values of all parameters and their standard deviations (see Fig. 48). If the parameter "xmid" had not been bounded (see step 7), then the second line of the dialog box shown in Fig. 48 would display the name of the Gaussian function's centroid "`%_1.center`". Because the previously mentioned bound was defined, that centroid is also used in the definition of the sigmoid's parameter "xmid" (xmid = center – $midoffset), so instead of the parameter name, the label "`(2 refs)`" is displayed. Consequently, in the case of Fig. 48, the final calibration spectrum Gaussian

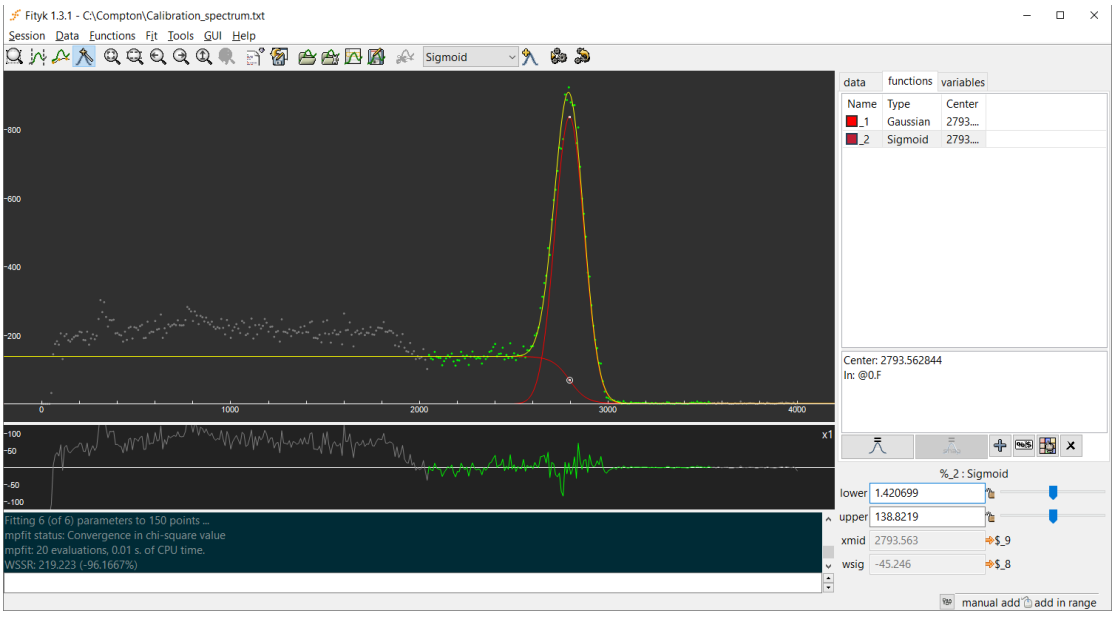


Fig. 47. The "Fityk" program window after the first fitting cycle.

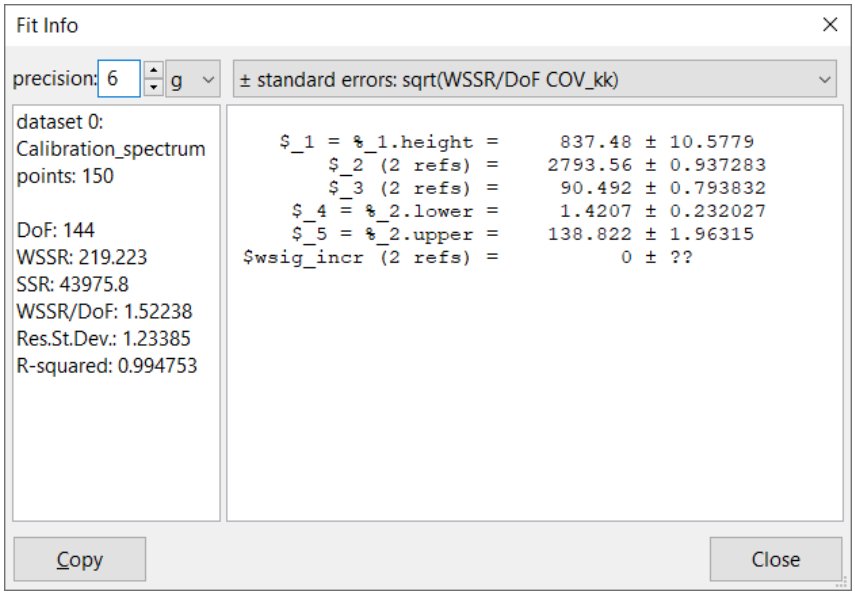


Fig. 48. The "Fit Info" dialog box of the "Fityk" program after completing the calibration spectrum fit.

centroid (H_0) is equal to 2793.06, and its standard deviation (δH_0) is equal to 1.08701.

11. The file containing all fitting data and results (`*.fit`) is saved using the menu command "*Session* > *Save Session...*" (later, that file can be opened using the menu command "*Session* > *Load Session*"). To save all previously entered commands, select "*Save History...*" instead of "*Save Session...*". In the latter case, instead of the data and final results, the sequence of entered commands is written into the `*.fit` file, and when opening that file, all those commands are executed automatically (since one of those commands is loading the initial data file, in that case you must ensure that the data file has not been deleted or renamed).

6.3.3. Calculation of the scattered spectrum peak centroid by non-linear least squares fitting

Fitting the scattered radiation spectra is very similar to fitting the calibration spectrum described in the previous subsection. There are only three differences:

A. The scattered spectrum data are saved in text files with *three* columns. The second column contains the difference between the total and background spectra, and the third column contains the standard deviation of the difference, which is equal to the square root of the sum of the total and background spectra (see Eq. (6.1.7)). Therefore, when loading data into "Fityk", you can no longer use the automatic standard deviation calculation option; instead, you must specify to the program that the standard deviations are located in the third column of the data file.

B. The histogram bin widths of the scattered spectra are equal to 20 or 50, i.e., two or five times larger than the histogram bin width of the calibration spectrum. Furthermore, as the scattering angle increases, the energy of the scattered photons decreases, i.e., the spectrum narrows. Both of these factors manifest themselves in a smaller number of data points used in the fit compared to the calibration spectrum. Therefore, the number of "extra" points on both sides of the full-energy absorption peak that must be included in the fitting interval is also several times smaller (those points are important for calculating the parameters of the sigmoid-shaped term (6.1.1)).

C. The sigmoid parameter "lower" (see the definition of the sigmoid (6.1.1)) is known in advance in the case of the scattered spectrum: it is equal to 0, because this term approximates the counts of recorded photons whose energy is greater than the energy of the scattered photons, and those counts cancel out after subtracting the background spectrum from the total spectrum (only random deviations from 0 remain). Consequently, the number of unknown parameters is one fewer than in the case of the calibration spectrum.

Below is a description of how to fit the scattered radiation spectra using the data analysis program "Fityk", highlighting the steps that differ from the corresponding steps in Section 6.3.2 when fitting the calibration spectrum (step numbers have not been changed):

1. Launch the "Fityk" program and select the menu command "*Data* > *Load File*" (instead of the "*Quick Load File*" command that was used for the calibration spectrum). The "Load Data" dialog box then opens, an example of which is shown in Fig. 49. Check the "σ" radio button located at the bottom of this dialog box (see Fig. 49). This instructs the program that the standard deviation values should not be calculated automatically, but rather read from the third column.

2. In the upper-left panel of the "Load Data" dialog box, select the text file containing the scattered radiation spectrum data and click the "Replace @0" button (see Fig. 49). Then close the "Load Data" dialog box (it does not close automatically).

3. Once the data plot window opens (e.g., see Fig. 50), you can change the size of the data points using

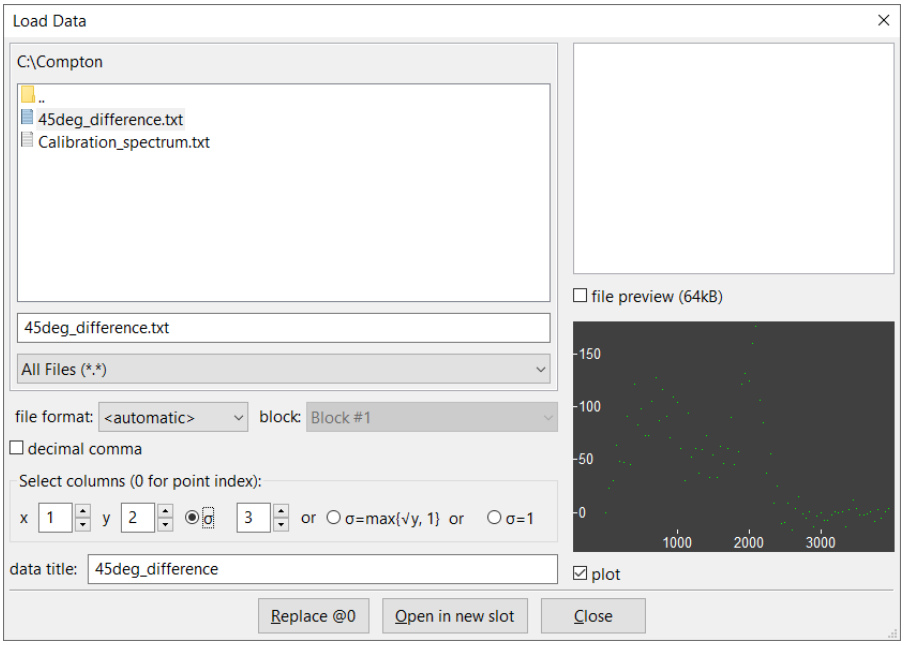


Fig. 49. The "Load Data" dialog box of the "Fityk" program.

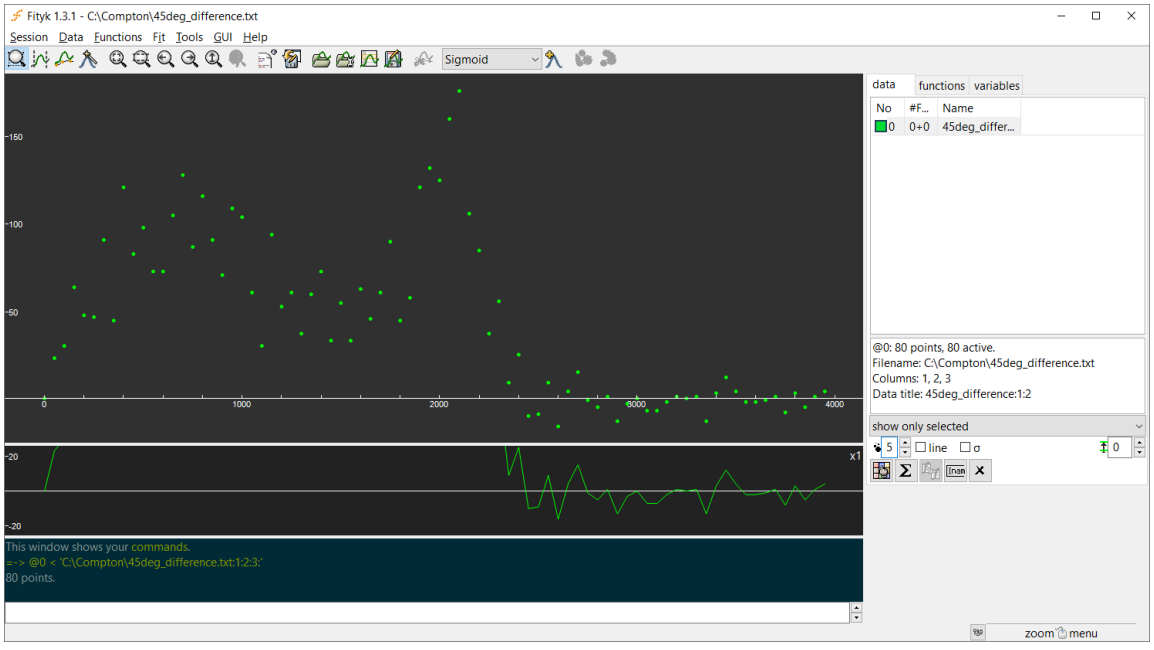


Fig. 50. Main window of the "Fityk" program after loading the scattered radiation spectrum data.

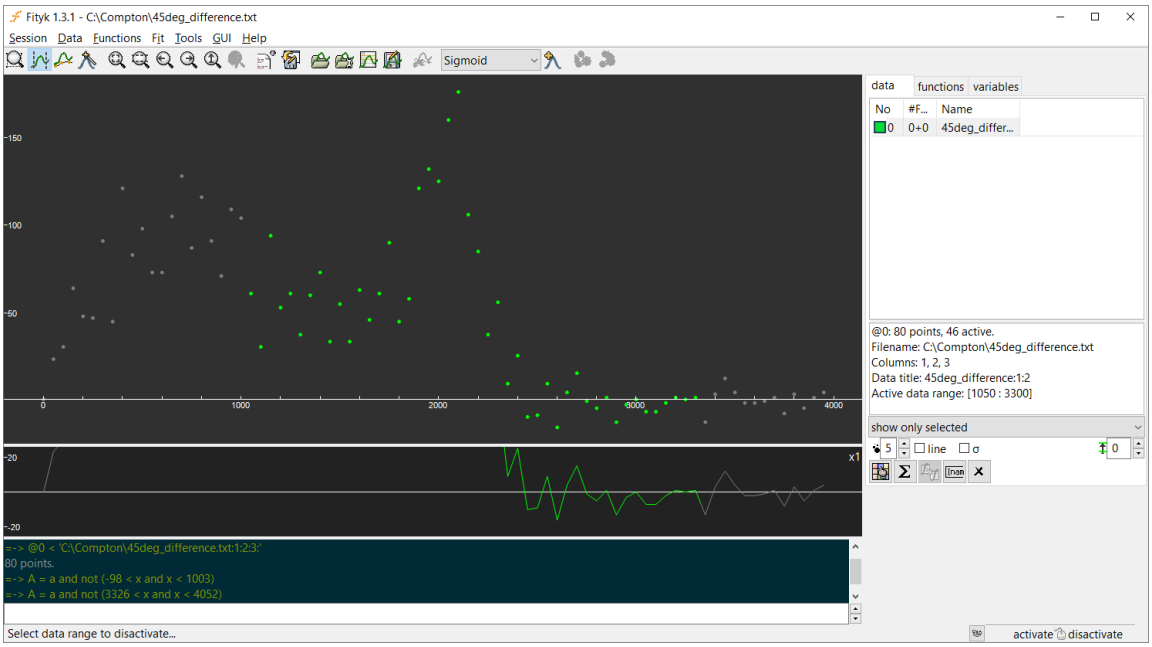


Fig. 51. Main window of the "Fityk" program after marking the points to be used in the fit.

the spin control located in the lower-right part of the window (e.g., in Fig. 50, the selected point size is 5). This spin control is visible only when the "data" tab is selected in the upper-right corner of the window (see Fig. 50).

4. Set the *X*-axis fitting interval. To do this, click the second toolbar button "" (see Fig. 50). Then drag the mouse across the plot window while holding down the right mouse button. Points whose *X*-values the mouse passes over will be excluded from the fitting region (those points turn gray in the plot). To restore points back into the fitting region, drag the mouse while holding down the left mouse button. In this way, define a fitting interval that encompasses the entire peak located at the right edge of the spectrum, plus another 10–15 points on both sides of that peak (the latter points must be chosen such that the *Y*-values are approximately constant within their interval, apart from random variations). For example, in the case of Fig. 50, the optimal fitting interval is approximately $1000 < x < 3500$. The selected interval is displayed on the right side of the main window after the words "Active data range" (e.g., in Fig. 51, that interval is $1050 \leq x \leq 3300$).

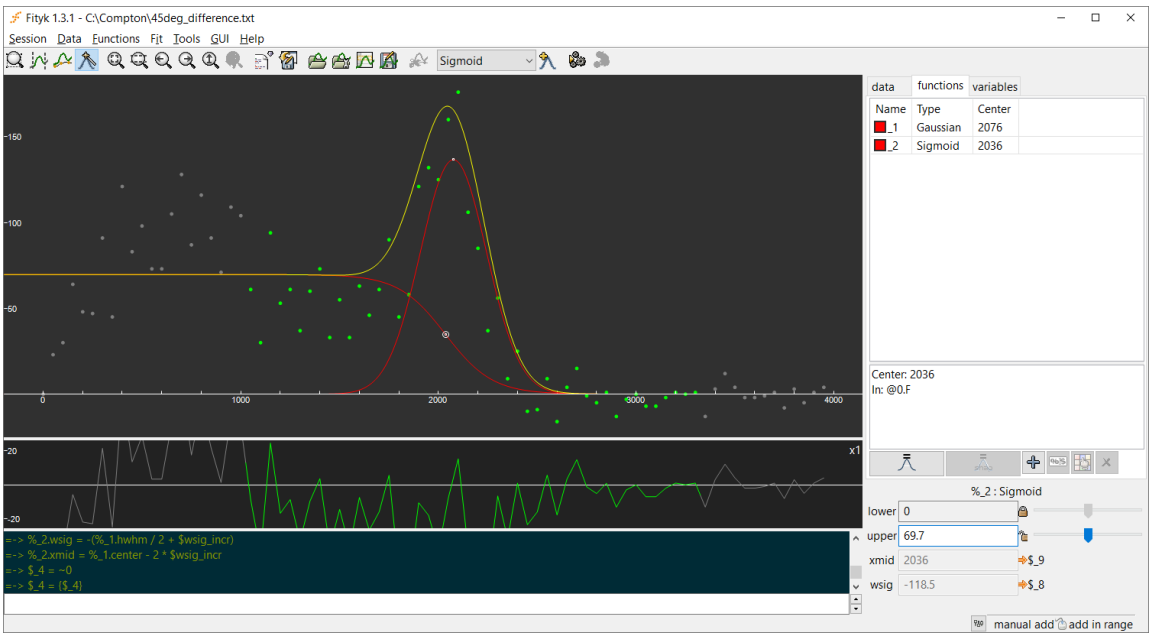


Fig. 52. Main window of the "Fityk" program after constraining the sigmoid parameters "lower", "xmid", and "wsig".

5. The Gaussian function is selected and its initial parameter values are defined in the exact same way as for the calibration spectrum (see step 5 in the previous subsection).

6. The sigmoid is selected and its initial parameter values are defined in the exact same way as for the calibration spectrum (see step 6 in the previous subsection).

7. Just as in the case of the calibration spectrum, the sigmoid parameter "xmid" must be bounded from above so that it does not exceed the Gaussian function's centroid "center". The corresponding steps are described in step 7 of the previous subsection. In addition, the sigmoid parameter "lower" must be fixed: as mentioned, it must be equal to 0. This is done by typing the number 0 into the text field "lower" and clicking the padlock-shaped icon next to that field. The "unlocked padlock" icon then turns into a "locked padlock" icon (see Fig. 52), and it is no longer possible to change the "lower" value manually (the background of the corresponding text field turns gray).

All subsequent steps are identical to those when fitting the calibration spectrum (see the descriptions of steps 8–11 in Section 6.3.2). The result is the peak centroid H and its standard deviation δH. All actions described in this subsection must be performed for each of the seven scattered radiation spectra.

6.3.4. Verification of the Compton formula and calculation of the Compton wavelength

1. From the centroids H_0 and H of the calibration and scattered radiation spectrum peaks, calculate the energies E of the photons scattered at each angle (Eq. (5.7.3)), and from the standard deviations δH and δH_0, calculate the error bounds ΔE of those energies (Eqs. (6.1.12) and (6.1.13)).

2. Calculate the wavelengths λ of the radiation scattered at each angle and their error bounds $\Delta\lambda$ (Eqs. (6.1.14) and (6.1.15)).

3. For each scattering angle, calculate the change in wavelength $\lambda - \lambda_0$, where λ_0 is the wavelength of the primary radiation (λ_0 is calculated using the known ^{137}Cs radiation photon energy $E_0 = 661.7$ keV). The error bound of the wavelength change is equal to the previously calculated error bound $\Delta\lambda$ of the wavelength λ.

4. Plot the measurement data in a graph where the wavelength change $\lambda - \lambda_0$ is plotted on the Y-axis, and the expression $1 - \cos\theta$ is plotted on the X-axis. In this graph, the experimental data must be represented by seven individual data points with their corresponding error bars (in the form of vertical tick bars). According to the Compton formula (3.3.5), within the error bars, those points should follow a linear dependence with zero intercept.

5. To verify the Compton formula, perform a linear fit. Various programs can be used for this purpose, e.g., the previously mentioned program "Fityk". When using "Fityk", the main fitting steps are the same as in the previously described spectrum fits: **(a)** create a text file with three columns and seven rows: the first column contains the $1 - \cos\theta$ values, the second column contains the experimental values of the difference $\lambda - \lambda_0$, and the third column contains the corresponding error bounds, **(b)** load the data from that file into "Fityk" using the menu command "*Data* > *Load File*" and checking the "σ" radio button in the "Load Data" dialog box, **(c)** select the linear fitting function (menu command "*Functions* > *Function Type* > *Linear*"), **(d)** after clicking the fourth toolbar button "", draw an initial straight line in the plot window (it does not necessarily have to match the data, since the coefficients of a straight line will be optimized anyway and their final values will not depend on the initial approximations), **(e)** perform the fit by clicking the next-to-last toolbar button "", **(f)** copy the coefficient estimates and their standard deviations of the straight-line equation "$a_0 + a_1 \cdot x$" from the "Fit Info" window, which opens after selecting the menu command "*Fit* > *Info*", **(g)** calculate the error bounds Δa_0 and Δa_1 of the coefficients "a_0" and "a_1" by multiplying their standard deviations by the Student's t-coefficient corresponding to a 95 % confidence level and $n - 2$ degrees of freedom, where n is the number of experimental points used in the fit (Student's t-coefficients are given in Table 4). If all errors are purely random, then the confidence interval of the slope coefficient "a_1" (i.e., the interval $[a_1 - \Delta a_1,\ a_1 + \Delta a_1]$) encompasses the exact value of the Compton wavelength expressed by formula (3.3.6) with 95 % probability, and the confidence interval of the intercept "a_0" encompasses zero with 95 % probability (i.e., $\Delta a_0 > |a_0|$).

6. Repeat the linear fit using a zero intercept. To do this, in the text field containing the value of the coefficient "a_0", type the number 0 and click the padlock-shaped icon next to that field (so that the "unlocked padlock" icon turns into a "locked padlock" icon), and then repeat the fit (the next-to-last toolbar button ""). Now only the estimate of the slope coefficient a_1 and its standard deviation will be visible in the "Fit Info" window. When calculating its error bound Δa_1, you must use a number of degrees of freedom greater by one than in the previous step, i.e., $n - 1$, because only one parameter is now being optimized instead of two. If all errors are purely random, then the confidence interval of the slope coefficient "a_1" (i.e., the interval $[a_1 - \Delta a_1,\ a_1 + \Delta a_1]$) encompasses the exact value of the Compton wavelength expressed by formula (3.3.6) with 95 % probability.

7. Plot the fitted linear dependences obtained in steps 5 and 6 in the same graph as the experimental wavelength shifts.

8. Based on the fitting results of steps 5 and 6, discuss and compare the accuracy of the two linear fits performed. Compare the experimental value of the Compton wavelength with the exact value.

Table 4. Student's *t*-coefficients corresponding to various confidence levels and various numbers of degrees of freedom

Degrees of freedom \ Confidence level	50%	60%	70%	80%	90%	95%	98%	99%	99.5%	99.8%	99.9%
1	1.000	1.376	1.963	3.078	6.314	**12.71**	31.82	63.66	127.3	318.3	636.6
2	0.816	1.061	1.386	1.886	2.920	**4.303**	6.965	9.925	14.09	22.33	31.60
3	0.765	0.978	1.250	1.638	2.353	**3.182**	4.541	5.841	7.453	10.21	12.92
4	0.741	0.941	1.190	1.533	2.132	**2.776**	3.747	4.604	5.598	7.173	8.610
5	0.727	0.920	1.156	1.476	2.015	**2.571**	3.365	4.032	4.773	5.893	6.869
6	0.718	0.906	1.134	1.440	1.943	**2.447**	3.143	3.707	4.317	5.208	5.959
7	0.711	0.896	1.119	1.415	1.895	**2.365**	2.998	3.499	4.029	4.785	5.408
8	0.706	0.889	1.108	1.397	1.860	**2.306**	2.896	3.355	3.833	4.501	5.041
9	0.703	0.883	1.100	1.383	1.833	**2.262**	2.821	3.250	3.690	4.297	4.781
10	0.700	0.879	1.093	1.372	1.812	**2.228**	2.764	3.169	3.581	4.144	4.587
11	0.697	0.876	1.088	1.363	1.796	**2.201**	2.718	3.106	3.497	4.025	4.437
12	0.695	0.873	1.083	1.356	1.782	**2.179**	2.681	3.055	3.428	3.930	4.318
13	0.694	0.870	1.079	1.350	1.771	**2.160**	2.650	3.012	3.372	3.852	4.221
14	0.692	0.868	1.076	1.345	1.761	**2.145**	2.624	2.977	3.326	3.787	4.140
15	0.691	0.866	1.074	1.341	1.753	**2.131**	2.602	2.947	3.286	3.733	4.073
16	0.690	0.865	1.071	1.337	1.746	**2.120**	2.583	2.921	3.252	3.686	4.015
17	0.689	0.863	1.069	1.333	1.740	**2.110**	2.567	2.898	3.222	3.646	3.965
18	0.688	0.862	1.067	1.330	1.734	**2.101**	2.552	2.878	3.197	3.610	3.922
19	0.688	0.861	1.066	1.328	1.729	**2.093**	2.539	2.861	3.174	3.579	3.883
20	0.687	0.860	1.064	1.325	1.725	**2.086**	2.528	2.845	3.153	3.552	3.850
21	0.686	0.859	1.063	1.323	1.721	**2.080**	2.518	2.831	3.135	3.527	3.819
22	0.686	0.858	1.061	1.321	1.717	**2.074**	2.508	2.819	3.119	3.505	3.792
23	0.685	0.858	1.060	1.319	1.714	**2.069**	2.500	2.807	3.104	3.485	3.767
24	0.685	0.857	1.059	1.318	1.711	**2.064**	2.492	2.797	3.091	3.467	3.745
25	0.684	0.856	1.058	1.316	1.708	**2.060**	2.485	2.787	3.078	3.450	3.725
26	0.684	0.856	1.058	1.315	1.706	**2.056**	2.479	2.779	3.067	3.435	3.707
27	0.684	0.855	1.057	1.314	1.703	**2.052**	2.473	2.771	3.057	3.421	3.690
28	0.683	0.855	1.056	1.313	1.701	**2.048**	2.467	2.763	3.047	3.408	3.674
29	0.683	0.854	1.055	1.311	1.699	**2.045**	2.462	2.756	3.038	3.396	3.659
30	0.683	0.854	1.055	1.310	1.697	**2.042**	2.457	2.750	3.030	3.385	3.646
40	0.681	0.851	1.050	1.303	1.684	**2.021**	2.423	2.704	2.971	3.307	3.551
50	0.679	0.849	1.047	1.299	1.676	**2.009**	2.403	2.678	2.937	3.261	3.496
60	0.679	0.848	1.045	1.296	1.671	**2.000**	2.390	2.660	2.915	3.232	3.460
80	0.678	0.846	1.043	1.292	1.664	**1.990**	2.374	2.639	2.887	3.195	3.416
100	0.677	0.845	1.042	1.290	1.660	**1.984**	2.364	2.626	2.871	3.174	3.390
120	0.677	0.845	1.041	1.289	1.658	**1.980**	2.358	2.617	2.860	3.160	3.373
∞	0.674	0.842	1.036	1.282	1.645	**1.960**	2.326	2.576	2.807	3.090	3.291